NOVEL APPROACHES TO THE STUDY OF SYNAPTIC PLASTICITY IN THE RAT HIPPOCAMPUS

by

Borbala Podor

Submitted in partial fulfilment of the requirements
for the degree of Doctor of Philosophy

at

Dalhousie University
Halifax, Nova Scotia
June 2017

Szüleimnek és nagyszüleimnek

TABLE OF CONTENTS

LIST OF TABLES

LIST OF FIGURES

ABSTRACT

Synaptic plasticity refers to changes in the strength of connections between neurons in response to previous activity. Its experimental correlates, i.e., long-term-potentiation (LTP), a persistent increase in synaptic efficacy, and long-term-depression (LTD), a persistent decrease in synaptic efficacy, are the leading cellular models of learning and memory. The observed changes in LTP and LTD are detected by electrophysiological methods as lasting modifications of synaptic transmission, but they may be accompanied by morphological changes in the synapses undergoing plasticity. However, published accounts of the relationship between functional and structural changes are incomplete and often inconsistent. This is partially due to the lack of available tools and technologies allowing direct observations and interpretations of obtained results. In this thesis I explore potential technological advances for investigating neuronal activity, and examine the relationship of functional and structural changes at synapses undergoing plasticity.

First, I evaluate a number of novel genetically-encoded calcium indicators (GECIs) for optical monitoring of neuronal activity in rat hippocampal slices. The results indicate that most GECIs are too slow and/or insensitive to follow individual action potentials at high frequencies necessary for some intended uses. Next, I demonstrate that recently-developed ultrafast GECIs provide vastly improved kinetics, but at the expense of weaker fluorescent signals. Further improvements in these indicators may be highly valuable for future applications. Finally, I present a multifaceted approach combining double intracellular electrophysiological recordings from pairs of synaptically connected hippocampal neurons with two-photon-excitation fluorescence microscopy and calcium imaging to study structural plasticity of individually identified synapses undergoing plasticity. My results suggest that physiological stimulation and plasticity induction do not cause significant persistent changes in size of either pre- or postsynaptic elements. In this context, I also describe how optimizing a variety of recording variables (e.g., days *in vitro*, sub-regional localization, distance between cell pairs) contribute to the success of paired recordings in rat organotypic hippocampal slices, and how it can aid our studies on structural and functional plasticity.

LIST OF ABBREVIATIONS USED

3D – Three dimension

7CK – 7-Chlorokynurenic acid

A/C – Associational/commissural pathway

ACSF – Artificial cerebrospinal fluid

Ala - Alanine

AMPA - α-amino-3-hydroxy-5-methyl-4-isoxazolepropionic acid

AMPAR - α-amino-3-hydroxy-5-methyl-4-isoxazolepropionic acid receptor

AP – Action potential

Arc 2/3 – Actin-related protein 2/3

ASAP-1 – Accelerated sensor of action potentials 1

Asp – Aspartic acid

AZ – Active zone

BDNF – Brain derived neurotrophic factor

BFP – Blue fluorescent protein

B-GECO – Blue GECO

$[Ca^{2+}]$ – Calcium concentration

C/A – Commissural/associational

CA – Conru ammonis

CA3a – Subregion “a” of CA3

CA3b – Subregion “b” of CA3

CA3c – Subregion “c” of CA3

CaM – Calmodulin

CaMKII – Calcium/calmodulin-dependent protein kinase II

CAR-GECO – Carmine GECO

Cdc42 – Cell devision control protein 42

CEPIA – Calcium-measuring organelle entrapped protein indicator

CICR – Calcium-induced calcium release

cLTP – Chemically-induced LTP

CMV – Cytomegalo virus

CNS – Central nervous system

cp – Circularly permuted

EF – Helix-loop-helix structural domain

EGFP – Enhanced green fluorescent protein

eLTP – Early LTP

DCV – Dense core vesicles

DG – Dentate gyrus

DIV – Days *in vitro*

DNA – Deoxyribonucleic acid

EBSS – Earle's balanced salt solution

EC – Entorhinal cortex

EM - Electron microscopy

EPSCaT - Evoked postsynaptic calcium transient

EPSP – Excitatory post-synaptic potential

ER – Endoplasmic reticulum

F-actin – Filamentous actin

FlaSH – Fluorescent shaker

FP – Fluorescent protein

FRET - Fluorescence Resonance Energy Transfer

GABA – gamma-Aminobutyric acid

G-actin – Globular actin

G-CaMP - Calmodulin-based genetically encoded fluorescent calcium indicators

GCaMPer – Endoplasmic reticulum targeted low affinity GCaMP3

GCaMP-HS – Hyper-sensitive GCaMP

GCaMP6f – Fast GCaMP6

GCaMP6m – Medium GCaMP6

GCaMP6s – Slow GCaMP6

$GCaMP6f_u$ – Ultrafast GCaMP6f

GECI – genetically encoded calcium indicator

GECO - Green Fluorescent Genetically Encoded Calcium Indicators for Optical Imaging

GEM-GECO – Green emission GECO

GFP – Green fluorescent protein

G-GECO – Green GECO

GEVI – Genetically encoded voltage indicator

GluR1 – Glutamate receptor 1

GTP – Guanosine triphosphate

HBSS – Hank's balanced salt solution

HEK – Human embryonic kidney cell

HeLa – Henrietta Lacks cervical cancer cell line

HEPES - 4-(2-hydroxyethyl)-1-piperazineethanesulfonic acid

HFS – High frequency stimulation

hVOS – Hybrid voltage sensor

IPSP – Inhibitory postsynaptic potential

IP3R – Inositol trisphosphate receptor

K_d – Dissociation constant

LFS – Low frequency stimulation

LTD – Long-term depression

LTP - Long-term potentiation

l-LTP – Late LTP

MAP - Mitogen-activated protein

MF – Mossy fiber

MEM – Minimum essential medium

mGluRI – Metabotropic glutamate receptor type I

MNI-glu - Methoxy derivative of nitroindolino glutamate

MSB – Multi-synaptic boutons

NMDA - N-methyl-D-aspartate

NMDAR - N-methyl-D-aspartate receptor

NO – Nitric oxide

NR2B – N-methyl-D-aspartate receptor subtype 2B

n.s. – Not significant

O-GECO – Orange GECO

OHSC - Organotypic hippocampal slice culture

oLFS – Optogenetic low frequency stimulation

p38MAPK – p38 mitogen-activated protein kinase

PK – Protein kinase

PKA – Protein kinase A

PKC – Protein kinase C

PKMζ – Protein kinase M zeta

PMT – Photomultiplier tube

PND – Post Natal Day

PP - Perforant path

PP1 – Protein phosphatase 1

P_r - Probability of transmitter release

PSD – Post-synaptic density

PSD-95 - Post-synaptic density protein 95

RIM - Rab3-interacting molecule

RIM-BP – RIM binding protein

RS20 - Smooth muscle myosin light chain kinase-derived peptide

S/A – Schaffer collateral/associational

SC – Schaffer collateral

S.E.M. – Standard error of the mean

st. –Stratum

s.l.m. – Stratum oriens-lacunosum

s.o. – Stratum oriens

s.r. – Stratum radiatum

STED - Stimulated emission depletion (microscopy)

STDP – Spike timing-dependent plasticity

SSH - Slingshot protein phosphatase

Sy-GCaMP2 – Fusion of synaptophysin and GCaMP2

TBS – Theta burst stimulation

Trp - Tryptophan

Tyr - Tyrosine

VGCC - Voltage-gated calcium channel

Y-GECO – Yellow GECO

ACKNOWLEDGEMENTS

I would like to express my sincere gratitude for my supervisors, Dr. Alan Fine and Dr. Roger Croll. Thank you for taking a chance and welcoming me on your team first as an exchange student and then to extend that into supervising me throughout a PhD degree. Thank you for setting high standards and examples for me to learn from and looking out for me throughout the ups and downs of a scientific endeavour.

I would also like to thank members of my supervisory committee, Dr. Stefan Krueger and Dr. William Baldridge, and my external examiner, Dr. Katalin Tóth, for participating in the preparation and the defense of this thesis.

I am grateful for all collaborative opportunities, specifically with Dr. Nordine Helassa, Dr. Katalin Török, Dr. Masamichi Ohkura, and Dr. Junichi Nakai.

I would like to extend my gratitude for past and present members of the Fine and Croll laboratories. Special thank you to Dr. Yi-ling Hu for her amazing work, patience, support and love. Thank you to Dr. Ulli Hoeger for all the lessons in electrophysiology and for the countless times of fixing my setup. Ryuichi, Oliver, Matthew, Ranga, Aram, Stephanie, Hershel, Matt, Jillian, Neil for being fun lab members. Thank you to all members of the Department of Physiology and Biophysics, specifically to Jennifer, Annette, Dylan, Andrea, Alexander and Alexey.

Thank you for all the personal support from the Lakner and Allen families, and my close friends near and far.

I am forever grateful for my family. This work is dedicated to them as it would not have been possible without the constant love, support and inspiration from my parents, grandparents, and siblings, who always encouraged me to pursue my goals even when they take me across the Atlantic ocean.

Finally, I would like to thank my husband for his patience, understanding and loving support throughout this degree. Thank you for knowing when to push me further and when to offer me shelter.

Köszönöm!

CHAPTER 1

INTRODUCTION

1.1 Hippocampal Formation

The hippocampus has served as a substrate for numerous pioneering discoveries in neuroscience, particularly in the field of learning and memory. The role of this structure, however, was a topic of a long-standing debate in the eighteenth and nineteenth century. Its undeniable function in memory has since been validated in numerous human and animal studies by demonstrating how injury to the hippocampal formation leads to memory deficits (Scoville & Milner, 1957; Zola-Morgan *et al.*, 1986; Thornton *et al.*, 1997; Ramos, 1998). It is now also accepted that the hippocampal formation receives and integrates widespread sensory information from the neocortex, is part of the limbic system, has an important role in spatial memory and navigation (Moser, Kropff, & Moser, 2008; O'Keefe & Dostrovsky, 1971) and the process of consolidation of short to long-term memory (Dudai, 2004).

1.1.1 Anatomy of the Hippocampus

Besides the hippocampus' prominent role in memory its unique and highly organized anatomy has led to its becoming a preferred model system in neurobiology. In humans it is part of the medial temporal lobe located adjacent to the lateral ventricle, and

in rodents it is a C-shaped structure located caudoventrally, in both cases bilaterally (Figure 1.1). The principal cells of the hippocampal formation are organized in layers and its mainly unidirectional inputs are arranged in laminar ways. The hippocampus proper consists of areas CA1, CA2, and CA3 (cornu ammonis, abbreviated CA) and together with other regions such as the dentate gyrus (DG), subiculum, pre- and parasubiculum, and the entorhinal cortex they form the hippocampal formation.

1.1.2 Hippocampal processing loop

The information flow in the hippocampus is generally described as the "Hippocampal Processing Loop" (Figure 1.1). It begins in the superficial layers of the entorhinal cortex, where multimodal sensory information from the neocortex arrives, and ends in the deep layers of the same region. Information from the entorhinal cortex travels via the Perforant Path (PP) and synapses onto the granule cells of the DG. The axons of the granule cells give rise to the Mossy Fibers (MF) and make multiple *en passant* boutons, or mossy fiber expansions, that form large synapses with the "thorny excrescences" of the pyramidal cells in area CA3. The axons of CA3 pyramidal cells that target CA1 pyramidal cells make up the Schaffer collaterals, whereas the associational/commissural fibers of CA3 cells form multiple recurrent synapses on other CA3 cells. CA1 pyramidal cells receiving information via the Schaffer collaterals from area CA3 subsequently project to the subiculum and the entorhinal cortex. The pathways of the tri-synaptic circuit (Andersen et al., 1971) consisting of the Perforant Path, Mossy Fibers and Schaffer collaterals are largely unidirectional projections.

1.1.3 Principal cells and synapses of the hippocampus

Most of the cells of the hippocampus as well as its excitatory and inhibitory synapses are now identified, localized and their function described, including their role in some of the underlying mechanisms of learning and memory. Many of these advances are attributable to the development of transverse hippocampal slice preparations (Skrede & Westgaard, 1971) that allows one to access the neatly organized principal cells and pathways of the hippocampus, to record intra- and extracellularly, and to achieve quick pharmacological manipulation of the preparation. In addition, the innovation of *in vitro* organotypic hippocampal cultures (Gähwiler, 1981*a*; Stoppini *et al.*, 1991) allows normal differentiation, development, and organization of the hippocampal tissue, ultimately reserving the normal cytoarchitecture and resulting in properties close to that of acute slices (Gähwiler, 1997). Much of the literature on synaptic plasticity, a model of learning and memory, not surprisingly comes from these hippocampal preparations. The next two sections will focus on the principal cells and synapses of areas CA1 (Figure 1.2) and CA3 (Figure 1.3) of the rodent hippocampus, followed by a brief description of their synaptic plasticity.

1.1.4 Pyramidal cells of area CA1

The most studied cells of the hippocampus are arguably the CA1 pyramidal cells (Figure 1.2), due to the fact that they can be easily reached for electrical recordings, their input pathway through the Schaffer collaterals can be reliably stimulated extracellularly,

and that they are often more viable than CA3 cells in slice preparations (Spruston & McBain, 2007). Morphologically CA1 and CA3 cells are similar: their cells bodies are of a pyramidal shape and they both typically display an apical and basal dendrites with extensive arborization. In both cases the basal dendrites reach into stratum (st.) oriens, whereas apical dendrites reach to st. radiatum and st. lacunosum-moleculare (Bannister & Larkman, 1995; Pyapali *et al.*, 1998). The total dendritic length of CA1 cells is shorter (12 mm) than that of CA3 cells (16 to 18 mm); however, the apical dendrite of CA1 cells is longer compared to CA3, which bifurcates sooner (Megias *et al.*, 2001).

The pyramidal cells of the hippocampus receive thousands of excitatory inputs from presynaptic boutons that mainly associate with postsynaptic dendritic spines, small protrusions of the dendritic shaft. Typically one can differentiate four classes of dendritic spines according to their morphology: thin, stubby, mushroom, and branched (Sorra & Harris, 2000). Thin spines are long and skinny; stubby spines are short and lacking a distinguishable neck; mushroom spines have narrow necks and bulbous heads; and branched spines arise from the same dendritic shaft and via a neck that branches contact different axons (Sorra & Harris, 2000). CA1 cells harbor approximately 30 000 spines, but they are almost lacking on the first 100 μm from the soma (Megias *et al.*, 2001). CA1 cells receive excitatory inputs from two major sources, the entorhinal cortex through the PP targeting mainly the apical tuft, and the Schaffer collaterals from CA3 cells projecting to st. radiatum and st. oriens. Inhibitory synapses are found mainly on the soma, shaft, and apical dendrites with a total number of approximately 1700 (Megias *et al.*, 2001). In addition a variety of neuromodulatory inputs are also received, such as cholinergic input

from the septum, noradrenergic from locus coeruleus, serotonin from raphe nuclei, and dopamine from the ventral tegmental area (Spruston & McBain, 2007).

Axons of CA1 cells have a diameter of less than 1 μm, and their boutons have an oblong shape with a diameter of ~1 μm (Tamamki & Nojyo, 1990). They mainly project to the subiculum and to the deep layers of the entorhinal cortex, completing the hippocampal information processing loop (Amaral *et al.*, 1991). Recurrent connections between CA1-CA1 cells are negligible compare to cells of the CA3 area, and they almost never project back to CA3 cells (Amaral *et al.*, 1991; Debanne *et al.*, 1995).

CA1 and CA3 cells have similar conductances, but the specific location and density of the channels vary (Spruston & McBain, 2007). Importantly for imaging studies, for example, calcium transients in CA1 and CA3 cells are mediated by different sources based on the type of stimulation. Back-propagating action potential-induced calcium signals are provided by high-threshold voltage-gated calcium channels (VGCCs) (Yuste & Denk, 1995; Yuste *et al.*, 1999); synaptically evoked calcium signals originating from N-methyl-D-aspartate receptor (NMDAR) mediated calcium entry are amplified by calcium-induced calcium release (CICR) from intracellular stores (Emptage *et al.*, 1999; Yuste *et al.*, 1999); and in some cases can be mediated by calcium permeable non-glutamate receptors (Yuste *et al.*, 1999).

Regarding electrophysiological properties, there is a distinct difference between CA1 and CA3 pyramidal cells (Golding & Spruston, 1998; Kim, Guzman, Hu, & Jonas, 2012). In CA1 pyramidal cells action potentials back-propagate into the dendrites with large attenuation (Golding & Spruston, 1998), whereas in the proximal dendritic region of CA3 cells action potential back-propagation is only moderately decremented with

minimal temporal differences (Kim et al., 2012). APs back propagate in CA3 even with high frequencies which is aided by a higher density of voltage-gated Na^+ channels, compared to CA1, resulting in dendritic spikes (Kim et al., 2012). The dendritic spikes originating from converging synaptic input may serve in coincident detection, rendering CA3 pyramidal cells well suited for spike timing-dependent plasticity (STDP) in their commissural and auto-associational connections, as well as formation of associative learning and memory (Kim et al., 2012).

Although CA1 and CA3 pyramidal cells share numerous similar properties, CA3 cells are unique due to their extensive recurrent synapses, their giant MF synapses, and their bursting properties, some of which are discussed in further detail below.

1.1.5 Pyramidal cells of area CA3

The principal cells of CA3 area (Figure 1.3) have a prevalent dendritic tree with a total dendritic length of up to 18 mm (Megias *et al.*, 2001). Their dendritic spines are more diverse than those of CA1 cells, and they harbor a particular additional type of dendritic spine, the thorny excrescences. These complex spines, originating with a single stalk from the dendritic shaft, can branch many times and make contact with a single axon. The distributions of different spine classes and morphologies are varied; where the thorny excrescences are generally found only on proximal basal and apical branches (before the first branching point), other spine forms are not particularly associated with specific regions (Amaral & Witter, 1995). Simple spines are far more abundant, forming approximately 30 000 dendritic spines (Trommald & Hulleberg, 1997). Besides the MF

inputs, CA3 spines receive inputs from the PP originating in the entorhinal cortex, but the most numerous inputs are the associational CA3-CA3 connections (Amaral & Witter, 1995), making the CA3 region unique. Additionally to the three main excitatory inputs, CA3 pyramidal cells receive modulatory cholinergic input from the septum (Frotscher & Léránth, 1985), and a variety of inhibitory inputs from hippocampal interneurons (Tóth *et al.*, 1993; Amaral & Witter, 1995; Miles *et al.*, 1996), as well as ascending monoaminergic modulatory inputs including noradrenaline, dopamine and serotonin (Törk, 1990; Hörtnagl *et al.*, 1991; Guo & Li, 2007; Prince *et al.*, 2016).

Axons of the CA3 pyramidal cells give rise to multiple collaterals that reach both ipsi- and contra-laterally to CA1, CA2, and interneurons, however an estimated 30 to 70 % of the connections reach and synapse onto other CA3 pyramidal neurons, the latter referred to as recurrent synapses (Li *et al.*, 1994; Debanne *et al.*, 1995). CA3 axons overlap with both apical and basal dendrites of other hippocampal CA1 and CA3 pyramidal cells. CA3 axons also project to the lateral and medial septal nuclei and to the diagonal band of Broca (Kesner, 2007). The total axonal length in CA3 pyramidal cells is longer than the total dendritic length contributing to the most extensive axonal projection network in the rodent hippocampus (Ropireddy *et al.*, 2011). Axons of CA3 pyramidal cells form an estimated 15 000 to 60 000 terminals along their total length at intervals of two to five μm (Sik *et al.*, 1993; Li *et al.*, 1994). Axonal boutons typically have a diameter of ~0.4 μm, approximately twice the axonal diameter of ~0.2 μm (Li *et al.*, 1994). Electron microscope (EM) studies show that these presynaptic boutons have active zones (the site of neurotransmitter release; AZ) and synaptic vesicles and oppose postsynaptic partners with postsynaptic densities (a protein-dense specialization

associated with the post-synaptic membrane; PSD) (Shepherd & Harris, 1998; Holderith *et al.*, 2012). Boutons of the recurrent CA3 axons in roughly one out of five cases have multiple postsynaptic partners, but most commonly establish single contacts (Holderith *et al.*, 2012).

The spine and bouton structure and morphology of CA3 cells, as well as of other neurons in the central nervous system (CNS), are plastic to some extent and may experience a varying level of change in response to development, activity and inactivity as I will discuss further below in section 1.2 and in Chapter 4.

1.1.6 CA3-CA3 recurrent synapses

The CA3-CA3 projections are referred to as associational connections or recurrent synapses. The majority of these associational connections are found in st. radiatum (along the apical dendrites) and, less commonly, in st. oriens (along the basal dendrites), where they mostly form excitatory synapses on dendritic spines (Gulyas *et al.*, 1993). The extent of connectivity estimated from paired recordings is low in acute hippocampal slices (2 to 3 %) though much higher in cultured, organotypic hippocampal slices (30 to 60 %) (Debanne *et al.*, 1995).

The function of the associational connections has been linked to physiological and pathological synchronous pattern generation in spatial learning (Wilson and McNaughton, 1994), place cell activity (O'Keefe & Dostrovsky, 1971) associative learning (Marr, 1971), and epilepsy (Kandel and Spencer 1961). As reviewed by Kesner (2007), the CA3 area of the hippocampus is involved in rapid encoding of new

information, encoding over multiple trials, arbitrary associations, cued recall, pattern completion and retrieval of memory with short delays (Kesner, 2007).

Short- and long-term synaptic plasticity can be achieved both at CA3-CA3 and at CA3-CA1 synapses (Debanne *et al.*, 1998), and will be discussed in the following section. For further details on recurrent synapses of CA3-CA3 cells the reader is referred to Chapters 4 and 5.

1.2 Synaptic plasticity and cellular models of learning

The term "synaptic plasticity" as a long-lasting change in the strength of synapses was used as early as 1948 by Jerzy Konorski (Zieliński, 2006) and by Hebb in his synaptic model hypothesis (Cooper, 2005). Cajal however had decades earlier postulated that the functional connections between neurons (e.g., synapses) can undergo anatomical change (Sherrington, 1897). Experimental evidence that the efficacy of hippocampal synapses are altered by previous activity that could potentially be a way of memory storage came from Bliss and Lømo's discovery of long-term potentiation (LTP) (Bliss & Lømo, 1973), where brief trains of high-frequency stimulation of the PP led to a sustained increase in synaptic transmission on to granule cells.

The role of synaptic plasticity as a cellular substrate of learning and memory was later strengthened by Morris and colleagues (Morris *et al.*, 1986), who showed that blocking hippocampal LTP induction also leads to a severe weakening of memory acquisition and retention. Eventually LTP became the most accepted cellular model of

learning and memory (Bliss & Collingridge, 1993). It has since been shown that both LTP and its counterpart, long-term depression (LTD; sustained decrease in synaptic efficacy) occur in most parts of the brain. Both processes can be divided up into induction, expression and maintenance phases. Experimentally, LTP and LTD can be induced by a number of activity patterns, summarized in the next section, followed by a brief description of the molecular processes of LTP and LTD expression.

1.2.1. Common LTP and LTD inducing protocols in the rodent hippocampus

Since the original LTP studies showing that high frequency stimulation (tetanization) of afferent pathways can lead to a persistent increase of synaptic transmission (Bliss & Lømo, 1973), it has also been shown that theta burst and prime burst stimulation, spike timing-dependent plasticity, chemical LTP and patterned glutamate uncaging are also reliable ways to enhance synaptic strength.

1.2.1.1 Tetanization

Typically, tetanization involves one or more trains of pulses at 100 Hz for 1 second with 10 minute intervals. Three of these trains can lead to LTP saturation that may last for many hours, and in some cases up to a year (Abraham, 2003). It has been suggested though that such high frequency trains are uncommon under physiological

circumstances and that theta burst stimulation (TBS) is much closer to natural hippocampal activity patterns (Buzsaki, Haas, & Anderson, 1987; Buzsaki, 2002).

1.2.1.2 Theta-burst stimulation

TBS usually consists of a few brief bursts of 4 or 5 pulses at 100 Hz repeated at 5 Hz. TBS involves a variety of mechanisms leading to LTP. These include activation of NMDAR, VGCC, CICR, back-propagating action potentials, and the activity of neurotrophic factors (Buzsaki, 2002; Morgan & Teyler, 2001; Raymond & Redman, 2006).

1.2.1.3 Prime-burst stimulation

Prime-burst stimulation, where 200 ms after a single priming stimulus is followed by a single bursts of 4 shocks at 100 Hz, is also considered a more physiological LTP inducing paradigm as similar firing patterns can occur in the hippocampus during learning (Otto *et al.*, 1991).

1.2.1.4 Chemical LTP

Chemically induced LTP (cLTP) is often the method of choice when maximizing the number of synapses undergoing potentiation is favored. The cLTP inducing protocols

mostly rely on either elevated Ca^{2+} and reduced Mg^{2+} levels and the addition of tetraethylammonium (Aniksztejn & Ben-Ari, 1991; Hosokawa *et al.*, 1995), or the NMDAR co-agonist glycine (Musleh *et al.*, 1997), to the extracellular solution of artificial cerebrospinal fluid (ACSF), amongst many others (Otmakhov *et al.*, 2004; Molnár, 2011).

1.2.1.5 Two-photon uncaging

Two-photon uncaging of a methoxy derivative of nitroindolino glutamate (MNI-glu) as a way of imitating synaptic transmission at the individual synapse was described by Matsuzaki and colleagues (Matsuzaki *et al.*, 2001) and has since been used extensively (Harvey & Svoboda, 2007; Kwon & Sabatini, 2011; Meyer *et al.*, 2014). This technique circumvents the activation of presynaptic cell by using light to free caged glutamate via photolysis with high spatio-temporal resolution directly onto the postsynaptic cell, mostly on dendritic spines, which it is then possible to visualize via calcium imaging (Carter & Sabatini, 2004). MNI-glutamate can be applied in mM concentration directly in the ACSF or by puff application, and uncaging light pulses (~30 to 40 pulses at 0.5 Hz with 4 ms pulse duration) are delivered ~0.5 μm from the dendritic spine (Kwon & Sabatini, 2011; Meyer *et al.*, 2014). Plasticity induction via MNI-glu uncaging can be done independently or in combination with depolarization, low extracellular Mg^{2+}, or with the induction of postsynaptic action potentials (Harvey & Svoboda, 2007).

1.2.1.6 LTD induction protocols

In contrast to LTP, LTD can result from longer episodes of low frequency stimulation, e.g., 15 minutes of 1 Hz stimulation (Dudek & Bear, 1992; Collingridge *et al.*, 2010) or low frequency glutamate uncaging (Oh *et al.*, 2013). Furthermore, both LTP and LTD can be evoked by spike timing-dependent plasticity (STDP) (Song *et al.*, 2000; Bi & Poo, 2001; Markram, 2011).

1.2.1.7 Spike timing-dependent plasticity for LTP and LTD

Spike timing-dependent plasticity (STDP; Figure 1.4) refers to a precisely timed and ordered pairing of pre- and postsynaptic activity leading to synaptic plasticity (Markram *et al.*, 1997; Bi & Poo, 1998; Song *et al.*, 2000; Feldman, 2012). In general, STDP results from the coincident actions of presynaptic inputs (leading to excitatory postsynaptic potentials; EPSPs) and postsynaptic action potentials. The postsynaptic action potential can back-propagate into the dendrites and relieve the Mg^{2+} block from the NMDAR (Bi & Poo, 2001), rendering it permeable to cations in the presence of glutamate. NMDAR activation results in Ca^{2+} influx, and the magnitude of intracellular [Ca^{2+}] increase at the postsynaptic site along with temporal factors may determine the direction of plasticity (Bliss & Collingridge, 1993; Wang, Gerkin, Nauen, & Bi, 2005).

Most studies find that LTP occurs when the presynaptic spike proceeds that of the postsynaptic spike by approximately 15 ms, and that LTD is induced when the

postsynaptic spike arises 15 to 70 ms before the presynaptic one and when such pairings are repeated ~100 times (Figure 1.4) (Markram *et al.*, 1997; Bi & Poo, 1998; Debanne *et al.*, 1998; Wittenberg & Wang, 2006). In addition, perfectly synchronized pre- and postsynaptic action potentials will lead to LTD (Debanne *et al.*, 1998), whereas longer than 200 ms delay between the pairing pulses will generally not alter plasticity (Markram *et al.*, 1997). Thus the degree of plasticity is time-dependent, that is LTP and LTD are strongest when pre- and postsynaptic firing is closest together (Buchanan & Mellor, 2010). However, in a 2001 study of Sjöström and colleagues, it was shown that irrespective of the order of pre- and postsynaptic firing, HFS promoted LTP and LFS preferred LTD (Sjöström *et al.*, 2001). It has since been proposed that the requirement of a particular order of pre- and postsynaptic activity for STDP induction is debatable, and that STDP depends on linking pre- and postsynaptic activity together by the coincidence of EPSPs and postsynaptic depolarization by back-propagating action potentials or dendritic spikes, serving as an associative signal (Stuart & Sakmann, 1994; Magee & Johnston, 1997; Debanne *et al.*, 1998; Golding *et al.*, 2002; Buchanan & Mellor, 2010).

In a recent study by Mishra and colleagues (Mishra *et al.*, 2016), plotting changes in EPSP amplitude against pairing time interval in CA3-CA3 recurrent synapses the STDP curve proved to be symmetrical and broad with a ~150 ms half-width. Potentiation was therefore independent of relative order of pre- and postsynaptic activation, but required the supra-linear summation of spine calcium signals through NMDAR and L-type calcium channels. Such summation may be due to the combination of synaptic input and action potential after-depolarization. More and more studies indicate that the classical

STDP requirements might be influenced and potentially altered by the location of the activated synapse and active dendritic mechanisms (Kampa *et al.*, 2007).

Taken together, LTP and LTD can be induced by several techniques, however, some processes are arguably closer to naturally occurring activity patterns, hence suggested as more physiological in nature. STDP is considered to be one of these induction protocols, and is linked to associative learning in CA3 cells. Thus we selected STDP as a mean to induce and study the physiological and structural aspects of synaptic plasticity in recurrent CA3-CA3 synapses, which is applied and detailed in Chapter 4.

1.2.3 Molecular processes of NMDAR-dependent hippocampal LTP and LTD

CA3-CA3 connections, similarly to CA3-CA1 synapses, but unlike MF-CA3 synapses (Harris and Cotman, 1986), both express NMDAR-dependent and support bidirectional LTP and LTD (Bliss & Collingridge, 2013; Debanne et al., 1998; Zalutsky & Nicoll, 1990). The term NMDAR-dependent LTP and LTD signifies how the processes of postsynaptic NMDAR activation by glutamate and subsequent Ca^{2+} entry is necessary in inducing LTP or LTD (Bliss & Collingridge, 1993; Coan, Saywood, & Collingridge, 1987; Lynch, Larson, Kelso, Barrionuevo, & Schottler, 1983).

During synaptic transmission glutamate is released from the presynaptic terminal and acts on postsynaptic AMPAR at low frequencies and on AMPA and NMDA receptors at high frequencies. If the Na^{+} entry through the AMPAR sufficiently depolarizes the postsynaptic cell to relieve the Mg^{2+} block of the NMDAR, Ca^{2+} can flow

into the cell (Nowak *et al.*, 1984). The elevated postsynaptic [Ca^{2+}] originating through the NMDARs – and potentially augmented by VGCCs and CICR from internal stores - then activates a variety of protein kinases (PKs), such as PKA, PKC, Ca^{2+}/calmodulin-dependent protein kinase II (CaMKII), and mitogen-activated protein (MAP) kinases. These initial steps make up the phase of LTP induction (Bliss, Collingridge, & Morris, 2007).

The mechanism of LTP expression is less clear, and has been a topic of heated debate over the last few decades, with evidence pointing to presynaptic (Emptage, Reid, Fine, & Bliss, 2003; Lamanna, Signorini, Cerutti, & Malgaroli, 2015; Lisman & Raghavachari, 2006; Malgaroli & Tsien, 1992; Zakharenko, Zablow, & Siegelbaum, 2001), postsynaptic (Malinow & Malenka, 2002; Collingridge *et al.*, 2004), or potentially both pre- and postsynaptic mechanisms (Bliss & Collingridge, 2013; Macdougall & Fine, 2013). Possible presynaptic means could be the increase in the number of release sites (Lisman, 2009), the number of vesicles released (Malgaroli et al., 1995), amount of glutamate released (Choi *et al.*, 2000), or probability of transmitter release (P_r) (Enoki *et al.*, 2009; Lamanna *et al.*, 2015). Alternatively, postsynaptic mechanisms of LTP expression could include post-translational modifications of existing receptors (Huganir & Nicoll, 2013; Lee, Barbarosie, Kameyama, Bear, & Huganir, 2000), AMPAR trafficking including exocytosis, lateral diffusion, and trapping (Lu *et al.*, 2001; Malinow & Malenka, 2002; Bats *et al.*, 2007; Opazo *et al.*, 2010, 2012), and/or alterations of ion channels (Matsuzaki *et al.*, 2004; Collingridge *et al.*, 2004). The steps reviewed above describe LTP induction and early expression, after which PKMζ

activation in the dendritic spine may contribute to LTP maintenance (Ron *et al.*, 2012), a topic beyond the scope of this overview.

NMDAR-dependent LTD shares the initial step in this signal transduction pathway, that is the Ca^{2+} entry through the NMDAR, though it is believed that a more modest yet longer lasting calcium entry takes place in LTD compared to in LTP (Collingridge *et al.*, 2010). Similarly to LTP, evidence for both pre- (Stanton *et al.*, 2003; Enoki *et al.*, 2009) and postsynaptic expression mechanisms (Kandler *et al.*, 1998; Collingridge *et al.*, 2004) have been put forward for LTD. These include changes in release probability of glutamate from the presynaptic compartment, or alternatively various changes in postsynaptic receptors, such as endocytosis of AMPARs and changes of receptor conductances (Collingridge *et al.*, 2004, 2010; Enoki *et al.*, 2009). The initial Ca^{2+} influx through the NMDARs then activates calmodulin (CaM), which in turn activates calcineurin. Calcium sensitive enzymes could alternatively be activated by CICR from internal stores (Nishiyama, Hong, Mikoshiba, Poo, & Kato, 2000). Subsequently, calcineurin dephosphorylates inhibitor-1, leading to the activation of protein phosphatase 1 (PP1), which dephosphorylates various target proteins, ultimately leading to AMPAR internalization, after which protein synthesis is required for further maintenance of LTD (Mulkey *et al.*, 1993; Carroll *et al.*, 1999; Manahan-Vaughan *et al.*, 2000; Collingridge *et al.*, 2010).

In contrast to plasticity induction, mechanisms of LTP and LTD expression and maintenance as well as the accompanying molecular and possible ultra-structural aspects remain controversial, and many of the above mentioned aspects are still highly debated.

1.3 Structural plasticity of the synapse

The possibility that memory formation is linked to alterations in either the number of synapses, by addition or elimination of spines, or morphological changes affecting existing synapses has been suggested by many over the last century. In support of this theory are observations such as the individual correlation of the size of the pre- and postsynaptic compartments and its components, despite of the large overall heterogeneity of synapse shapes and sizes (Shepherd & Harris, 1998). Namely, correlations between the size of the bouton and opposing spine, the size of the active zone and PSD, the number of AMPA- and NMDA receptors located in the PSD, AMPAR and NMDAR and PSD size, PSD size with the postsynaptic currents have all been reported previously (Harris & Stevens, 1989; Nimchinsky, Yasuda, Oetner, & Svoboda, 2004; Nusser et al., 1998; Takumi, Ramírez-León, Laake, Rinvik, & Ottersen, 1999; but see Holderith *et al.*, 2012; Takasaki & Sabatini, 2014). In addition, several kinds of experimental manipulations, e.g., learning, LTP and LTD, are often reported to be accompanied by morphological changes of the synapses. However, despite countless studies there is still disagreement regarding the existence and extent of the aforementioned structural and functional changes as well as how these changes in plasticity and morphology relate to each other. In the following sections I will systematically review evidence supporting and arguing against structural changes of the pre- and postsynaptic compartments of hippocampal synapses undergoing plasticity, including addition and elimination of existing synapses as

well as changes of existing synapses, and Chapter 4 will discuss our experimental results on this topic.

1.3.1 Addition or elimination of synapses

Synapses of the CNS may go through phases of genesis and elimination throughout their life (Desmond *et al.*, 1994). This dynamic turnover is most pronounced during development and slows considerably in the mature brain but has been speculated as a potential way for continuous adaptation to experience (Caroni *et al.*, 2012). With LTP and LTD inducing electrical stimulating protocols or activity and experience driven learning, some claim to witness a change in synapse density. A variety of stimulation protocols, including tetanus in the rat DG (Trommald *et al.*, 1996) and CA1 (Chang & Greenough, 1984; Maletic-Savatic *et al.*, 1999), TBS (De Roo *et al.*, 2008) and carbachol superfusion in CA1 pyramidal cells (Engert & Bonhoeffer, 1999), spatial learning in CA1 and CA3 (Moser *et al.*, 1994; Mahmmoud *et al.*, 2015), trace-conditioning in CA1 (Leuner *et al.*, 2003) have all been reported to increase spine density in the hippocampus. In addition, HFS has also been associated with an increased number of multiple spine synapses (Toni *et al.*, 1999; Medvedev *et al.*, 2014), and bifurcated spines (Trommald *et al.*, 1996) compared to un-stimulated controls. On the other hand LFS of glutamate uncaging (Oh *et al.*, 2013), LFS of optogenetic stimulation (Wiegert & Oertner, 2013) and fear conditioning (Sanders *et al.*, 2012) all led to spine elimination. Others have reported that LFS has led to synapse separation but not to spine loss (Bastrikova *et al.*, 2008).

However, there are a vast amount of papers showing just the opposite: that manipulations leading to LTP and LTD, and associative learning do *not* lead to a change in spine density. In particular, electron microscopy (EM) studies show that tetanization neither results in an elevated number of synapses of CA1 cells nor does it increase the number of multiple synapse boutons or bifurcated spines (Sorra & Harris, 1998). Similarly, spatial learning did not alter spine density in the DG or CA1 regions of the rat hippocampus (Rusakov et al., 1997). Lee and colleagues also found no changes in the total number of synapses and number of spine synapses in HFS animals (Lee, Schottler, Oliver, & Lynch, 1980).

Other tetanization protocols (Popov *et al.*, 2004; Medvedev *et al.*, 2010) and fear conditioning (Gu et al., 2014) also showed no effect on spine densities. Similarly, cLTP was not linked to an increase in spine density (Hosokawa *et al.*, 1995; Stewart *et al.*, 2005).

Lastly, some reports claim an initial increase in the number of spines following LTP or associative learning, which is then followed by a loss of synapses (Bourne & Harris, 2011; Gu et al., 2014) or report an increase in the basal protrusion turnover rate (De Roo *et al.*, 2008) and no overall change in spine density as the opposing processes balance each other out.

Besides inducing synaptic plasticity by electrophysiological and optical methods, or alternatively by learning paradigms, hormonal changes (Cooke & Woolley, 2005; Bailey *et al.*, 2011; Suri & Vaidya, 2013), physical activity (Russo-Neustadt, Ha, Ramirez, & Kesslak, 2001; Stranahan, Zhou, Martin, & Maudsley, 2009), and an enriched environment (Altschuler, 1979; Faherty, Kerley, & Smeyne, 2003; Moser,

Trommald, Egeland, & Andersen, 1997) have all been linked to alterations of spine numbers in the hippocampus.

In contrast to the dendritic spine, very little is known about the presynaptic side of the synapse. A small number of studies mention the increase of multiple spine boutons (Toni *et al.*, 1999; Geinisman *et al.*, 2001; Medvedev *et al.*, 2014) and highly motile filopodia-like protrusions (Tashiro *et al.*, 2003) as presynaptic contributors to the structural remodeling and dynamics of stimulated synapses but most attention has focused on alterations to the postsynaptic spine.

Notwithstanding how a variety of manipulations seem to have an effect on synapse turnover, reservations remain regarding the degree, importance, and necessity of addition and elimination of boutons and spines in synaptic plasticity in the mature hippocampus. The existing discrepancies between the reported changes in spine density following learning and synaptic plasticity inducing protocols, evident from this overview, might be partially attributable to a non-uniform timeline of investigation, different induction protocols, age of the animals, specific hippocampal areas, and imaging techniques used.

1.3.2 Alteration of existing synapses

Correlating morphological changes of already-existing boutons and spines with synaptic plasticity has been an intriguing yet highly controversial topic of the last few decades. Research groups have found everything from synapse enlargement (Matsuzaki,

Honkura, Ellis-Davies, & Kasai, 2004) to shrinkage (Zhou, Homma, & Poo, 2004), and transient expansions (Lang et al., 2004) to no structural change at all (Sorra & Harris, 1998) of the synapses undergoing LTP or LTD. The following section will review evidence for and against structural changes of existing dendritic spines and boutons undergoing LTP and LTD.

1.3.2.1 Postsynaptic structural changes in LTP

Early research on structural plasticity used EM to explore potential morphological changes associated with LTP. Eva Fifkova's lab investigated the effects of tetanus on DG granule cells in mice with rapid-freeze EM and found an immediate and long-lasting increase in spine size, where changes were visible within two minutes post-stimulus and lasted for at least one hour (Van Harreveld & Fifkova, 1975). They showed, moreover, that spine swelling was accompanied by a 30 % spine neck shortening and a 40 % increase in neck width (Fifkova & Anderson, 1981). A major flaw to these studies was however the lack of proof that in fact LTP was elicited in these preparations.

Similarly to Fifkova and her colleagues, Desmond and Levy reported an increase in the density of concave/large spines, a concomitant decrease in nonconcave spines, an increase in shaft synapses and an increase in the mean PSD length after LTP (Desmond & Levy, 1983, 1986). These studies did confirm potentiation electrophysiologically but still could not identify whether potentiation affected imaged spines.

In sharp contrast to the findings of Fifkova and Desmond, *in vivo* (Deadwyler *et al.*, 1979) and *in vitro* (Lee, Oliver, Schottler, Creager, & Lynch, 1979) studies by the Lynch group found no structural changes of the dendritic spines in CA1 cells after HFS. Their EM studies showed no change in the density of synapses, however, the incidence of shaft synapses was increased by 33 %. Other than this increase in the number of shaft synapses, they found no significant change in the mean size of the following parameters: area of synaptic boutons contacting spines or shafts, area of spines, width of spine neck, length of PSD, or density of perforated synapses (Lee et al., 1980).

In agreement with Lynch, Chang and Greenough reported no changes in the area of the spine head or bouton, PSD length, neck width, or even the length or number of presynaptic vesicles in area CA1 of the *in vitro* hippocampal slice after HFS (Chang & Greenough, 1984). They did however find an increase in the density of stubby and shaft synapses, but importantly not in the total number of spines or the incidence of perforated synapses.

EM serial reconstruction studies by the Andersen lab were in favour of changing numbers and shapes of the synapses after LTP induction in the DG, with initial reports of 50 % increase in spine density, along with increased numbers of bifurcated spines, and changes of the spine neck dimensions (Trommald *et al.*, 1990). Later, however, they reported a more moderate (30 %) increase in spine numbers and no structural changes of the existing dendritic spines were observed (Trommald *et al.*, 1996).

Similarly, tetanus induction in CA1 of mature rats, revealed by serial EM showed no change in a number of properties, such as synapse density, shaft synapse density, distribution of synapse types (e.g., thin, mushroom, stubby), PSD type (macular,

perforated, segmented), PSD length, or single or MSBs (Sorra & Harris, 1998). A high degree of variability of synapse density between different braches of the same cell, between cells and animals was however reported here and also in the Andersen studies, which makes interpretation of the results rather difficult even with increased sample sizes. In addition, the above mentioned EM studies come with other serious limitations: (i) without a marker for potentiated spines it is impossible to confirm whether potentiation was achieved at specific spines, (ii) controls are demonstrated in different preparations, (iii) impossible to image at multiple time points, (iv) cannot distinguish between changes in existing spines and a substitution of *de novo* spines or (v) a possible balancing between an increase in potentiated spine size and a decrease in unpotentiated spine size, and (vi) potential artifacts of tissue preparation methods. Therefore caution has to be taken with the interpretation of these results.

The introduction of longitudinal studies was a great improvement. Repeated imaging of live CA1 cells of acute hippocampal slices showed that cLTP did not alter spine density or spine length, but increased the number of a subpopulation of medium length spines and lower that of the smaller spines. In addition, the authors reported an increase of spine reorientation in slices that underwent potentiation when compared to control (Hosokawa *et al.*, 1995).

The majority of reports referenced above used distinct time points to compare synapse structure and size in LTP or LTD but were unable to show the existence or lack of changes in a longitudinal study. Two-photon time-lapse imaging studies aim to do just that. One of the earliest of such studies in the rat hippocampal slice showed that tetanization in area CA1 led to an NMDAR–dependent spinogenesis and growth of

existing protrusions 40 minutes post-stimulus (Maletic-Savatic *et al.*, 1999). Approximately a third of the new filopodia turned into bulbous dendritic spines after one hour and the net growth reached baseline levels after 45 minutes (Maletic-Savatic *et al.*, 1999). However, the authors used developing hippocampal slices in which filopodia outgrowth is much more prominent than in the adult brain (Fiala *et al.*, 1998), did not confirm that LTP was achieved, had limited z-axis access so only laterally projecting filopodias could be detected, and by placing the stimulating electrode adjacent to the dendritic spines overstimulation, direct depolarization of the membrane likely occurred. In addition, the rapid onset of LTP cannot be explained by the growth of the filopodia at a much delayed time point.

Two-photon imaging of acute hippocampal slices of adult mice showed a transient enlargement of a small subpopulation of spines with a fast, 30 seconds onset, maximal effect at one to two minutes and a return to baseline levels at 10 to 20 minutes after tetanic stimulation. Besides this effect they found no evidence for spinogenesis, or filopodia outgrowth (Lang *et al.*, 2004).

The first 3D EM reconstruction from *in vivo* studies noted no change in the total number of synapses, but found that shaft and stubby spines developed into thin dendritic spines, and that the volume and area of mushroom spines significantly increased at six hours post tetanus (Popov *et al.*, 2004). They also found an increase in macular and perforated PSDs.

Two consecutive cLTP studies in 2005 and 2006 had rather different outcomes. EM and confocal studies on CA1 area in mice showed a decrease in the number of macular PSDs but an increase in perforated and complex PSDs (Stewart *et al.*, 2005).

They did not find, however, an increase in volume of either mushroom or thin spines. In contrast, cLTP in organotypic hippocampal slices imaged with time-lapse two-photon microscopy showed quick spine enlargement post-LTP pairing protocol (Kopec *et al.*, 2006). In addition they provided evidence for GluR1 AMPAR incorporation at the synapse, accompanied by a small decrease of NR2B NMDAR.

In 2004 Matsuzaki's paper received a lot of attention as it was the first of its kind showing simultaneous structural and functional plasticity measurements of a particular spine undergoing plasticity (Matsuzaki *et al.*, 2004). By using two-photon MNI-glutamate uncaging in CA1 area of rat hippocampal slice preparations, they showed a fast, large, and selective enlargement of stimulated spines. This growth was accompanied by an increase in AMPAR currents, and was NMDAR-, CaMKII-, calmodulin-, and actin polymerization-dependent. Spine enlargement began with a 10 to 60 second onset and a peak around one to five minutes. Interestingly though it was only persistent in small spines (but see Yang, Wang, Frerking, & Zhou, 2008), lasting over 100 minutes, whereas larger mushroom spines only exhibited a transient enlargement, and no new spines were detected. Since the original paper, many other studies have showed how glutamate uncaging leads to rapid spine enlargement (Harvey & Svoboda, 2007; Tanaka *et al.*, 2008; Govindarajan *et al.*, 2011; Bosch *et al.*, 2014; Meyer *et al.*, 2014; Oh *et al.*, 2015). However, uncaged glutamate can activate glutamate receptors at a distance of up to ~1 μm (Matsuzaki *et al.*, 2001), a distance much greater than the size of the PSD, with an average size of 0.008 - 0.54 μm^2 in CA1 (Harris & Stevens, 1989), or the 250 nm diameter of synaptic "hotspots" opposite of vesicle release where most channels are activated during vesicular glutamate release (Raghavachari & Lisman, 2004). Thereby

uncaged glutamate will most likely affect extrasynaptic receptors on the spine, presynaptic receptors, other spines or even other neighboring cells (Rusakov & Kullmann, 1998). In fact, Matsuzaki reported that 9 % of neighboring spines also enlarged without direct stimulation, located at a mean distance of 1.2 μm (Matsuzaki *et al.*, 2004). In addition these experiments were carried out in juveniles where silent synapses are more abundant than in adults (Durand *et al.*, 1996). In fact, in their earlier paper they demonstrate how small, thin spines often lack AMPARs (Matsuzaki *et al.*, 2001), therefore unsilencing may be attributable to the enlargement and plasticity of these spines. In conclusion, it is arguable that these glutamate uncaging studies report a combination of developmental phenomenon and overstimulation rather than a direct link between structural and functional plasticity in mature cells. Furthermore, they completely exclude the presynaptic terminal from the equation.

Using the supposedly more physiological potentiation protocol, TBS, Bourne and Harris noted no change regarding the size of the spines (Bourne & Harris, 2011). In contrast others have found spine swelling with this protocol (Yang *et al.*, 2008) which was apparent at five hours but was reversed by 24 hours post-stimulus (De Roo *et al.*, 2008).

This review shows how literature on postsynaptic structural remodeling is extensive but far from conclusive. The emerging picture is however that EM studies in general report an increase in the size of certain subpopulation of spines rather than an increase in spine density and that time-lapse imaging of two-photon uncaging experiments show a rapid and extensive enlargement of stimulated spines. However,

interpretation of both of these methods are difficult and confounded for reasons mentioned above. New methods are required for further clarification.

1.3.2.2 Presynaptic structural remodeling in LTP

The literature on presynaptic structural remodeling is far less extensive than that on postsynaptic changes. One study using EM and confocal imaging in organotypic hippocampal slices with DiI-labeled neurons showed that TBS leads to an increase in presynaptic protrusions and a remodeling of the presynaptic varicosities (Nikonenko *et al.*, 2003). These small filopodia were visible by five minutes, reached their maximum growth at 20 minutes and often disappeared after 60 minutes. However, some made contact with either dendritic shafts or spines around 30 minutes, and initiated spinogenesis. The presynaptic remodeling was shown to be NMDAR activation and NO-dependent. Serial section EM also revealed that the number of docked vesicles dropped by 30 minutes and even more by two hours post TBS (Bourne *et al.*, 2013). There was also an apparent decrease in presynaptic bouton densities by two hours. Both the decrease in presynaptic vesicles and bouton numbers seemed to depend on NMDAR activation as application of the receptor antagonist, APV, during TBS stimulation prevented both of these changes (Bourne *et al.*, 2013).

In recent findings two-photon glutamate uncaging led to not only spine enlargement but also to bouton swelling at one to three hours after potentiation (Meyer *et al.*, 2014). The spine and bouton growth showed correlated enlargement in stabilized

synapses and returned to baseline levels in unstabilized synapses. In alignment with this and their 2014 findings Bourne and Harris proposed a "conversion hypothesis" showing that LTP induced by TBS results in spine and PSD enlargement, which is mirrored by the AZ (Bell *et al.*, 2014). This growth could be attributed to the dense core vesicles (DCV) adding presynaptic scaffolding and adhesion molecules to the presynapse, and recruiting vesicles to nascent zones (Ahmari *et al.*, 2000; Shipman & Nicoll, 2012; Bell *et al.*, 2014). They propose that by this recruit existing nascent zones can convert to active zones, a process which may correspond to unsilencing functionally inactive regions. However, DCV were only present in a fraction of synapses indicating that this mechanism might only affect a subpopulation of (silent) synapses. It is most likely that structural and functional LTP mechanisms at these sites differ from LTP at mature, nonsilent synapses (Macdougall & Fine, 2013).

1.3.2.3 Pre- and postsynaptic structural remodeling in LTD

Compared to morphological changes in LTP, LTD appears to have received less attention. Nevertheless, some evidence has been presented. For example, a study on acute hippocampal slices from rats used two-photon time-lapse imaging to investigate the possible relationship between LFS and spine remodeling (Zhou et al., 2004). Their results indicated that LFS leads to a gradual reduction in spine head size, which was reversible with a consequent HFS, was NMDA-, calcineurin- and cofilin-dependent, but unlike

LTD, not protein phosphatase-dependent (Zhou et al., 2004). Therefore, LTD and spine shrinkage are arguably governed by, at least in part, divergent molecular mechanisms.

Another paper from the same year also found that LFS leads to spine shrinkage, or even disappearance, which was positively correlated with a shift of the globular (G)-actin/filamentous (F)-actin equilibrium towards an increase in G-actin (Okamoto *et al.*, 2004). In agreement with this, Oh also reported that LFS via glutamate uncaging at CA1 pyramidal cells produces LTD and spine shrinkage, rather than spine loss (Oh *et al.*, 2013). The changes due to subsequent uncaging proved to be saturable, reversible, and were NMDAR-dependent. In contrast to small spines, shrinkage of large-sized spines also was mGluRI and IP3R activation-dependent.

A more recent study showed that LFS via glutamate uncaging results in spine shrinkage even when calcium flow is blocked through the NMDARs by the antagonist 7CK (Stein *et al.*, 2015). Shrinkage was found to be a consequence of glutamate binding to the receptor and p38MAPK activity but not ionotropic functions of the NMDARs.

LFS was showed to result in a decrease in the co-localization of pre- and postsynaptic structures, therefore indicating synapse loss (Bastrikova *et al.*, 2008). The loss of synapses though was more of a separation of the pre- and postsynaptic compartments rather than spine elimination, which was never observed. However, shrinkage of spine size was noted, but there was no correlation between shrinkage and synapse separation. The degree of synapse loss was rather associated with greater LTD, and smaller spines were also more likely to separate from the bouton.

A recent study used low frequency optogenetic stimulation (oLFS) of the Schaffer collaterals in combination with postsynaptic calcium imaging and observed strong LTD

but no shrinkage of dendritic spines in CA1 cells (Wiegert & Oertner, 2013). However, oLFS did increase the incidence of a delayed spine elimination of a specific subgroup of depressed spines. Spines with initially high release probability were less likely to be eliminated. This spine elimination was not a gradual shrinkage but rather a quick loss, as at the very last time point before spine loss, the volume of the spines was *en par* with that of the average spines.

The aforementioned examples demonstrate the profound contradictions that exist in the field of structural plasticity of hippocampal synapses, spanning a spectrum from total absence of any detectable changes to radical and immediate changes in synapse structure. Nonetheless, a brief overview of the proposed mechanisms by which reorganization of the synapse structure might be possible is offered to the reader next.

1.3.3 Molecular processes of structural plasticity

Similarly to NMDAR-dependent LTP and LTD, structural plasticity of the synapse also requires the activation of NMDARs and subsequent Ca^{2+} inflow, the activation of small GTPases, and actin polymerization (Sala & Segal, 2014) but see (Stein *et al.*, 2015). The reader is offered a brief overview of how some of these key molecules might play a part in structural reorganization of the synapse.

Actin is a key cytoskeletal protein in the dendritic spines. Actin molecules are constantly undergoing a process referred to as “treadmilling” in which polymerization of

G-actin happens at the barbed end and depolymerization of F-actin at the pointed end of the actin filament. The turnover rate for dynamic pools of actin is around one to two minutes whereas it is approximately 17 minutes for stable actin pools (Star *et al.*, 2002; Honkura *et al.*, 2008). The equilibrium between G- and F-actin has major implications of spine structure and dynamics, and its reorganization could account for enlargement or alternatively shrinkage of the synaptic structures (Fischer *et al.*, 1998; Dunaevsky *et al.*, 1999; Okamoto *et al.*, 2004). It has been shown that LTP promotes an accumulation of F-actin and a concomitant decrease in G-actin, a decrease in actin motility and a subsequent spine stabilization, potentially of the increased spine head volume (Fischer *et al.*, 1998; Matus, 2000; Fukazawa *et al.*, 2003; Okamoto *et al.*, 2004). In addition, inhibiting actin polymerization blocks LTP (Krucker *et al.*, 2000). Actin polymerization can also be regulated by NMDAR activation, which when inhibited, causes the blocking of LTP and actin polymerization (Maletic-Savatic *et al.*, 1999; Star *et al.*, 2002; Lamprecht & LeDoux, 2004). LTD on the other hand promotes actin depolymerization (Okamoto *et al.*, 2004; Honkura *et al.*, 2008).

A number of molecules, e.g., small GTPases, profilin, cofilin, N-catenin, drebrin, synaptopodin, have all been implicated to play a role in actin reorganization, affecting the motility or stabilization of the dendritic spine (Abe, Chisaka, Van Roy, & Takeichi, 2004; Ackermann & Matus, 2003; Biou, Brinkhaus, Malenka, & Matus, 2008; Gu *et al.*, 2010; Murakoshi, Wang, & Yasuda, 2011). For example actin-binding protein Arp 2/3 is associated with spine enlargement after LTP induction and *de novo* actin polymerization (Kim et al., 2013; Korobova & Svitkina, 2010; Rocca, Martin, Jenkins, & Hanley, 2008). Profilin and N-catenin accumulate rapidly in dendritic spines after activity-induced Ca^{2+}

increase, and promote spine stability by reducing actin dynamics (Ackermann & Matus, 2003; Abe *et al.*, 2004). Similarly, drebrin and synaptopodin aid spine stabilization after LTP induction (Biou *et al.*, 2008; Zhang *et al.*, 2013). Cofilin content increases fast in the dendritic spine following plasticity, and influence actin polymerization (Bosch et al., 2014; Gu et al., 2010). The phosphorylated form of cofilin promotes less actin severing, and the un-phosphorylated cofilin promotes more actin severing (Calabrese *et al.*, 2014). The balance between the two forms of cofilin is regulated by LIM, and slingshot protein phosphatase (SSH), where cofilin inactivation supports the stabilization of actin cytoskeleton (Calabrese *et al.*, 2014). Small GTPases (Ras, Rho, Cdc42, Rac) can regulate structural plasticity and actin polymerization through downstream effectors, and are believed to mediate the effects of neurotransmitters and adhesion molecules (Lamprecht & LeDoux, 2004; Biou *et al.*, 2008; Murakoshi *et al.*, 2011; Zhou *et al.*, 2012). The activation of small GTPases can also lead to the activation of actin-binding proteins, like cofilin (Nishiyama & Yasuda, 2015).

CaMKII has been shown to be necessary for LTP induction (Lisman, Yasuda, & Raghavachari, 2012; Malenka et al., 1989; Malinow, Schulman, & Tsien, 1989) and for activity-driven spine growth (Yamagata *et al.*, 2009; Bosch & Hayashi, 2012; Chang *et al.*, 2017). When activated, CaMKII translocates to the PSD and can phosphorylate several proteins, including PSD-95 and stargazin, leading to PSD disassembly and AMPAR insertion in the PSD (Shen & Meyer, 1999; Hayashi *et al.*, 2000; Dosemeci *et al.*, 2001; Tomita *et al.*, 2005; Steiner *et al.*, 2008). Furthermore, CaMKII may destabilize actin filaments directly and allow for reorganization and later polymerization (Okamoto *et al.*, 2007). CaMKII also phosphorylates AMPARs, promoting an increase in

AMPAR externalization, AMPAR conductance, and synaptic efficacy (Barria, Muller, Derkach, Griffith, & Soderling, 1997; Benke, Luthi, Isaac, & Collingridge, 1998; Derkach, Barria, & Soderling, 1999; Lisman et al., 2012; but see Hosokawa *et al.*, 2015).

Both NMDARs and AMPARs interact with PSD scaffolding proteins through their C-termini. Meyer and colleagues showed that although LTP was immediately followed by spine enlargement, the PSD scaffolding molecules Homer1c and PSD-95 both increased with a delay of 20 minutes and 3 hours, respectively, and that a correlated enlargement of the presynaptic bouton displayed a one to three hour delay (Meyer *et al.*, 2014). On the contrary, following LTD induction, the size of the PSD decreases with no significant time delay, and PSD-95 loss is not required for the spine head shrinkage (Woods *et al.*, 2011). PSD-95 forms a complex with NMDARs and help to stabilize new spines, but it is not necessary for NMDAR localization (Kornau *et al.*, 1995; Niethammer *et al.*, 1996; Passafaro *et al.*, 1999; Wenthold *et al.*, 2003; Ehrlich *et al.*, 2007). Shank can also bind to NMDARs and to Homer, and the two of them promote spine enlargement (Naisbitt *et al.*, 1999; Sala *et al.*, 2001).

It has been proposed that the increased membrane surface of an enlarged spine might be accounted for from exocytosis, which is also an important avenue of AMPAR insertion (Park *et al.*, 2004, 2006; Kennedy *et al.*, 2010; Murakoshi & Yasuda, 2012). In fact, AMPAR numbers increase on the same time scale and in proportion with the spine head enlargement (Kopec *et al.*, 2006; Patterson *et al.*, 2010). Lateral diffusion of AMPARs is, however, the major source of AMPAR increase in the PSD after LTP induction (Borgdorff & Choquet, 2002; Makino & Malinow, 2009) and the trapping of AMPARs in the PSD is CaMKII-dependent (Opazo *et al.*, 2010).

Finally, adhesion molecules have been also implicated to play roles in structural and functional plasticity. Namely, N-cadherin has been implicated to couple structural and functional changes at the synapse during LTP but not affect LTD, baseline morphology or baseline function of mature CA1 synapses (Bozdagi *et al.*, 2010). It has also been shown in cultured hippocampal neurons that N-cadherin can directly bind to the GluR2 subunit of AMPARs and help recruit them to the membrane surface. N-cadherin immobilization also reduces lateral diffusion of GluR2 (Saglietti *et al.*, 2007). Through α- and β-catenin N-cadherin additionally interacts with F-actin which may be an avenue for potentially mediating structural changes (Ozawa *et al.*, 1990; Hirano *et al.*, 1992; Murase *et al.*, 2002). Besides cadherins, various members of the cell adhesion molecule family have been previously implicated in plasticity, stabilization and morphological remodeling of the synapse (Fazeli *et al.*, 1994; Lüthl *et al.*, 1994; Cremer *et al.*, 1998; Stäubli *et al.*, 1998; Henkemeyer *et al.*, 2003; Dityatev *et al.*, 2008; Blundell *et al.*, 2010). Cell adhesion molecules could also fulfill the role of coordinating pre- and postsynaptic structural and molecular plasticity.

The electron dense protein network of the presynaptic active zone aligns with the postsynaptic density, and is enriched, amongst many, in RIM (Rab3-interacting molecule), RIM-BP (RIM-binding protein) Munc13, ELKs, α-liprin, bassoon and piccolo (Lazarevic *et al.*, 2011; Südhof, 2012; Davydova *et al.*, 2014). These molecules interact with each other, and orchestrate vesicle release by associating with synaptic vesicles and Ca^{2+} channels as well as potentially playing a part in regulating synaptic efficacy and structural changes of the presynapse (Michel *et al.*, 2015).

Structural plasticity affecting the presynaptic bouton remains enigmatic. Nonetheless, it is suggested that the remodeling of the AZ is assisted by the ubiquitin-proteasome system (UPS) by regulating the amount of Munc-13 and RIM, for example (Bruckner *et al.*, 2015). Munc-13 in turn, however, has been proposed to promote elongation of the bouton in LTP (Zhao *et al.*, 2012). The structure of the bouton can also be altered by TBS which can significantly reduce the number of docked vesicles, followed by a greater reduction in the vesicle pool at later time points (Bourne *et al.*, 2013). Dense core vesicles (DCV), transporting scaffolding proteins, have been shown to be inserted at nascent zones and convert previously silent nascent zones to active zones and have also been proposed as means for an increase in bouton size during LTP (Bell *et al.*, 2014).

1.4 Summary of LTP/LTD/learning and structural plasticity

Similarly to the long-standing debate of the location of LTP expression, structural plasticity has fueled countless debates. However, several lines of evidence and theories have been put forward from which the following "postivist" (Macdougall & Fine, 2013) model arises: LTP induction at excitatory synapses is generally agreed upon to be of a postsynaptic nature as it requires Ca^{2+} influx into the dendritic spine through NMDARs, and a consequent CaMKII activation (Bliss & Collingridge, 2013). According to the postivists, LTP expression is also postsynaptic as it involves AMPAR exocytosis, lateral diffusion, and trapping at the PSD (Malinow & Malenka, 2002). This addition of AMPARs is believed to account for the increased synaptic efficacy as well as an increase

in the dendritic spine size, along with exocytosis and molecular reorganization of the spine head, including actin polymerization (Harvey *et al.*, 2008; Lee *et al.*, 2009; Makino & Malinow, 2009; Patterson *et al.*, 2010; Murakoshi *et al.*, 2011; Lisman *et al.*, 2012; Murakoshi & Yasuda, 2012). Conversely, in LTD, it is believed that NMDAR activation leads to a moderate but long-lasting increase in intracellular calcium levels, which through calcineurin and PP1 leads to LTD (Collingridge *et al.*, 2010). It is also believed that consecutive spine shrinkage is mediated by cofilin (Calabrese et al., 2014; Zhou et al., 2004). These changes in LTP and LTD are then mirrored by the presynaptic bouton (Meyer *et al.*, 2014). A postivist summary of structural changes in LTP and LTD as well as a timeline of the synchronous steps leading to these changes in LTP and synapse growth are presented in Figures 1.5 and 1.6.

Despite the vast support of a postivist approach, "preists" offer compelling evidence and a different framework for LTP/LTD expression, in which presynaptic events, such as an increase or decrease in release probability can account for LTP or LTD, respectively (Macdougall & Fine, 2013). In addition, countless examples were put forward that question not only the relationship between witnessed structural plasticity and LTP or LTD, but the importance and even existence of such changes.

Notably, Holderith *et al*. showed how despite previous correlation studies the bouton volume seemed to be a poor predictor of the opposing dendritic spine volume of hippocampal pyramidal cells (Holderith *et al.*, 2012). Another interesting study by Dhanrajan aimed to control for the possible role of the stimulating protocols and not LTP's effect *per se* on morphological changes by using aged rats and dividing them up in groups where animals could sustain LTP and where the animals could not (Dhanrajan *et*

al., 2004). They showed that LTP leads to an increase in perforated PSDs, however, HFS alone will increase the number of branched spines without necessarily inducing LTP, as was demonstrated by the group where the rats could not sustain LTP.

Further evidence for partially different induction or signaling pathways for LTD and spine shrinkage were recently added to the literature (Bastrikova et al., 2008; Wang, Yang, & Zhou, 2007; Wiegert & Oertner, 2013). Wang and colleagues showed that LFS in acute hippocampal slices causes LTD, and a decrease in spine head diameter and fluorescence intensity (Wang et al., 2007). However, when they blocked spine shrinkage LTD expression was not affected, and similarly, when LTD was inhibited LFS could still reduce the size of spine heads. Furthermore, trafficking of NMDAR or AMPAR did not lead to changes in spine size, but by inhibiting actin polymerization, both LTD and spine shrinkage was abolished.

As it is evident from this review on structural plasticity in the rat hippocampus, an encompassing theory has not been formed, as the whole spectrum of changes in synapse structure from non-existing to immediate and robust have been reported. Although many point to a simultaneous occurrence of plasticity induction and changes in synapse size, the physiological relevance of the outcomes by the majority of these studies are questionable, as often are the interpretability of the results obtained by the traditional and indirect methods. Innovative and perhaps a multifaceted approach to these questions are necessary.

1.5 Comparison of methods for the investigation of neural behaviour

1.5.1 Electrophysiological vs. optical methods

Neuronal signal integration and communication is based on electrical signals, i.e., ionic current flow across the plasma membrane and resulting changes in membrane potential. Electrophysiological methods are the most common way to measure neuronal signaling activity, mainly because recording via intra- or extracellular electrodes from neurons provide high temporal resolution (tens of μs) of small electrical changes (μV-mV, pA-nA). In addition, it is possible to record electrically not just action potentials but also graded inhibitory and sub-threshold excitatory potentials. On the other hand, this method offers relatively low spatial resolution, as recordings only report electrical changes in close proximity to the recording electrode tip. Here, detectable signals have already been modified and integrated to various extent during their passage from their point of origin. True measurements of subtle voltage changes happening at the location of the main excitatory inputs (e.g. the dendritic spines) or at axon terminals are impossible to measure directly via electrodes, simply because of the small size of those structures. Another limitation of electrophysiology is its restriction to monitor very few identifiable neurons within a network. To be able to study multiple neurons and their interactions, electrophysiology is not ideal.

For multiple reasons, optical methods that use extrinsic small-molecule probes, genetically encoded fluorescent proteins, or optogenetics for imaging neuronal activity are becoming increasingly important. Optical tools are relatively non-invasive and they allow us to acquire data over an extended period of time from large groups of

individually identifiable neurons, making them ideal candidates for circuit analysis studies. Although they do not always give us a detailed readout of sub-threshold signals or inhibitory synaptic inputs, they can provide useful insight into local events such as synaptic transmission in dendritic spines.

1.5.2 Extrinsic small-molecule probes vs. genetically encoded probes

Two main approaches that have been used to image action potentials and synaptic activity in neurons are: indirectly by measurement with calcium indicators reporting changes in free intracellular [Ca^{2+}] due to the opening of calcium channels in response to membrane depolarization, or directly via voltage sensors. Importantly, to be able to monitor neuronal calcium signaling or membrane potential changes in a network of cells, or in subcellular compartments, genetically encoded voltage (GEVI) and calcium indicators (GECI) have great advantages over extrinsic small-molecule probes despite the latter's generally superior brightness, signal to noise ratio, multicolour availability, dynamic range, and response kinetics. In particular, with GECIs and GEVIs one can target specific populations of neurons when sensors are expressed under the control of cell-type specific promoters (Bozza *et al.*, 2004), or subcellular targets (e.g. plasma membrane, ER, mitochondria, Golgi, nucleus) via expression of appropriate fusion proteins (Shigetomi *et al.*, 2010).

Imaging action potential firing and graded potentials during synaptic activity with calcium sensors or voltage sensors thus holds great promise for understanding neuronal networking, single neuron behaviour, and intracellular signalling activity within

subcellular compartments. These tools have become increasingly important as the last decade has seen great progress in the development of existing GECIs and GEVIs. Nonetheless, most of these indicators still produce only a small fluorescence change (particularly GEVIs), and provide suboptimal temporal resolution (particularly GECIs).

Electrical and optical recordings as well as extrinsic small-molecule probes and genetically encoded indicators were all applied in this thesis and are described in the following chapters as I present and contemplate on data acquired by a variety of alternative and multifaceted approaches to the study of neuronal activity, particularly synaptic plasticity in the rat hippocampus.

1.6 Thesis objectives

Synaptic plasticity and its cellular models, LTP and LTD, have been intriguing topics and supplied a steady flow of discussions over the last few decades. Despite this great interest many questions remain unresolved, such as whether structural changes represent a requisite step, an accompanying but autonomous step, or rather a stimulation artifact in synaptic plasticity?

The aim of my thesis was to investigate such phenomena by using novel approaches in cultured hippocampal rat brain slices. Therefore I set out to examine whether there are, under near physiological circumstances, any morphological changes to either the pre- or postsynaptic compartment of an active synapse undergoing plasticity?

In quest of facilitating such technical approaches I turned to the use of GECIs, as such sensors could eliminate the use of dye loading. Although the produced comprehensive evaluation of available GECIs for imaging neuronal activity in rats was valuable, it identified a clear need for GECIs with improved kinetics. Therefore, I next tested the newly designed fastest available GECIs, important for our purposes. These, however, were trading fast on- and off kinetics for smaller fluorescence signals. Notwithstanding the efforts of aiding my experiments by the use of GECIs, and providing a standardized comparison of such sensors in mammalian neurons for the scientific community, I identified that further improvements of GECIs were necessary. I, therefore, proceeded to investigate structural plasticity with the use of synthetic indicators with an alternative and more physiological approach of simultaneous imaging and

electrophysiological recording of a single synapse between nearby CA3 cells undergoing plasticity.

1.6.1 Specific aims of the thesis

1. **Quest for alternative imaging tools** – Comparison of genetically encoded calcium indicators for monitoring action potentials in mammalian brain by two-photon excitation fluorescence microscopy – Chapter 2
2. **Quest for GECIs with improved kinetics** - Design and mechanistic insight into ultrafast calcium indicators for monitoring intracellular calcium dynamics - Chapter 3
3. **Studying physiological and morphological changes of an active synapse undergoing plasticity** – Chapter 4
4. **Optimization of paired CA3-CA3 intracellular recordings** – Chapter 5

Collectively, I concluded that a standardized evaluation of the promising GECIs needed to be provided, which is presented in Chapter 2. The results indicated that most of these GECIs are too slow to follow individual action potentials at high frequencies. Furthermore, I showed that the advancement of fast GECIs trade the strong fluorescent signals for improved kinetics (Chapter 3), hence not being ideal without additional improvements for single action potential monitoring. I then presented a multifaceted approach to study structural plasticity, where our results suggest that physiological stimulations and plasticity induction do not cause immediate and robust changes in

synapse size (Chapter 4). Finally, I conducted a systematic evaluation of how particular recording variables contribute to the success of paired CA3-CA3 recordings of the rat hippocampus, and how optimizing these factors can aid our studies on structural plasticity, among others. An overall discussion is offered for the reader in Chapter 6.

Figure 1.1 Hippocampal anatomy and the Hippocampal Processing Loop. The hippocampus is a C-shaped structure located bilaterally and caudoventrally in the rat. The principal cells of the dentate gyrus (DG), CA1, CA2, and CA3 of the hippocampus are organized in layers and its predominantly unidirectional inputs are arranged in laminar ways. The hippocampal processing loop begins in the superficial layers of the entorhinal cortex (EC), which receives multimodal sensory information from the neocortex. From the EC the information reaches the granule cells of the DG via the Perforant Path (PP). The granule cell axons, forming the Mossy Fibers (MF), synapse onto CA3 pyramidal cells. In turn, CA3 projection axons, collectively referred to as Schaffer collaterals, target CA1 pyramidal cells. CA1 cell then project to the subiculum and the EC. Associational/commissural axons of CA3 cells forming recurrent synapses onto other CA3 cells are also depicted. Figure is reprinted by permission from Macmillan Publishers Ltd: Nature Reviews Neuroscience (Neves *et al.*, 2008). Reprint permission is found in Appendix A.

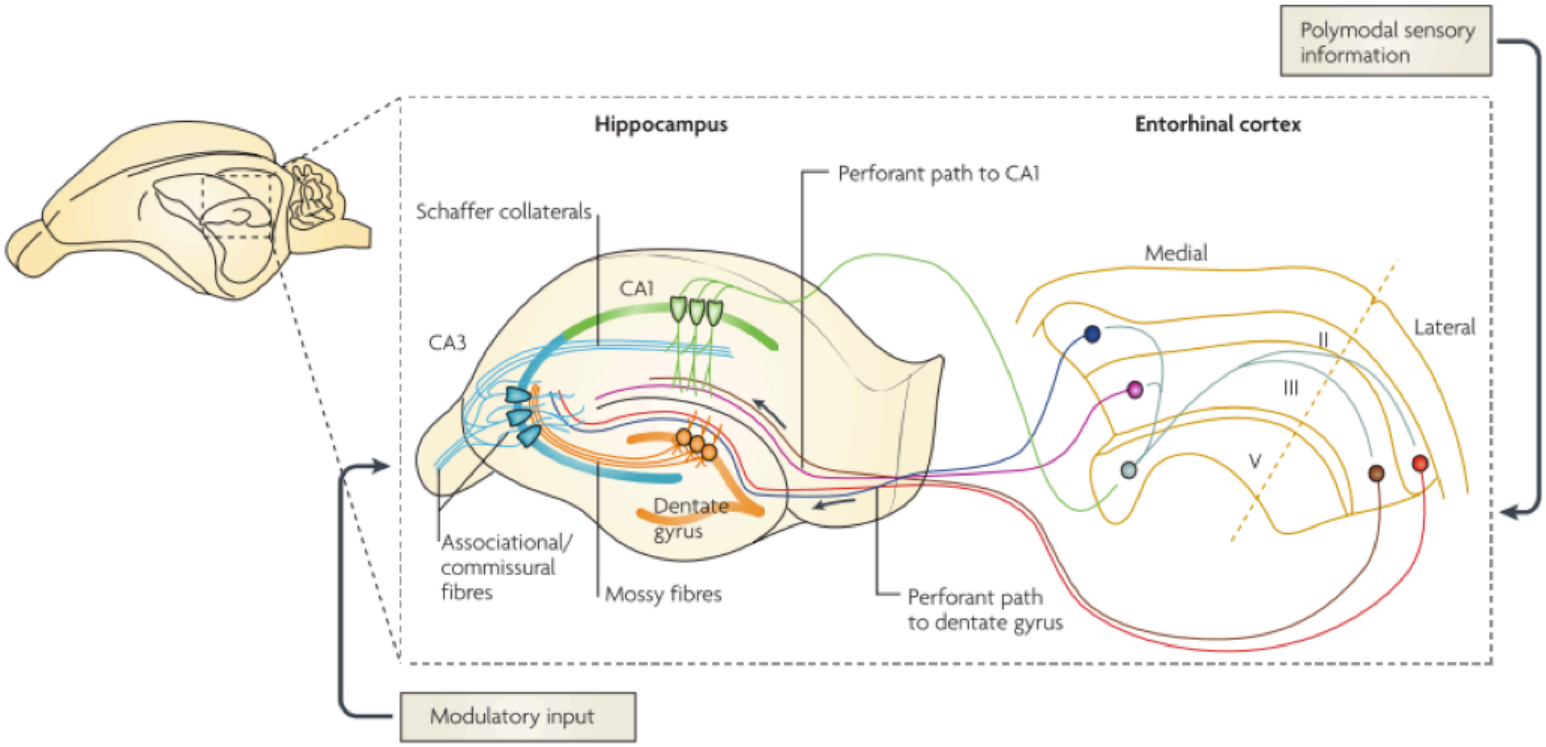

Figure 1.1 Hippocampal anatomy and the Hippocampal Processing Loop. Adapted with permission from (Neves *et al.*, 2008)

Figure 1.2 CA1 pyramidal cell adapted with permission from The Hippocampus Book, 2007 (Andersen *et al.*, 2007) Chapter 5 (Spruston & McBain, 2007). (**A**) Camera lucida drawing of a CA1 cell with cell body in stratum pyramidale, apical dendrites reaching stratum lacunosum-moleculare (s.l.m.) and basal dendrites in stratum oriens (s.o.). Major synaptic inputs and outputs are also depicted in panels A and B. Bar = 100 μm. (Source: adapted with permission from Bannister & Larkman, 1995) (**B**) Variety and density of a s.r. dendritic branch segment of a CA1 pyramidal cell from three angles. Bar = 1 μm. (Source: adapted from SynapseWeb, Kristen M. Harris, PI, https://synapseweb.clm.utexas.edu). Reprint permissions are found in Appendix A.

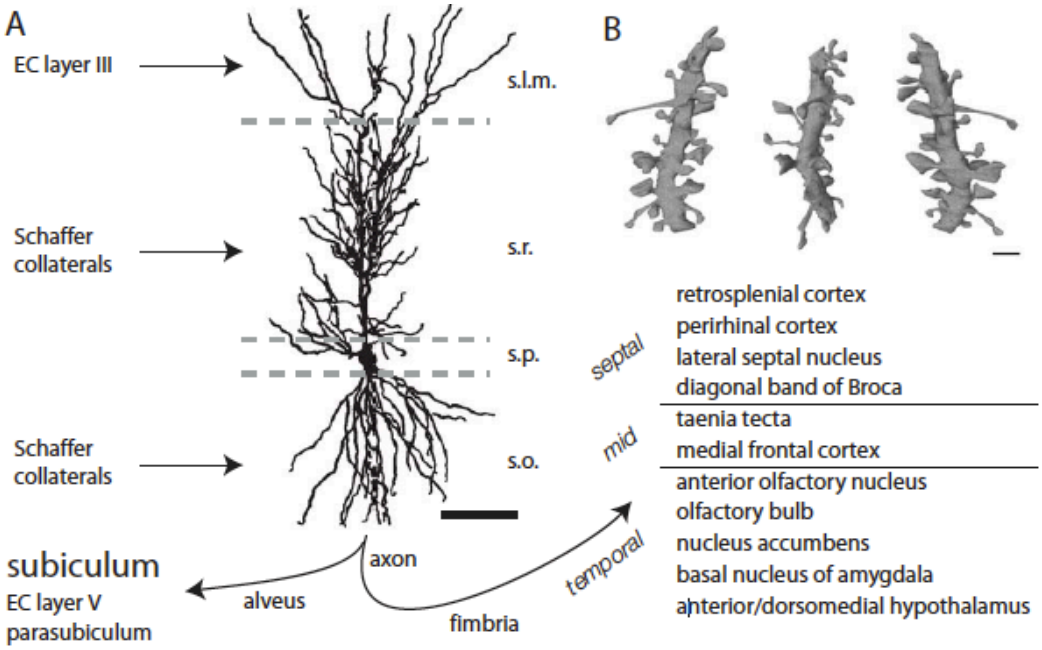

Figure 1.2 CA1 pyramidal cell adapted with permission from The Hippocampus Book, 2007 (Andersen *et al.*, 2007), Chapter 5 (Spruston & McBain, 2007).

Figure 1.3 CA3 pyramidal cell adapted with permission from The Hippocampus Book, 2007 (Andersen *et al.*, 2007). (**A**) Dendritic morphology, major synaptic inputs and outputs are shown in panel A. Bar = 50 μm. (Source: Adapted with permission from Gonzales, DeLeon Galvan, Rangel, & Claiborne, 2001) (**B**) The distribution of different spine types are varied and not associated with specific regions. The giant mossy fiber synapses, the thorny excrescences, are an exception, making contacts only on proximal basal and apical branches. Bar = 25 μm. (Source: Adapted with permission from Gonzales, DeLeon Galvan, Rangel, & Claiborne, 2001) (**C**) Three-dimensional reconstruction of a thorny excrescence, PSD are highlighted in white. Bar = 1 μm. (Source: Adapted with permission from Chicurel & Harris, 1992). Reprint permissions are found in Appendix A.

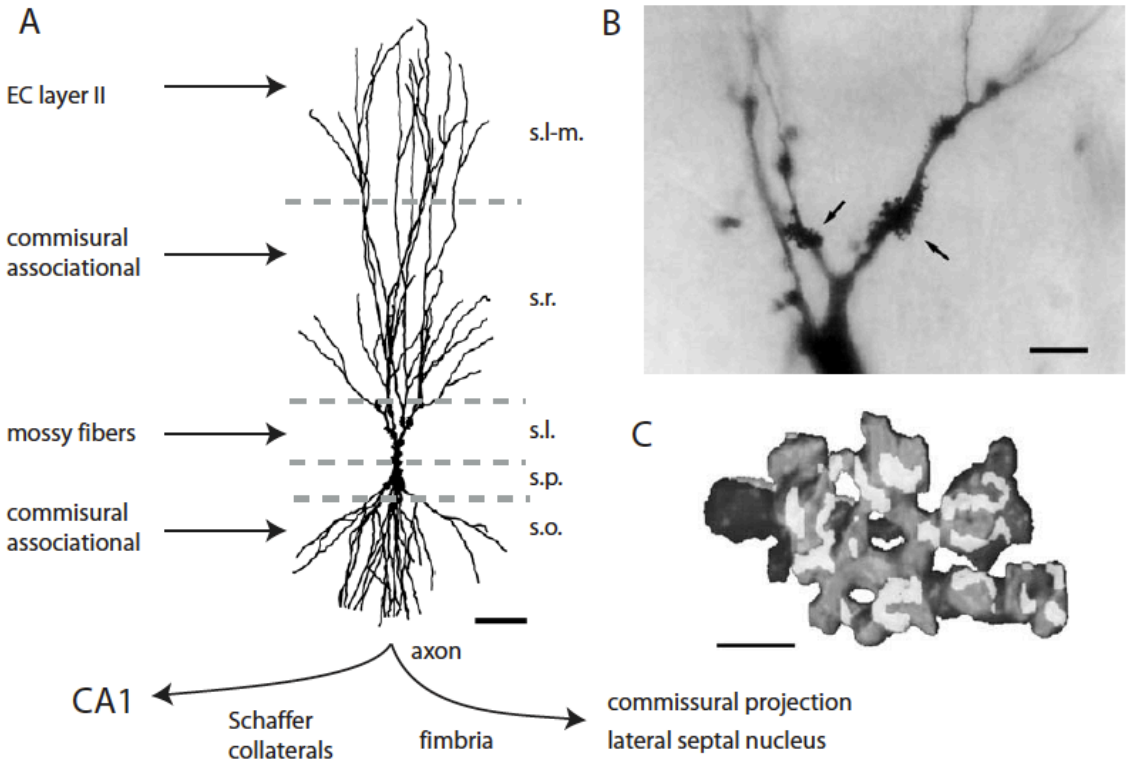

Figure 1.3 CA3 pyramidal cell adapted with permission from The Hippocampus Book, 2007 (Andersen *et al.*, 2007), Chapter 5 (Spruston & McBain, 2007).

Figure 1.4 Classical Spike Timing-Dependent Plasticity (STDP; adapted with permission from Feldman, 2012). **(A)** Pairing of pre- and postsynaptic spikes resulting in excitatory postsynaptic potential (EPSP) and back-propagating action potential, respectively, in the postsynaptic cell. **(B)** Repeated pre- before postsynaptic spiking drives long-term potentiation, whereas post- before presynaptic spiking drives long-term depression (adapted from Feldman, 2000). **(C)** Critical timing for the induction of STDP in cultured hippocampal neurons from Bi & Poo, 1998. Percentage of synaptic change before and after the pairing protocol are plotted against pre-post spike timing interval. Reprint permissions are found in Appendix A.

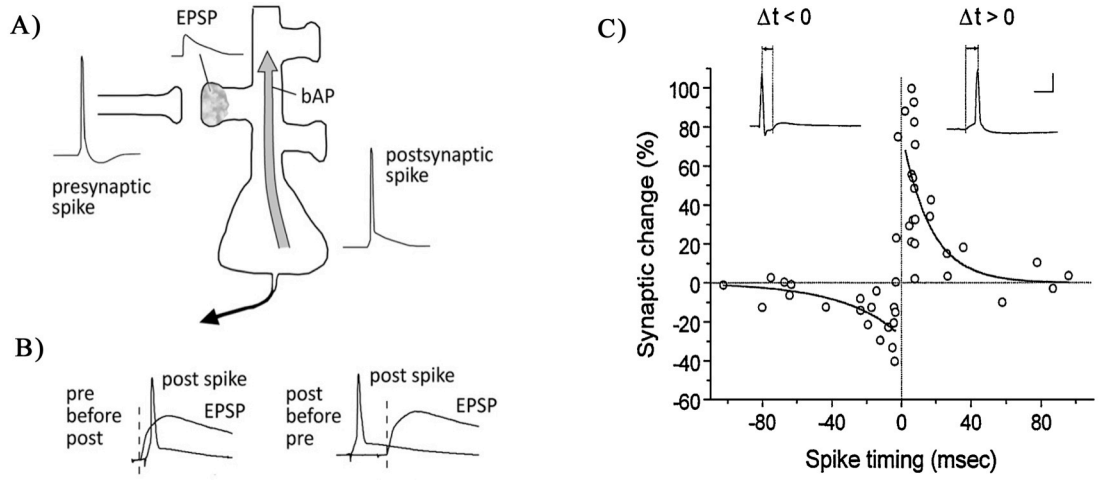

Figure 1.4 Classical Spike Timing-Dependent Plasticity (adapted with permission from Feldman, 2012).

Figure 1.5 Proposed structural and molecular reorganization of excitatory synapses in long-term potentiation (LTP) and long-term depression (LTD) (adapted with permission from Choquet & Triller, 2013). During LTP AMPA receptor numbers are suggested to increase by exocytosis, lateral diffusion, and synaptic trapping, and be responsible for enhanced synaptic strength as well as increase dendritic spine size but see (Enoki *et al.*, 2009; Macdougall & Fine, 2013). Opposing mechanisms during LTD such as AMPA receptor internalization, decreased synaptic strength, and spine shrinkage are presumed to evolve. Reprint permission is found in Appendix A.

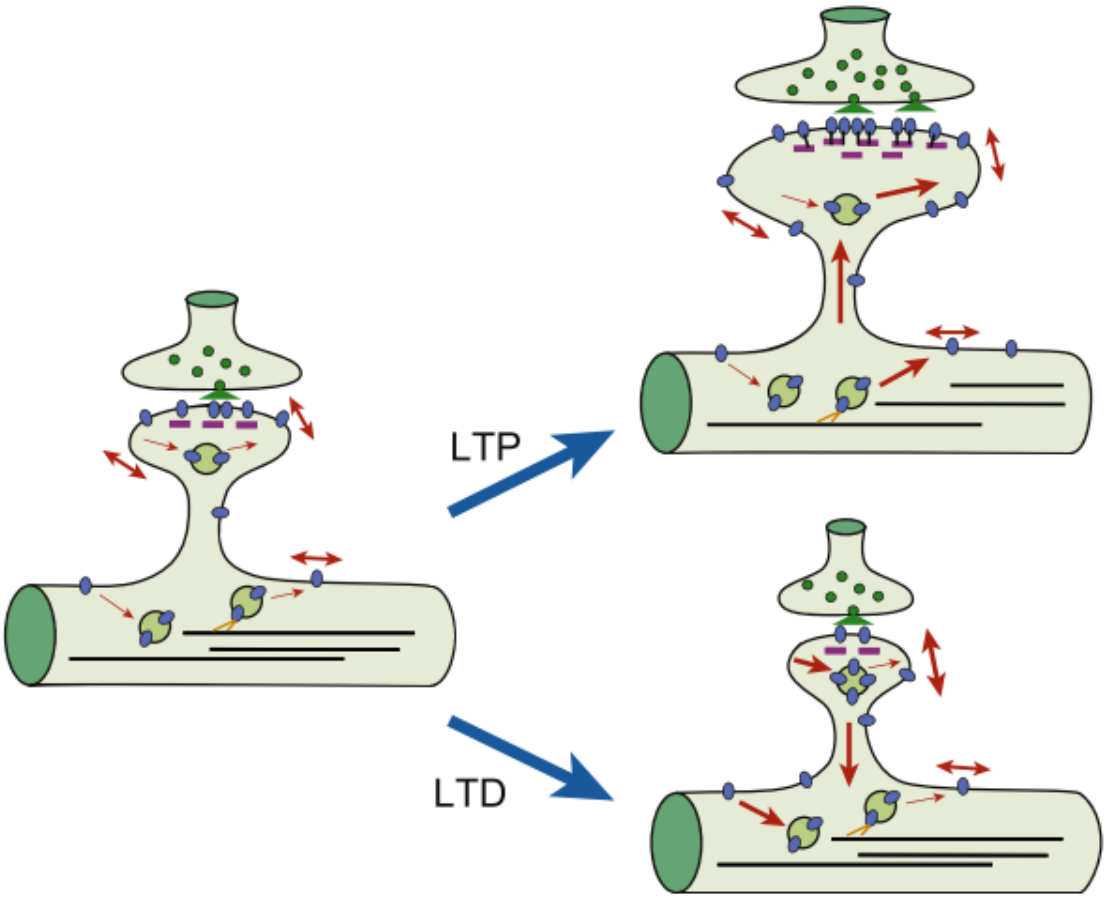

Figure 1.5 Proposed structural and molecular reorganization of excitatory synapses in long-term potentiation (LTP) and long-term depression (LTD) (adapted with permission from Choquet & Triller, 2013).

Figure 1.6 Proposed spatio-temporal regulation of structural and functional changes in glutamate uncaging-induced LTP (adapted with permission from Murakoshi & Yasuda, 2012). Calcium influx through the NMDAR activates CaMKII, which itself activates several targets including Cdc42, RhoA, HRas, stargazin, PSD-95. These lead to actin reorganization in the dendritic spine as well as AMPAR insertion in the postsynaptic membrane. Their combination is suggested to result in spine enlargement and LTP. White arrowhead indicates glutamate uncaging-stimulated spine. Reprint permission is found in Appendix A.

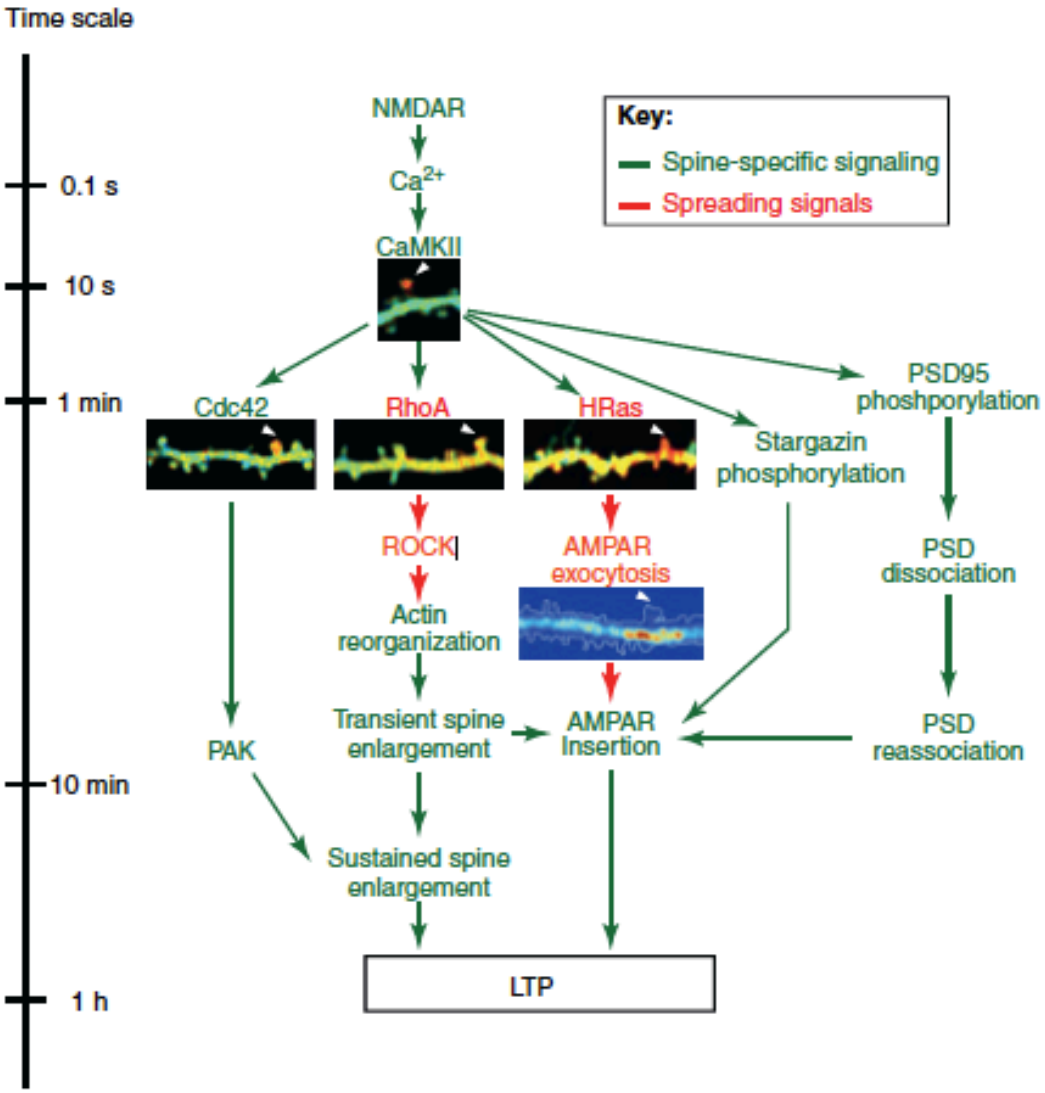

Figure 1.6 Proposed spatio-temporal regulation of structural and functional changes in glutamate uncaging-induced LTP (adapted with permission from Murakoshi & Yasuda, 2012).

CHAPTER 2

COMPARISON OF GENETICALLY ENCODED CALCIUM INDICATORS FOR MONITORING ACTION POTENTIALS IN MAMMALIAN BRAIN BY TWO-PHOTON EXCITATION FLUORESCENCE MICROSCOPY

The content of this chapter has been previously published and modified only to meet formatting requirements (Borbala Podor, Yi-ling Hu, Masamichi Ohkura, Junichi Nakai, Roger Croll, Alan Fine. 2015. Comparison of genetically encoded calcium indicators for monitoring action potentials in mammalian brain by two-photon excitation fluorescence microscopy. Neurophotonics 2015 Apr;2(2):021014. doi: 10.1117/1.NPh.2.2.021014).

Re-print permission from the publisher was granted and is found in Appendix A.

Key words: genetically encoded calcium indicators, G-CaMP, GECO, two-photon microscopy, calcium transients, organotypic hippocampal slice

Acknowledgements

We thank Yongxin Zhao, Jiahui Wu, and Robert Campbell for the GECO constructs and Alexander Goroshkov for technical assistance. This work was supported by grants from the Canadian Institutes of Health Research; Alzheimer Society of Canada; and Natural Sciences and Engineering Research Council of Canada.

2.1 Abstract

Imaging calcium transients associated with neuronal activity has yielded important insights into neural physiology. Genetically encoded calcium indicators (GECIs) offer conspicuous potential advantages for this purpose, including exquisite targeting. While the catalogue of available GECIs is steadily growing, many newly developed sensors that appear promising *in vitro* or in model cells perform less usefully when expressed in mammalian neurons. We have, therefore, evaluated the performance of GECIs from two of the most promising families of sensors, G-CaMPs (Nakai *et al.*, 2001) and GECOs (genetically encoded calcium indicators for optical imaging; Zhao *et al.*, 2011), for monitoring action potentials in rat brain. Specifically, we used two-photon excitation fluorescence microscopy to compare calcium transients detected by G-CaMP3; GCaMP6f; G-CaMP7; Green-GECO1.0, 1.1 and 1.2; Blue-GECO; Red-GECO; Rex-GECO0.9; Rex-GECO1; Carmine-GECO; Orange-GECO; and Yellow-GECO1s. After optimizing excitation wavelengths, we monitored fluorescence signals associated with increasing numbers of action potentials evoked by current injection in CA1 pyramidal neurons in rat organotypic hippocampal slices. Some GECIs, particularly Green-GECO1.2, GCaMP6f and G-CaMP7, were able to detect single action potentials with high reliability. By virtue of greatest sensitivity and fast kinetics, G-CaMP7 may be the best currently available GECI for monitoring calcium transients in mammalian neurons.

2.2 Introduction

Monitoring changes of free intracellular calcium ion concentration in living neurons offers a valuable window on calcium-dependent processes within the cell. It can also provide a surrogate readout of electrical activity, as membrane depolarization by action potentials or sufficiently large graded potentials opens voltage-gated calcium channels, resulting in calcium influx. During synaptic transmission, calcium ions can enter the postsynaptic cell through calcium-permeable receptors such as N-methyl-D-aspartate (NMDA) and alpha7 nicotinic receptors. In addition, calcium-induced calcium release from intracellular stores can substantially amplify calcium transients (Emptage *et al.*, 1999). Since the proportional change of free cytosolic concentration during electrical activation is commonly larger for calcium than for other ions, calcium sensors are particularly attractive for imaging neuronal activity.

Importantly, to monitor neuronal calcium signaling in a network of cells or in subcellular compartments, GECIs have great advantages compared with synthetic, extrinsic indicators. In particular, with GECIs, investigators can target specific populations of neurons or subcellular organelles when sensors are expressed under the control of cell type-specific promoters (Bozza *et al.*, 2004) or as appropriate fusion proteins (Shigetomi *et al.*, 2010), respectively, and can control the specific timing of expression while also eliminating the need for loading cells with extrinsic indicators.

Since the development of the first GECIs, various strategies have been used to generate more useful tools for optical imaging of neuronal activity. GECIs described to date include aequorin-based reporters (Shimomura *et al.*, 1962; Baubet *et al.*, 2000),

ratiometric fluorescence (Förster) resonance energy transfer (FRET)-based indicators (Miyawaki *et al.*, 1997) and single fluorescent protein (FP)-based calcium sensors (Baird *et al.*, 1999).

Single-wavelength GECIs typically consist of a calcium-binding element (*e.g.*, calmodulin or its fragments) inserted into an FP such as green fluorescent protein (GFP) or its variants. Currently, the growing G-CaMP family of GECIs is the most widely used of the genetically encoded calcium probes (*e.g.*, (Tian & Looger, 2008; Dombeck *et al.*, 2010; Shigetomi *et al.*, 2010; Muto *et al.*, 2011, 2013; Maisak *et al.*, 2013)). Over the past decade, successive generations of these high affinity calcium indicators have yielded progressively better signal-to-noise ratio, dynamic range and kinetics than their predecessors (Mank & Griesbeck, 2008; Looger & Griesbeck, 2011) .

The first G-CaMP, developed by Nakai *et al*. (Nakai *et al.*, 2001) was based on circularly permuted enhanced GFP and displayed a fivefold increase in fluorescence intensity upon calcium binding. This sensor, however, was pH sensitive, required temperatures below 37 ºC for best folding, and was suboptimal for measurements in the micromolar calcium concentration range (Nakai *et al.*, 2001). It was followed by the development of successive variants: G-CaMP2 (Tallini *et al.*, 2006), GCaMP3 (Tian *et al.*, 2009), "hyper-sensitive" GCaMP-HS (Muto *et al.*, 2011), G-CaMP4 (Shindo *et al.*, 2010), GCaMP5 (Akerboom *et al.*, 2012), two variants numbered "6" (GCaMP6 from Janelia Farm (Chen *et al.*, 2013), and G-CaMP6 from Saitama University (Ohkura *et al.*, 2012)), G-CaMP8, and G-CaMP7 (Ohkura *et al.*, 2012; Muto *et al.*, 2013).

G-CaMPs have been successfully expressed and used to detect calcium transients in a wide variety of cells and tissues, including HEK cells and mouse myotubes (Nakai *et*

al., 2001), chemosensory neurons of worms, antennal lobe neurons of flies, mouse somatosensory cortex neurons (Tian *et al.*, 2009) and place cells (Dombeck *et al.*, 2010), and zebrafish spinal motor neurons and optic tectum (Muto *et al.*, 2011, 2013).

Directed evolution of the GCaMP3 sensor has yielded improved green, blue, and red intensiometric and ratiometric indicators referred to as genetically encoded calcium indicators for optical imaging (GECOs (Zhao *et al.*, 2011)). The enhanced green probe (G-GECO) was reported to display approximately twice the calcium-dependent fluorescence change of GCaMP3 (Zhao *et al.*, 2011). The availability of G-GECO, blue-GECO (B-GECO) and red-GECO (R-GECO) has enabled simultaneous multicolour calcium imaging in three subcellular compartments of HeLa cells (Zhao *et al.*, 2011).

While the catalog of available GECIs is steadily growing (*e.g.*, (Wu *et al.*, 2013)), many newly developed sensors that appear promising *in vitro* or in model cells have performed less well in vertebrate neurons in organized brain tissue using two-photon excitation for improved depth penetration. We, therefore, set out to test and compare the two-photon performance of GECIs from both G-CaMP and GECO families in rat organotypic hippocampal slices. Action potentials were evoked in CA1 pyramidal neurons by direct current injection. Two-photon excitation wavelengths were selected for each probe to obtain maximum fractional changes in intensity in response to action potentials. Subsequently, we monitored calcium transients in proximal apical dendrites in response to increasing numbers of action potentials, via line-scans. Responses were recorded and compared from neurons expressing either GCaMP3, GCaMP6f, G-CaMP7, G-GECO1.0, 1.1, 1.2, B-GECO, R-GECO, Rex-GECO0.9, Rex-GECO1, CAR-GECO, O-GECO or Yellow-GECO1s (Y-GECO1s).

2.3 Materials and Methods

2.3.1 Preparation

Transverse organotypic hippocampal slices (350 μm) were made from brains of Wistar rat pups aged 6 to 8 postnatal days and cultured on Millicell CM membranes for 5 to 6 days prior to transfection as described previously (Stoppini *et al.*, 1991; Emptage *et al.*, 1999).

GECIs constructs were verified by DNA sequencing and introduced into target cells by biolistic (”gene-gun”) transfection (Lo *et al.*, 1994). Briefly, complementary DNAs encoding all GECIs were placed under cytomegalovirus (CMV) promoter, except for Rex-GECO0.9, Rex-GECO1, and Y-GECO, which used the human Synapsin I promoter, as CMV promoter yielded inadequate expression with these sensors (Table 1). Mammalian expression plasmids for all GECIs were constructed using pcDNA32 (Life Technologies). Most GECIs were too dim at resting conditions for reliable identification of expressing cells. To facilitate identification of transfected cells, GCaMPs and GECOs with dim basal fluorescence (all except GCaMP3 and GCaMP6f) were co-transfected with spectrally distinct cytoplasm-filling markers, *i.e.*, blue fluorescent protein (BFP) or GFP, as indicated in Table 2. GECI plasmid DNA (50 μg), mixed with equal amount of cytoplasmic FP vector DNA (total of 100 μg DNA) as required, was coated on 1.0 μm gold particles (Lo *et al.*, 1994; McAllister, 2000). GECI plasmid DNAs were delivered to organotypic hippocampal slices after five to six days *in vitro* by biolistics using a pressure of 120 psi with customized barrel at a distance of 4 cm above the slice through a

Millipore filter membrane (10 μm pore size) directly above the target. Imaging was carried out 1 to 4 days post-transfection.

Prior to imaging, slice preparations were transferred to the recording chamber for at least 30 minutes, where they were superfused with oxygenated (95% O_2/5% CO_2 gas mixture) artificial cerebrospinal fluid (ACSF) at 30 to 32°C. The ACSF contained, in mM: 120 NaCl, 3 KCl, 2 $MgSO_4$, 4 $CaCl_2$, 1.2 NaH_2PO_4, 23 $NaHCO_3$, 11 glucose.

2.3.2 Imaging and electrophysiology

Slices were viewed on an upright focusing-nosepiece epifluorescence microscope (Olympus, BX51WI) using a 60x NA 1.0 IR water immersion objective (Olympus) and an MRC1024MP laser scanner (Bio-Rad Microscience, Hemel Hempstead, United Kingdom) with nondescanned photomultiplier tube detectors. Available two-photon excitation wavelengths ranged between 710-970 nm (Coherent MIRA or Spectra-Physics MaiTai titanium:sapphire laser). Average energy levels measured at the specimen plane were 17 mW at 710 nm, 33 mW at 800 nm, and 10.5 mW at 970 nm. Specific excitation wavelengths used for each sensor are listed in Table 2.

Pyramidal cells expressing GECIs in the CA1 region were identified by single-photon widefield epifluorescence and impaled under visual control with sharp microelectrodes (60-80 MΩ) filled with 3 M KCl in 20 mM 2-[4-(2-hydroxyethyl)piperazin-1-yl]ethanesulfonic acid. Electrophysiological data were acquired and analyzed using AxoGraph software (AxoGraph Scientific, Sydney, Australia), and images were collected and analyzed using LaserSharp (Bio-rad Microscience) and

ImageJ (http://rsb.info.nih.gov/ij) software. In brief, one or more action potentials were evoked by 8 ms, 600 to 1200 pA current injections at 100 Hz via the intracellular electrode. Ten line scan images (each extending over 400 to 500 ms) were collected for each stimulus condition (one to eight action potentials) from two to five cells. Calcium transients were measured by collecting line scans across the proximal apical dendrite and expressed as percent fractional change in fluorescence: $\% \Delta F/F = 100 (F_{transient} - F_{initial})/(F_{initial} - F_{background})$, where $F_{initial}$ is the mean fluorescence intensity of the imaged cell over a 70 ms period prior to stimulation, and $F_{transient}$ was measured over 330 ms for one to four action potentials and 430 ms for eight action potentials (Figure 2.1).

2.4 Results

2.4.1 Expression and basal fluorescence of GECIs

Of the sensors tested here, GCaMP3 had the brightest fluorescence at resting calcium levels, which allowed for reliable detection of expressing cells. GCaMP6f also displayed adequate basal fluorescence for identification of transfected cells. Cotransfection with bright spectrally distinct cytoplasmic markers, such as BFP and GFP, was required for all other sensors tested (Table 2) in order to identify transfected cells. Expressing R-GECO in CA1 pyramidal cells often resulted in bright punctate, rather than diffuse, fluorescence throughout the cell; although unique to R-GECO among the sensors tested here, this pattern is a common phenomenon with red FPs (Katayama *et al.*, 2011; Yamada & Mikoshiba, 2012).

Our reported comparison for each indicator is based on values of fractional change in fluorescence and is, therefore, independent of the different excitation energies available at the different optimized wavelengths. We found that the optimal wavelengths (over the range available with our laser) for maximal fractional change in intensity in response to action potentials for the various GECIs were as follows: 910 nm for GCaMP3, G-CaMP7, and G-GECO 1.0, 1.1 and 1.2; 930 nm for GCaMP6f; 800 nm for B-GECO; 888 nm for R-GECO, Rex-GECO0.9, and Rex-GECO1; 970 nm for CAR-GECO and O-GECO; and 810 nm for Y-GECO1s (Table 2). (When imaging Y-GECO1s with 520 nm single-photon excitation or with 990 nm two-photon excitation, fluorescence

of resting cells is bright but decreases as ambient calcium ion concentration increases (Zhao *et al.*, 2014). Conversely, with 410 nm single-photon excitation or with two-photon excitation below 850 nm the resting fluorescence is dimmer but increases in proportion to the calcium ion concentration (Zhao *et al.*, 2014).)

2.4.2 Comparison of the two-photon performances of selected G-CaMPs and GECOs as demonstrated by their ability to report apical dendritic calcium transients associated with action potentials

After optimizing excitation wavelength for each GECI, fluorescence responses to one, two, three, four, and eight action potentials were determined. In general, G-CaMPs detected low numbers of action potentials (one to four) more reliably than GECOs. Of the sensors tested here, G-CaMP7, GCaMP6f and G-GECO1.2 were able to detect single action potentials with high reliability (Figure 2.2).

Fluorescence changes from G-CaMPs in response to a single action potential were 26 ± 7 % (all values ± standard error of the mean) with GCaMP3, 120 ± 58 % with GCaMP6f, and 302 ± 39 % with G-CaMP7 (Figure 2.2/A). Among the GECOs, G-GECO1.2 performed best in reporting low numbers of action potentials. The performance of G-GECO1.2 was superior to that of GCaMP3 both in the ΔF/F values and in linearity of responses to increasing numbers of action potentials (Figure 2.2/A and B). G-GECO 1.2 showed a 51 ± 7 % ΔF/F for a single action potential, and 384.5 ± 26 % ΔF/F for eight action potentials, whereas these values were 26 ± 7.7 % and 329 ± 33 % for GCaMP3 (Figure 2.2/B). G-GECO 1.0 and 1.1 displayed smaller fluorescence transients

(22.5 ± 18 %, and 16.5 ± 9 %, respectively) than G-GECO 1.2 in response to single action potentials (Figure 2.2/B). B-GECO demonstrated a 35 ± 11 % fluorescent change upon a single action potential, but the signals saturated beyond three action potentials and the maximal ΔF/F values only reached 52 ± 10 % with eight action potentials (Figure 2.2/C).

Performance of the longer-wavelength GECOs was modest. O-GECO and CAR-GECO performed similarly, with CAR-GECO displaying slightly higher ΔF/F values. The fluorescence transients ranged from 9.5 ± 4.5 % to 22 ± 11 % for CAR-GECO in response to one to eight evoked action potentials, respectively, versus from 7.5 ± 10 % to 18.7 ± 15 % for O-GECO (Figure 2.2/C). R-GECO responded with a slight increase in fluorescence of 6.5 % ± 7 and 12.5 % ± 15 to a single or 8 action potentials, respectively (Figure 2.2/C). Two other red indicators, Rex-GECO0.9 and Rex-GECO1, displayed greater fluorescence changes than R-GECO. The maximum ΔF/F values in response to eight action potentials were 65 ± 56 % with Rex-GECO0.9 and 47 ± 28 % with Rex-GECO1. Moreover, Rex-GECO0.9 showed a linear increase in ΔF/F values over one to eight action potentials at 100 Hz. On the other hand, Rex-GECO1 fluorescence shows a larger fluorescence increase in response to one to three action potentials.

The performance of the yellow sensor, Y-GECO1s, was comparable to that of Rex-GECO0.9 when imaged at 810 nm. Both indicators have similar ΔF/F values as well as linear responses over the range of one to eight action potentials, though Rex-GECO0.9 offers slightly higher fluorescent response than Y-GECO1s to eight action potentials but is considerably more variable (65 ± 56 % versus 53 ± 11 %, respectively).

The most robust calcium transients by far were obtained with G-CaMP7, which showed an immense 302 ± 39 % ΔF/F in response to individual action potentials (Figure 2.2/A), sufficient to render spontaneous electrical activity clearly visible by eye. Beyond four action potentials at 100 Hz, however, this sensor began to deviate from linearity, and it displayed a 1351 ± 147 % change with eight action potentials (Figure 2.2/A). The G-CaMP7 ΔF/F was significantly larger than those of GCaMP6f over the entire one to eight action potential range ($p < 0.0001$, analysis of variance), but GCaMP6f provided a more linear response over this range with 120 ± 58 % ΔF/F in response to single action potentials and 876 ± 145 % ΔF/F in response to eight action potentials.

On- and off-kinetics of all these sensors were too slow to follow individual action potentials reliably at frequencies above approximately 20 Hz, as the fluorescence in general rose with a time constant around 100 ms and decayed with a time constant around 400 to 700 ms, with the exception of Rex-GECO0.9 with ~320 ms and O-GECO with ~350 ms tau-off values (Table 1). Our data acquisition epoch was too short for reliable determination of tau-off values, but our observation that G-CaMP7 fluorescence transients evoked by single action potentials decayed at a rate intermediate between that of GCaMP3 and Rex-GECO0.9 allowed us to estimate that its decay time constant was ~470 ms. Our data did permit determination of tau-on values for all sensors, and these are reported in Table 1.

2.5 Discussion

G-CaMP7 stands out among the GECIs evaluated here. Using G-CaMP7, Muto *et al*. recently identified direction-selective neurons in the optic tectum of zebrafish, correlating visually evoked neuronal activity with behavior in real time (Muto *et al*. 2013). In the present study, G-CaMP7 was distinctly superior to the other tested indicators in terms of its ability to report action potential-evoked calcium transients (Figure 2.2/A). The second-most sensitive indicator we tested, GCaMP6f, displayed ΔF/F values only a third as great as G-CaMP7 over the one to four action potential range (Figure 2.2/A). At eight action potentials, G-CaMP7 ΔF/F values were not quite twice the GCaMP6f values, as G-CaMP7 begins to be saturated in response to more than four action potentials at 100 Hz (Figure 2.2/A). Of note, the measured and estimated time constants for G-CaMP7 (tau-on, 79 ms; tau-off, ~470 ms, respectively) are only slightly longer than those of GCaMP6f (tau-on, 74 ms; tau-off, 400 ms), which has been considered the fastest GECI for cytoplasmic free calcium in neurons (Chen *et al.*, 2013). G-CaMP7 would appear also to be superior to the slower GCaMP6 variants GCaMP6s and GCaMP6m, which display ΔF/F values not more than twice as great as GCaMP6f in response to single action potentials (Chen *et al.*, 2013). Thus, G-CaMP7 may be the GECI of choice at this time for monitoring Ca^{2+} signals, at least for low rates of action potentials in mammalian neurons.

Because signal amplitudes with some GECIs - particularly GCaMP6f, GECO1.2, Rex-GECO0.9, and Y-GECO1s - were more linearly related to the number of spikes at 100 Hz over the tested range (Figure 2.2/B), those sensors may be advantageous for

analysis of bursts of firing. An earlier study (Yamada & Mikoshiba, 2012) found that neither the G-GECOs nor R-GECO are significantly superior to GCaMP3. We have confirmed this, while extending the comparison to blue, orange, carmine, yellow, and two new red GECOs. We find that cells expressing GECOs are, in general, dimmer than cells expressing G-CaMPs under the same promoter, in both the calcium-free and calcium-bound states. It should be noted that the useful wavelength range of the lasers used in this work extended only to 970nm. It is possible that a laser source with useful output power at higher wavelength may improve the performance of Y-GECO1s, Rex-GECO1 and their derivatives. Nevertheless, these multicolour GECOs can facilitate simultaneous calcium imaging in multiple cellular or subcellular compartments (Zhao *et al.*, 2011).

Recent years have witnessed extraordinary advances in genetically encoded fluorescent calcium sensors. Notwithstanding this progress, further improvements are desirable. First, the changes in GECI fluorescence are substantially slower than the actual changes in calcium concentration, which are, in turn, much slower than membrane potential changes during action potentials. This deficiency compromises the ability of these GECIs to resolve individual action potentials at high frequencies. Second, GECIs are not capable of reporting inhibitory synaptic activity or other events that are not associated with a calcium transient. Third, GECIs act as calcium buffers, and thus may affect cell functions by interfering with intracellular calcium signaling, particularly after prolonged expression which was accompanied by bright nuclear fluorescence (Tian *et al.*, 2009). We note, however, that during the course of our experiments we detected no nuclear accumulation of GECIs. Finally, as most indicators are tested *in vitro*, in model cells, or in a variety of model organisms, there is a need for a uniform, standardized basis

for comparison among the increasing variety of sensors to help investigators choose the most suitable GECI for their specific requirements. The present study represents a step in that direction.

Figure 2.1 Simultaneous calcium imaging and electrophysiological recordings. **(A)** G-CaMP7 expressing CA1 pyramidal neuron; location of line scan is indicated by the white line across the proximal apical dendrite. Increasing fluorescence intensity in this and the following line scan images is represented by colours from black through red and yellow to green, blue and purple. **(B)** Representative line scans during one action potential and **(C)** eight action potentials with GECO1.2. The vertical white lines in (B) and (C) and corresponding deflections in (D) and (E) are time stamps, the first indicating the start of current injection, and the second, 50 ms later, serving as an internal time marker. Traces above the line scans show the simultaneously recorded action potentials on the same time scale; these are visible in more detail in panels (F) and (G). **(D)** and **(E)** Quantifications of line scans: **(D)** one action potential and **(E)** eight action potentials. X axis shows time, Y axis shows $\Delta F/F$ values. Traces are representations of single line scans. **(F)** and **(G)** show simultaneously recorded membrane potentials showing one or eight action potentials.

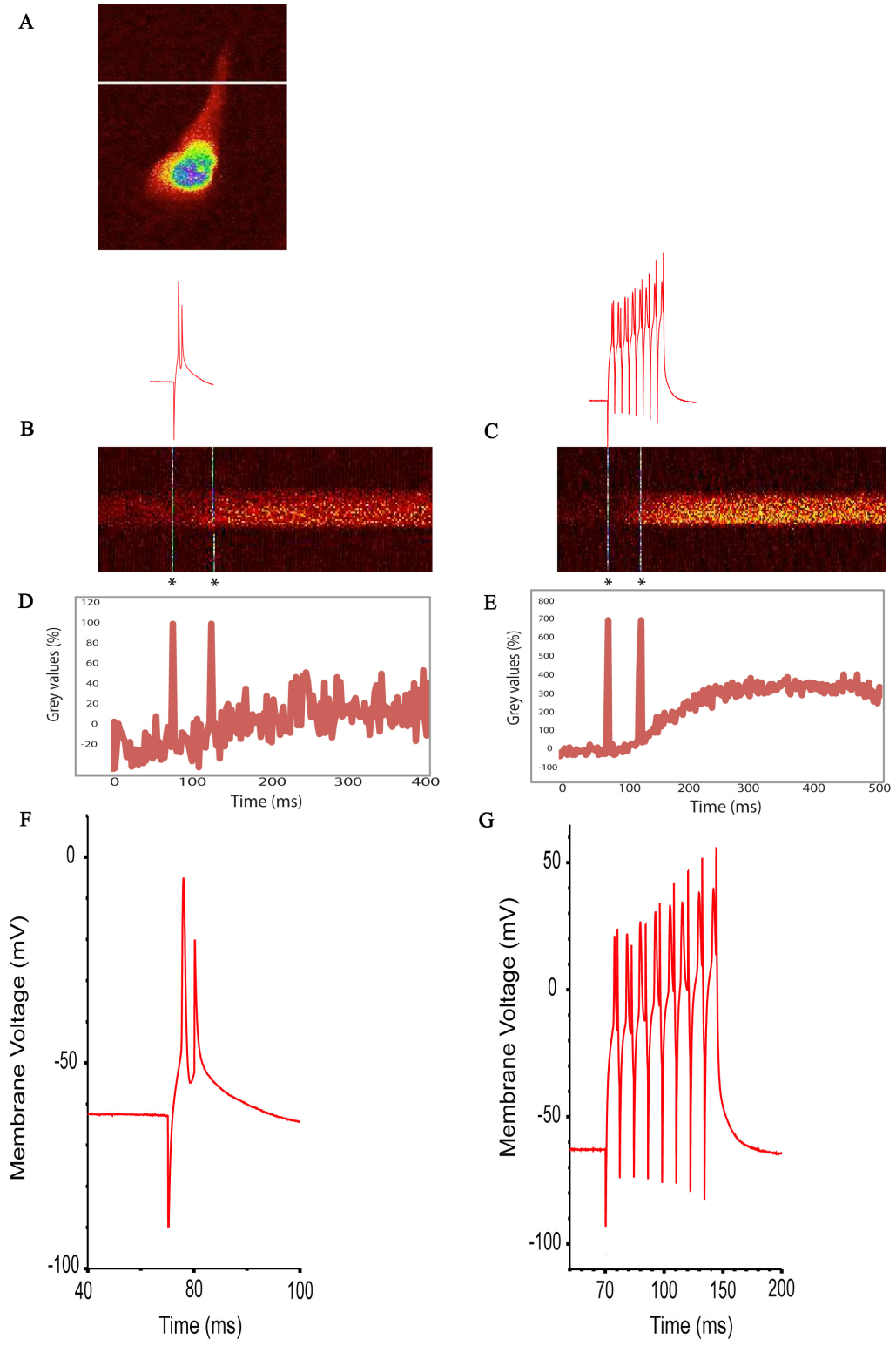

Figure 2.1 Simultaneous calcium imaging and electrophysiological recordings.

Figure 2.2 Summary of changes in fluorescence intensity corresponding to one to eight action potentials at 100 Hz. **(A)** Summary of changes in fluorescence intensity corresponding to one to eight action potentials at 100 Hz for all GCaMPs and GECOs tested. **(B)** Summary of changes in fluorescence intensity corresponding to one to eight action potentials at 100 Hz for all genetically encoded calcium indicators tested, excluding GCaMP6f and G-CaMP7. **(C)** Summary of changes in fluorescence intensity corresponding to one to eight action potentials at 100 Hz for blue-, orange-, carmine-, red-, and yellow-GECOs. Each data point corresponds to n = 10 measurements from multiple neurons. Error bars represent standard error of the mean.

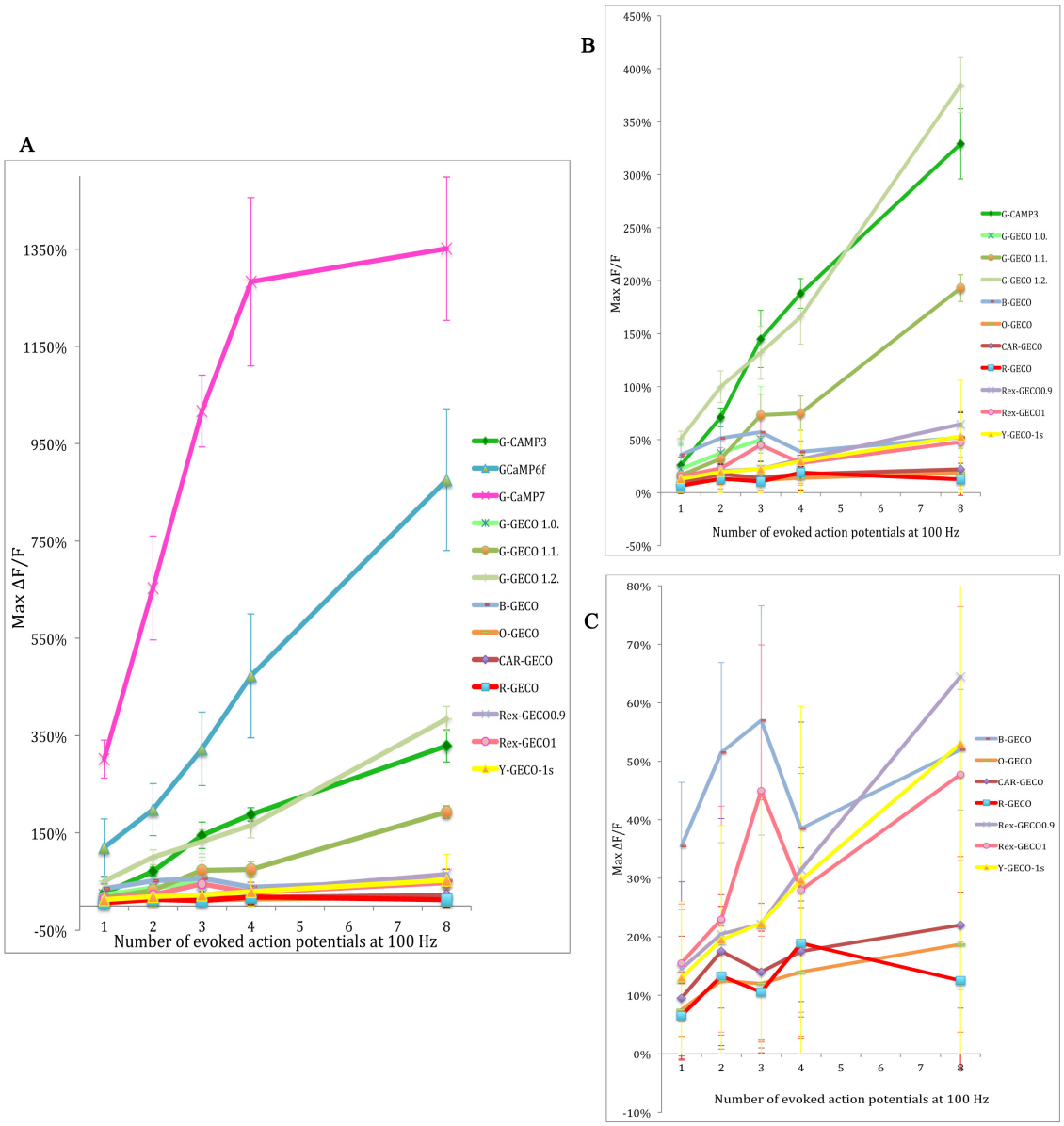

Figure 2.2 Summary of changes in fluorescence intensity corresponding to one to eight action potentials at 100 Hz.

Table 1 Measured fluorescence on- and reported off-kinetics, reported K_d for Ca^{2+}, promoters used for each GECI, and references.

	τ_{on}	τ_{off}	K_d (nM)	Promoter	Reference
G-CaMP3	95 ms	610 ms	542	Cytomegalovirus	(Zhao *et al*., 2011)
GCaMP6f	74 ms	400 ms	375	Cytomegalovirus	(Chen *et al*., 2012)
G-CaMP7	79 ms	~470 ms	243	Cytomegalovirus	(Ohkura *et al*., 2012)
G-GECO 1.2	114 ms	700 ms	1150	Cytomegalovirus	(Zhao *et al*., 2011)
B-GECO	156 ms	490 ms	260	Cytomegalovirus	(Zhao *et al*., 2011)
R-GECO	200 ms	660 ms	482	Cytomegalovirus	(Zhao *et al*., 2011)
Rex-GECO0.9	102 ms	320 ms	240	Human Synapsin I	(Wu *et al*., 2014)
Rex-GECO1	104 ms	590 ms	680	Human Synapsin I	(Wu *et al*., 2014)
O-GECO	102 ms	350 ms	1500	Cytomegalovirus	(Wu *et al*., 2013)
CAR-GECO	137 ms	600 ms	490	Cytomegalovirus	(Wu *et al*., 2013)
Y-GECO1s	127 ms	700 ms	190	Human Synapsin I	(Zhao *et al*., 2014)

Table 1 Measured fluorescence on- and off-kinetics, reported K_d for Ca^{2+}, promoters used for each GECI, and references.

Table 2 Optimal two-photon excitation wavelengths, specifications and references for each genetically encoded calcium indicator (GECI).

	Two-photon excitation	Co-transfection	Other information	References
G-CaMP3	910 nm	Not needed	Brightest basal fluorescence	(Tian *et al*., 2009)
GCaMP6f	930 nm	Not needed		(Chen *et al*., 2013)
G-CaMP7	910 nm	BFP	Highest ΔF/F values	(Ohkura *et al*., 2012)
GECO1.0	910 nm	BFP		(Zhao *et al*., 2011)
GECO1.1	910 nm	BFP		(Zhao *et al*., 2011)
GECO1.2	910 nm	BFP	Linear response to 1-8 APs @ 100 Hz	(Zhao *et al*., 2011)
B-GECO	800 nm	GFP		(Zhao *et al*., 2011)
R-GECO	888 nm	GFP	Often punctate expression	(Zhao *et al*., 2011)
Rex-GECO0.9	888 nm	GFP	Linear response to 1-8 APs @ 100 Hz	(Wu *et al*., 2014)
Rex-GECO1	888 nm	GFP		(Wu *et al*., 2014)
O-GECO	970 nm	GFP		(Wu *et al*., 2013)
CAR-GECO	970 nm	GFP		(Wu *et al*., 2013)
Y-GECO1s	810nm	BFP	Fluorescence proportional to $[Ca^{2+}]$ if exc <850nm, inversely proportional if >850nm	(Zhao *et al*., 2014)

Table 2 Optimal two-photon excitation wavelengths, specifications and references for each GECI.

CHAPTER 3

DESIGN AND MECHANISTIC INSIGHT INTO ULTRAFAST CALCIUM INDICATORS FOR MONITORING INTRACELLULAR CALCIUM DYNAMICS

Parts of this chapter have been previously published and the content modified to meet formatting and thesis requirements (Nordine Helassa, Borbala Podor, Alan Fine and Katalin Török. 2016. Design and mechanistic insight into ultrafast calcium indicators for monitoring intracellular calcium dynamics. Scientific Reports. 2016 Dec 6;6:38276. doi: 10.1038/srep38276.).

Keywords GCaMP6f, calcium, calmodulin, RS20 peptide, hippocampus, action potential

Author contributions

Manuscript author contributions: N.H. generated mutant proteins, carried out biophysical characterisation and data analysis, cell imaging, generated figures; B.P. and A.F. designed, performed and analysed experiments in hippocampal slices, generated relevant figures; K.T. designed and supervised the project and carried out kinetic modelling. Paper was written collaboratively.

In this thesis we only included relevant sections of the manuscript: experiments primarily performed and analysed by B.P. A preface and a summary of Chapters 2 & 3 are added and the reader is also referred to Chapter 6 for further discussion.

Acknowledgements

This work was funded by Wellcome Trust Project Grant 094385/Z/10/Z and BBSRC Project Grant BB/M02556X/1 to K.T., and by CIHR Grant MOP-123514 and NSERC Grant RGPIN-170421 to A.F. Dr Silke Kerruth and Dr Elizabeth R. Morris are thanked for comments on the manuscript. Use of the 3i-spinning confocal microscope at the Institute of Translational Medicine, Cellular and Molecular Physiology, University of Liverpool is acknowledged.

Preface to chapter 3

Chapter 2 evaluates how a variety of GECIs previously tested only in *in vitro* or in diverse model systems can monitor neuronal action potentials in organotypic hippocampal slice cultures. It demonstrates that GECIs are superior to synthetic extrinsic dyes in terms of eliminating the need for loading cells with fluorescents dyes (a lengthy process with potentially sub-optimal results), are relatively non-invasive, at least for the shorter time period of our experiments, and are available in multiple colours. Moreover, some GECIs, specifically G-GECO1.2, GCaMP6f, and G-CaMP7, are able to detect single action potentials. However, non-green indicators generally display smaller fluorescent changes upon stimulation, and many GECIs need co-transfection because of dim baseline fluorescence. Crucially, all are too slow to follow high frequency action potentials in mammalian neurons. The need for GECIs with improved kinetics is evident.

3.1 Abstract

Calmodulin-based genetically encoded fluorescent calcium indicators (GCaMP-s) are powerful tools for imaging calcium dynamics from cells to freely moving animals. High affinity indicators with slow kinetics, however, distort the temporal profile of calcium transients. Here we report that the newly developed variants of GCaMP6f, namely mGCaMP6f RS-1 EF-3 (GCaMP6f-ultrafast; GCaMP6f$_u$) and mGCaMP6 RS-1 EF-4, resulted in reduced affinity, ultrafast GECIs with improved kinetics.

Stimulation of hippocampal CA1 pyramidal neurons with five action potentials fired at 100 Hz resulted in a single dendritic calcium transient with a two-fold faster rise and seven-fold faster decay time than GCaMP6f.

The design strategy used to generate GCaMP6f$_u$ might also be applicable for the acceleration of the response kinetics of other GCaMP-type calcium indicators.

3.2 Introduction

Genetically encoded Ca^{2+} indicators (GECI) facilitate monitoring Ca^{2+} dynamics in intact and even freely moving animals. A limiting factor in the application of GECI has been their high Ca^{2+} affinity and slow response kinetics (Fernandez-Alfonso *et al.*, 2014). In GCaMP-type GECI (Nakai *et al.*, 2001; Ohkura *et al.*, 2005; Tallini *et al.*, 2006; Souslova *et al.*, 2007; Hendel *et al.*, 2008; Wang *et al.*, 2008; Akerboom *et al.*, 2009, 2012; Tian *et al.*, 2009; Muto *et al.*, 2011) Ca^{2+} binding to calmodulin (CaM) induces the formation of a complex with a target peptide which in turn restores the fluorescence of circularly permutated (cp) enhanced green fluorescent protein (EGFP; Baird *et al.*, 1999). The Ca^{2+}-induced binding of CaM to a target peptide allows the detection of Ca^{2+} signals also by GCaMP-related G-GECO-s (Zhao *et al.*, 2011), GEM-GECO-s (Zhao *et al.*, 2011), sub-cellularly targeted calcium-measuring organelle-entrapped protein indicators (CEPIA; Suzuki *et al.*, 2014) and GCaMPer (Henderson *et al.*, 2015). The most commonly used target peptide is RS20, a smooth muscle myosin light chain kinase-derived peptide.

GCaMP-s reported to have the greatest brightness and Ca^{2+} induced fluorescence enhancement to date are variants of a GCaMP6 generation termed GCaMP6 slow, GCaMP6 medium and GCaMP6 fast (GCaMP6s, GCaMP6m and GCaMP6f) (Chen *et al.*, 2013) as well as GCaMP7 (Muto *et al.*, 2013) and GCaMP8 (Ohkura *et al.*, 2012). Even though indicators such as GCaMP7 show sufficiently high level of brightness to

detect single action potentials (AP-s) (Podor *et al.*, 2015), their slow kinetic properties due to the Ca^{2+} - CaM - RS20 peptide interaction limit achieving temporal fidelity.

Typically, Ca^{2+} - CaM - RS20 interactions have a high affinity (half-maximal brightness concentration, K_d values of 100-300 nM) as for GCaMP6s and GCaMP6f (Chen *et al.*, 2013). Correspondingly, the Ca^{2+} dissociation rates and thus the signal decay rates are slow, 1-5 s^{-1} at 20 ^{o}C, comparable to that of GCaMP3 (Tian *et al.*, 2009). By rational design, mutations at the Ca^{2+} - CaM - RS20 binding interface have produced GCaMP3- and GCaMP6f-derived probes with improved decay kinetics (Sun *et al.*, 2013; Badura *et al.*, 2014). The probe with the fastest signal rise and decay kinetics so far is GCaMP3$_{fast}$ (Helassa *et al.*, 2015). The mutation strategy that gave rise to GCaMP3$_{fast}$ can serve as a template for generating fast-response CaM-based GECI.

3.2.1 Design template for ultrafast GCaMP-s

A strategy was developed to generate fast-response GCaMP-type GECI by introducing specific mutations at the Ca^{2+} - CaM - RS20 peptide interface to weaken their interactions (Figure 3.1/A). In CaM, Ca^{2+} binding sites are disabled by a single point- mutation of the first Asp to Ala in each EF-hand Ca^{2+} binding loop. The EF-3 mutation denotes a mutant with the third Ca^{2+} site inactivated, EF-4 with the fourth site. A mutation termed RS-1 which substitutes the Trp residue in position 43 for Tyr in the RS20 peptide sequence, further weakens the Ca^{2+}- CaM - peptide interaction (Török & Trentham, 1994) (Figure 3.1).

Four trends are commonly observed when the mutational strategy is applied to GCaMP3, G-GECO and GEM-GECO. First, mutation of EF-1 and/or EF-2 causes loss of fluorescence signal (Sun *et al.*, 2013; Helassa *et al.*, 2015). Second, the EF-4 and combined RS-1 EF-4 mutations consistently retain or have increased brightness and dynamic range together with faster kinetics than the parent proteins (Helassa *et al.*, 2015). Third, GCaMP3, G-GECO and GEM-GECO probes with the EF-3:4 double mutation alone or in combination with RS-1 have low affinity (mM K_d) and fast kinetics. Although the lower brightness and dynamic range of the EF-3:4 double mutants requires improvement, kinetically they are thus promising for development of extracellular or intra-organelle Ca^{2+} probes. Finally, the combination of mutations EF-3 and RS-1 results in the fastest response kinetics and has given the to-date most kinetically improved probe mGCaMP3 RS-1 EF-3 (also known as GCaMP3$_{fast}$), which has Ca^{2+} rise and decay times of 1-3 ms (Helassa *et al.*, 2015).

The strategy used to produce GCaMP3$_{fast}$ was applied to the popular bright probes GCaMP6s and GCaMP6f, and the hypothesis, that the EF-3, EF-4 and RS-1 mutations and their combinations result in significantly faster kinetics when applied to CaM-based GECI, was tested. Twelve mutant probes were generated, six each for GCaMP6s and for GCaMP6f (Chen *et al.*, 2013). Biophysical characterisation revealed that, as predicted, the fastest responding probe was given by the RS-1 (W43Y) EF-3 (D395A) mutation combination, followed by a combination RS-1 and EF-4 mutations. Fast response kinetic profiles of mGCaMP6f RS-1 EF-3, termed GCaMP6f-ultrafast

(GCaMP6f$_u$) and mGCaMP6 RS-1 EF-4 are demonstrated in neurons stimulated by high frequency action potentials and compared to GCaMP6f.

3.3 Materials and Methods

3.3.1 Materials

GCaMP6s and GCaMP6f plasmids were a gift from Douglas Kim (Addgene plasmid #40753 and #40755, respectively) (Chen *et al.*, 2013).

3.3.2 Two-photon imaging of GCaMP6f, GCaMP6f$_u$ and mGCaMP6 RS-1 EF-4 in hippocampal slices

Wistar rats were purchased from Charles River Laboratories. All experiments were conducted in accordance with the Canadian Council on Animal Care standard and guidelines, with approval of the Dalhousie University Committee on Laboratory Animals.

Transversely sectioned organotypic hippocampal slices (350 μm) were made from brains of rat pups aged 6 to 8 postnatal days humanely killed by Schedule 1 procedure (anaesthetic (ketamine) overdose followed by decapitation) and cultured on Millicell CM membranes for five to six days (Stoppini *et al.*, 1991; McAllister, 2000). Hippocampal slices were transfected using biolistics as described previously (see Chapter 2.3.1 and McAllister, 2000). Slice preparations were transferred to a recording chamber and superfused at 28 °C with artificial cerebrospinal fluid (containing 120 mM NaCl, 3 mM KCl, 2 mM $MgSO_4$, 4 mM $CaCl_2$, 1.2 mM NaH_2PO_4 and 11 mM glucose) saturated with a

gas mixture of 95% O_2/5% CO_2.

An upright epifluorescence microscope (Olympus BX51WI) with a 60X NA1.0 IR water immersion objective (Olympus) and an MRC1024MP (Bio-Rad Microscience, Hemel Hampstead, United Kingdom) laser scanner with nondescanned photomultiplier tube detectors were used to view slices. Two-photon imaging was carried out one to four days post-transfection using a MaiTai titanium sapphire laser at 930 nm.

Action potentials were evoked and recorded in expressing CA1 pyramidal neurons using a sharp intracellular electrode (60-80 MΩ) filled with 3 M KCl in 20 mM 2-[4-(2-hydroxyethyl)piperazin-1-yl]ethanesulfonic acid to buffer and maintain physiological pH. Line scans taken across proximal apical dendrites at 2 ms intervals were collected to determine the calcium transients measured as $\Delta F/F_0$ (defined as $\Delta F/F_0 = 100\ (F_{transient}\text{-}F_{initial})/(F_{initial}\text{-}F_{background})$ corresponding to 5 AP-s evoked by brief depolarizing current injection at frequencies between 10-100 Hz *via* a Multiclamp 700B amplifier (Molecular Devices, California). Evoking five action potentials was necessary as individual APs were not detectable with GCaMP6f$_u$ and mGCaMP6 RS-1 EF-4. Ca^{2+} decay kinetics of GCaMP6 variants were determined by monitoring fluorescence changes evoked by 5 APs at 100 Hz.

Electrophysiological and imaging data were collected and analysed with software from AxoGraph (AxoGraph Scientific, Sydney, Australia), LaserSharp (Bio-Rad Microscience) and ImageJ (Schneider *et al.*, 2012).

3.4 Results

3.4.1 Response of GCaMP6f, GCaMP6f$_u$ and mGCaMP6f RS-1 EF-4 to high frequency stimulation in neurons

Transfected CA1 pyramidal neurons of organotypic hippocampal slices showed homogenous GCaMP6f, GCaMP6f$_u$ and mGCaMP6f RS-1 EF-4 expression. Baseline fluorescence of all three indicators was bright enough to readily identify expressing cells (Figure 3.2).

Fluorescence dynamic ranges ($\Delta F/F_0$) were 5.9 ± 0.3, 0.8 ± 0.05 and 0.5 ± 0.04 for GCaMP6f, GCaMP6f$_u$ and mGCaMP6f RS-1 EF-4, respectively, consistent with small [Ca^{2+}] changes. Notably, GCaMP6f achieved a significantly higher $\Delta F/F_0$ value throughout the 10-100 Hz range tested compared to GCaMP6f$_u$ and mGCaMP6f RS-1 EF-4. Due to its low K_d for Ca^{2+}, only GCaMP6f was able to detect the low post-synaptic [Ca^{2+}] elevation evoked by 5 AP-s fired at 10 Hz. For the same reason, however, the kinetics of GCaMP6f response were the most prolonged. With their higher K_d values GCaMP6f$_u$ and mGCaMP6f RS-1 EF-4 did not show a response to stimulation up to 20-40 Hz frequency and the dynamic range remained low. The kinetic advantage of GCaMP6f$_u$ and mGCaMP6f RS-1 EF-4 became evident at stimulation at 40 Hz or greater (Figure 3.3) and was particularly clear at 100 Hz: compared to GCaMP6f, GCaMP6f$_u$ and mGCaMP6f RS-1 EF-4 responded with much faster rise and decay kinetics to the [Ca^{2+}] elevation evoked by trains of 5 AP-s. For GCaMP6f, following 50

ms stimulation at 100 Hz, the Ca^{2+} signal is still rising for another ~ 75 ms and then decays over ~ 400 ms (Chen *et al.*, 2013) (Figure 3.3). mGCaMP6f RS-1 EF-4 has improved kinetics with the signal decaying only ~ 20 ms after stimulation, with a $t_{1/2}$ of 91 ± 17 ms (Figure 3.3). The fastest response is achieved by GCaMP6f$_u$: the Ca^{2+} signal decay commences as soon as the stimulation is finished, and returns to baseline with a $t_{1/2}$ of 40 ± 2 ms, thus reducing the refractory period of detection following a stimulation event from hundreds to tens of milliseconds (Figure 3.3).

3.5 Discussion

This work reveals that modifications of fast-response GCaMP6f, resulting in probes GCaMP6f$_u$ and mGCaMP6f RS-1 EF-4, show more accurate time resolution of Ca^{2+} signalling events. The design template used to create these indicators could be applied in the future to other GCaMP-type GECIs.

The brightness and dynamic range of GCaMP6f$_u$ are not sufficient for the detection of the post-synaptic dendritic [Ca^{2+}] elevation evoked by a single AP. Although the kinetic properties of GCaMP6f$_u$ would allow the separation of individual AP-s even at 100 Hz, the actual Ca^{2+} transient reveals an integrated Ca^{2+} response for the five action potentials rather than individual peaks, raising the possibility that the Ca^{2+} dynamics associated with AP firing limit the use of Ca^{2+} as an indicator of fast neuronal activity.

Although unable to detect single AP-s, GCaMP6f$_u$ with its fast rise and decay kinetics may still be useful for the detection of repeated AP-s with between-train intervals of tens rather than hundreds of milliseconds. The Ca^{2+} rise rates following a train of 5 AP-s in organotypic hippocampal slices reported by the GCaMP6f$_u$ and mGCaMP6f RS-1 EF-4 probes were markedly faster than GCaMP6f. The novel variant GCaMP6f$_u$ show similar kinetic properties to GCaMP3$_{fast}$ (Helassa *et al.*, 2015). However GCaMP6f$_u$ has a 3-fold lower K_d (0.89 μM) compared to GCaMP3$_{fast}$ (2.8 μM) thus is more sensitive to small Ca^{2+} concentration changes and hence more suitable for

Ca^{2+} imaging in neurons. Improved brightness and fluorescence dynamic range would help make GCaMP6f$_u$ with its ultrafast kinetics a useful physiological tool.

Figure 3.1 Comparison of fast GCaMP probes ($GCaMP3_{fast}$ and $GCaMP6f_u$) and their parent variants (GCaMP3 and GCaMP6f). **(A)** Position of the mutations that gave rise to $GCaMP3_{fast}$ and $GCaMP6f_u$ variants, relative to GCaMP3. **(B)** Crystal structure of monomeric GCaMP6m in a Ca^{2+}-bound form with cpEGFP (green), Ca^{2+} ions (yellow), CaM (blue) and the RS20 peptide (light brown) (adapted with permission from Ding *et al.*, 2014). The amino acid residues highlighted in red are those that generated $GCaMP6f_u$ relative to GCaMP3.

A

	RS20	cpEGFP	linker		CaM					
GCaMP3	W43		T302	R303	A317	D380	T381	S383	R392	D395
GCaMP3$_{fast}$	W43Y									D395A
GCaMP5G			T302L	R303P		D380Y				
GCaMP6f			T302L	R303P	A317E	D380Y	T381R	S383T	R392G	
GCaMP6f$_{u}$	W43Y		T302L	R303P	A317E	D380Y	T381R	S383T	R392G	D395A

B

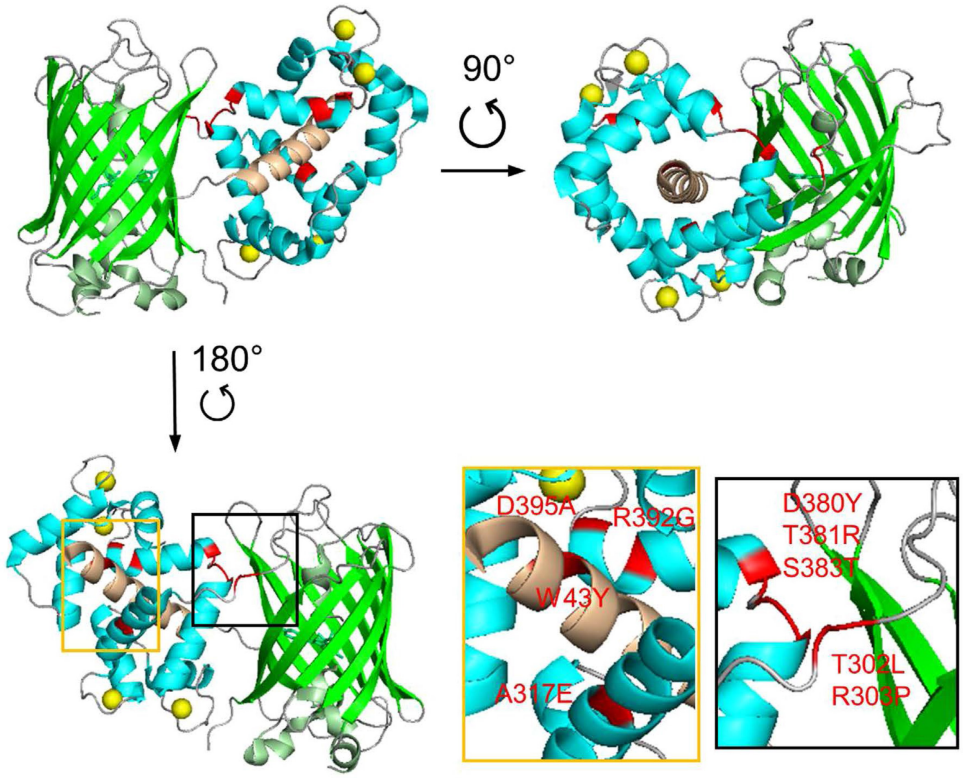

Figure 3.1 Comparison of fast GCaMP probes (GCaMP3$_{\text{fast}}$ and GCaMP6f$_{u}$) and their parent variants (GCaMP3 and GCaMP6f).

Figure 3.2 Representative images of baseline expression of GCaMP6f, GCaMP6f$_u$, and mGCaMP6f RS-1 EF-4. **(A)** GCaMP6f, **(B)** GCaMP6f$_u$, and **(C)** mGCaMP6f RS-1 EF-4 expressing CA1 pyramidal neurons. Expressing cells were readily detectible in all three cases. White lines denote the position of the line scan across the proximal apical dendrite.

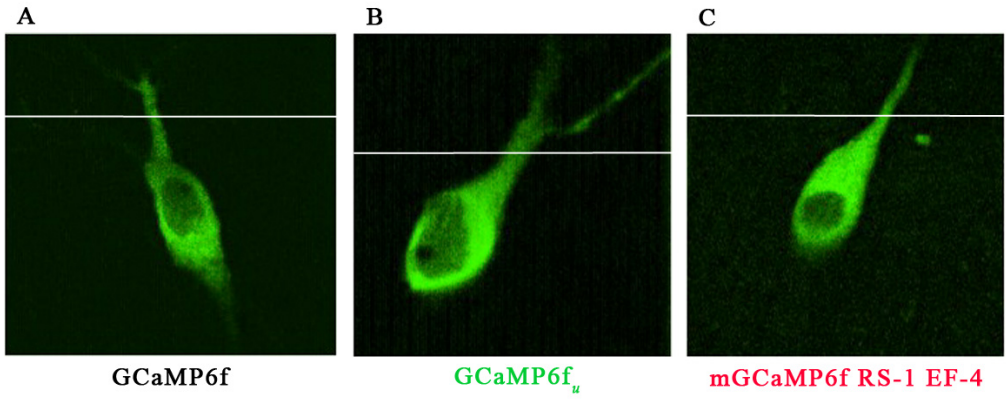

Figure 3.2 Representative images of baseline expression of GCaMP6f, GCaMP6f$_u$, and mGCaMP6f RS-1 EF-4.

Figure 3.3 Ca^{2+} response of GCaMP6f, GCaMP6f$_u$, and GCaMP6f RS-1 EF-4 in post-synaptic CA1 neurons in hippocampal slices. **(A)** Ca^{2+} response kinetics in post-synaptic CA1 neurons in hippocampal slices of GCaMP6f (28 °C) to stimulation by 5 action potentials (AP-s). Grey shaded areas indicate the duration of stimulation. GCaMP6f stimulated at (3 cells, n number of recordings in brackets) 10 Hz (n = 28), 20 Hz (n = 28), 40 Hz (n = 29), 50 Hz (n = 27), 75 Hz (n = 30) and 100 Hz (n = 19). **(B)** GCaMP6f$_u$ stimulated (4 cells, n number of recordings in brackets) at 10 Hz (n = 29), 20 Hz (n = 30), 40 Hz (n = 29), 50 Hz (n = 29), 75 Hz (n = 30) and 100 Hz (n = 26). The achieved maximum $\Delta F/F_0$ values are plotted against time. **(C)** GCaMP6f RS-1 EF-4 stimulated (3 cells, n number of recordings in brackets) at 10 Hz (n = 20), 20 Hz (n = 27), 40 Hz (n = 30), 50 Hz (n = 30), 75 Hz (n = 30) and 100 Hz (n = 30).

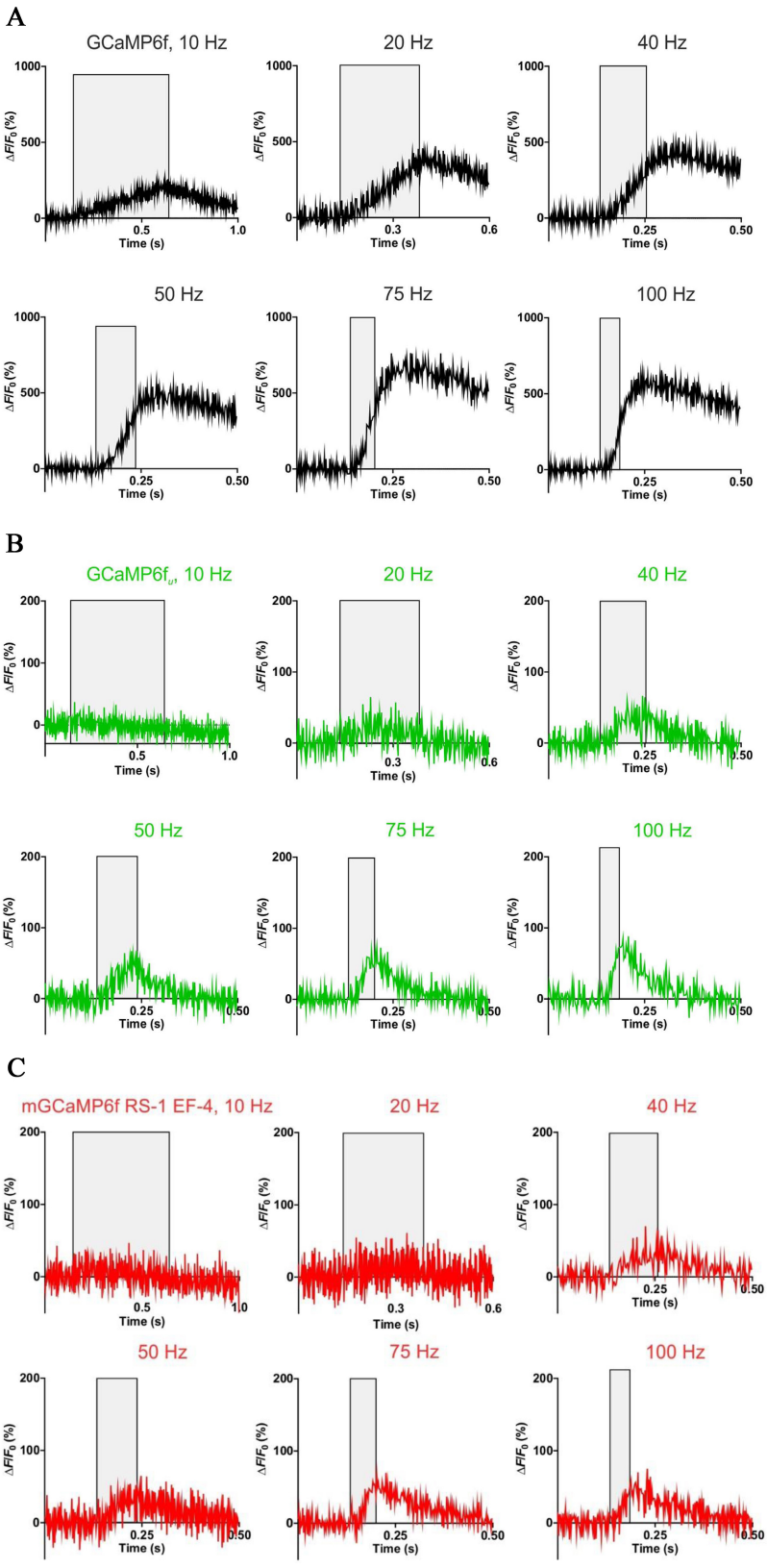
A
GCaMP6f, 10 Hz
20 Hz
40 Hz
50 Hz
75 Hz
100 Hz
ΔF/F0 (%)
Time (s)
B
GCaMP6f$_{u1}$, 10 Hz
20 Hz
40 Hz
50 Hz
75 Hz
100 Hz
ΔF/F0 (%)
Time (s)
C
mGCaMP6f RS-1 EF-4, 10 Hz
20 Hz
40 Hz
50 Hz
75 Hz
100 Hz
ΔF/F0 (%)
Time (s)

Conclusion of Chapters 2 and 3

As introduced in Chapter 1 the aim of this thesis was to explore and apply novel techniques for the study of neuronal activity and plasticity in rat organotypic hippocampal slices. A particular goal was to investigate structural and functional plasticity of recurrent synapses between CA3 neuron pairs. For that purpose recordings and stimulation of synaptically connected CA3 cell pairs, as well as identification and optical monitoring of each cell independently, and importantly of their synaptic contacts, is required. We anticipated that newly developed GECIs might aid our technically challenging studies if the cell pairs expressed spectrally different indicators thereby eliminating the need for dye-loading. However many GECIs have only been tested non-uniformly, *in vitro* or in different cells and organisms, e.g., B-GECO, G-GECO1.1 and G-GECO 1.2 in dissociated hippocampal cells (Zhao *et al.*, 2011), Y-GECO1, R-GECO and Rex-GECO in HeLa cell, dissociated cell cultures, organotypic hippocampal slices, *in vivo* tadpoles (Zhao *et al.*, 2014; Wu *et al.*, 2014), O-GECO, C-GECO in cell lines and mouse neocortical slice (Wu *et al.*, 2013), GCaMP3 in flies, worms, mice, rats (Tian *et al.*, 2009; Dombeck *et al.*, 2010; Mittmann *et al.*, 2011; Wiegert & Oertner, 2013; Rickgauer *et al.*, 2014), GCaMP6 in zebrafish, flies, mice, rats (Chen *et al.*, 2013; Lock *et al.*, 2015; Stein *et al.*, 2015; Liebscher *et al.*, 2016), GCaMP7 in HeLa cells and zebrafish (Ohkura *et al.*, 2012; Muto *et al.*, 2013), $GCaMP3_{fast}$ in cardiomyocytes (Helassa *et al.*, 2015), and other studies compared only a few indicators (Ohkura *et al.*, 2012; Yamada & Mikoshiba, 2012; Akerboom *et al.*, 2012; Zhao *et al.*, 2014). A

standardized comparison of GECIs in hippocampal pyramidal neurons was needed. Thus in Chapters 2 & 3 we evaluated promising GECIs in CA1 pyramidal cells of organotypic hippocampal slices based on their ability to report neuronal action potential firing. Our results indicate however that most GECIs tested are too slow and/or insensitive to follow individual action potentials at high frequencies.

Notwithstanding the valuable results of Chapters 2 and 3 I concluded that it is best to proceed with extrinsic fluorescent dyes for studying morphological changes associated with plasticity of recurrent CA3-CA3 synapses in the rat hippocampus instead of GECIs. After carefully weighting the pros and cons of using such GECIs, I resolve that: (i) Transfection efficiency is moderately controllable (Johnston, 1990; Lo *et al.*, 1994, 2014; McAllister, 2000): even with precise positioning of the slice preparation during gene-gun transfection, it is difficult to target only our region of interest and the number of expressing cells in each slice varies greatly between one to half a dozen or more (Murphy & Messer, 2001; Dunaevsky, 2013; Lo *et al.*, 2014). With multiple fluorescing cells in a field of view, following individual dendrites and axons for locating putative synaptic contacts between CA3 cell pairs for monitoring their structural plasticity proves to be particularly difficult. Therefore, fewer expressing cells are preferable, though less efficient. (ii) Using spectrally different GECIs as pre- and postsynaptic partners of a neuron pair is not ideal with current sensors: non-green GECIs are still suboptimal for our purposes, and the chances of finding synaptically connected pairs between expressing cells with only a handful each is low. (iii) In addition, gene-gun transfection uses golden particles to deliver GECI DNAs, which makes transfected cells particularly sensitive to

acquire damage during long periods of imaging, often a necessity of our paired recording experiments. (iv) Transfection efficiency is best at around three to five days *in vitro* (Lo *et al.*, 1994; Karra & Dahm, 2010), however, paired recordings are ideal around three weeks (see Chapter 5). (v) Lastly, transfection can, in some instances, compromise the health of the hippocampal slice evident by our observations of suboptimal visual appearance and electrophysiological properties of more cells than in non-transfected slices (Lo *et al.*, 1994; Karra & Dahm, 2010). Area CA3 seems to be specifically sensitive and often responds with lesions and swollen cells. Hence our synthetic dye approach for studying structural and functional plasticity of recurrent CA3 synapses in organotypic hippocampal slices was finalized and is detailed in the following chapters.

CHAPTER 4

SIMULTANEOUS ELECTROPHYSIOLOGICAL RECORDINGS AND OPTICAL IMAGING OF AN ACTIVE SYNAPSE UNDERGOING PLASTICITY

4.1 Introduction

The ability of neurons to change their synaptic strength according to their activity is referred to as synaptic plasticity (Zieliński, 2006). Two major forms of synaptic plasticity, long-term-potentiation (LTP), a persistent increase in synaptic efficacy, and long-term-depression (LTD), a persistent decrease in synaptic efficacy, are the leading cellular models of learning and memory (Bliss & Lømo, 1973; Morris *et al.*, 1986; Collingridge *et al.*, 2010; Bliss & Collingridge, 2013; Nicoll & Roche, 2013). Despite great interest in this phenomenon the underlying physiological and molecular mechanisms remain incompletely understood. Notably, molecular and structural aspects of synaptic plasticity, including the relative contribution of pre- and postsynaptic mechanisms in LTP or LTD expression (Malinow & Malenka, 2002; Macdougall & Fine, 2013) as well as the potential of associated morphological changes are highly debated (Holtmaat & Svoboda, 2009; Bosch & Hayashi, 2012).

Structural remodeling of existing synapses and formation or elimination of synaptic contacts during plasticity have been suggested as possible mechanisms

underlying LTP and LTD (Yuste & Bonhoeffer, 2001; Bosch & Hayashi, 2012; Bailey *et al.*, 2015). This notion is supported by evidence showing existing correlations between various aspects of the pre- and postsynaptic compartment of imaged synapses (Schikorski & Stevens, 1997; Holderith *et al.*, 2012; Meyer *et al.*, 2014; Nishiyama & Yasuda, 2015), as well as how numerous experimental manipulations (e.g., high- and low frequency stimulation or glutamate uncaging) can lead to changes in the size or ultrastructural composition of the synapse (Maletic-Savatic *et al.*, 1999; Yang *et al.*, 2008; Zhang *et al.*, 2013; Bell *et al.*, 2014; Calabrese *et al.*, 2014; Michel *et al.*, 2015). However, there has been a great deal of variability amongst the reported degree, timing, location, and even existence of such changes (Moser *et al.*, 1994; Hosokawa *et al.*, 1995; Sorra & Harris, 1998; Lang *et al.*, 2004; Matsuzaki *et al.*, 2004; Wang *et al.*, 2007; Meyer *et al.*, 2014; Stein *et al.*, 2015). Nonetheless, it has become increasingly accepted that dendritic spines enlarge during LTP, especially when spines are stimulated by MNI-glutamate uncaging (photolytic un-caging of methoxy derivative of nitroindolino glutamate) and monitored by patch-clamp recordings (Matsuzaki *et al.*, 2004; Tanaka *et al.*, 2008; Bosch *et al.*, 2014; Meyer *et al.*, 2014).

Patch clamp recordings and glutamate uncaging are, however, arguably far from physiological manipulations, as patch clamp recordings can disrupt the intracellular milieu of cells, and glutamate uncaging not only disregards the presynaptic cell but potentially releases an excess of glutamate. Thus both techniques possibly skew results and may reflect stimulation artifacts (Horn & Marty, 1988; Staley *et al.*, 1992; Scimemi *et al.*, 2004; Enoki *et al.*, 2009).

In contrast to postsynaptic LTP, structural changes in LTD or of the presynaptic bouton in LTP or LTD remain obscure (Buchs & Muller, 1996; Zhou *et al.*, 2004; Medvedev *et al.*, 2010, 2014; Chéreau *et al.*, 2017) and the outcomes of the numerous LTP and of the fewer LTD studies are often at odds (Hosokawa *et al.*, 1995; Harvey & Svoboda, 2007; Tanaka *et al.*, 2008; Bourne & Harris, 2011; Oh *et al.*, 2015). Some of those discrepancies can be explained by different preparations, age, and location of cells, but results are arguably limited and affected by available tools and chosen methods. For example, electron microscopy studies cannot follow longitudinal changes and might report large variability between animals rather than experimental conditions (Lee *et al.*, 1980; Fifkova & Anderson, 1981; Desmond & Levy, 1988; Nikonenko *et al.*, 2003; Medvedev *et al.*, 2014), the calcium precipitation method may label potentiated synapses but is biased for large spines (Buchs *et al.*, 1994; Buchs & Muller, 1996; Toni *et al.*, 1999), chemical LTP affects unspecified synapses (Otmakhov *et al.*, 2004; Stewart *et al.*, 2005; De Roo *et al.*, 2008), and even commonly-used induction protocols such as tetanization and glutamate uncaging can be regarded as unphysiological (Lang *et al.*, 2004; Matsuzaki *et al.*, 2004; Govindarajan *et al.*, 2011; Bosch *et al.*, 2014).

Besides the above mentioned techniques, a standard electrophysiological method to study synaptic connections between cells is to stimulate a bundle of unidentified presynaptic axons and record from the postsynaptic neuron (Figure 4.1/A). This, however, leaves the experimenter blind to many aspects of the presynaptic cell and also compromises the interpretation of the obtained results.

To overcome some of these limitations here we present an alternative approach in cultured hippocampal rat brain slices (Figure 4.1/B, C & D): working with pairs of identified CA3 neurons allows us to study simultaneously both compartments, which gives us the most direct evidence on how physiological neuronal activity in the presynaptic cell affects the postsynaptic cell. Moreover, combining these paired electrophysiological recordings with coincident optical imaging of an active synapse allows us to investigate the physiological and structural aspects of synaptic plasticity, thus potentially revealing whether there are, under near-physiological conditions, any morphological changes to either the pre- or postsynaptic compartment of an active synapse undergoing plasticity. We found that inducing LTD between pairs of CA3 pyramidal cells in organotypic hippocampal slices of the rat via spike timing-dependent plasticity (STDP) can happen without a significant change to the synapse as was confirmed by two-photon imaging.

4.2 Materials and methods

4.2.1 Animals

Experimental usage of all animals were approved by Dalhousie University Animal Care Committee and was in accordance to the Canadian Council of Animal Care. Pregnant female Wistar rats were purchased from Charles River Laboratories and were housed in cages with free access to food and water. Pups were sacrificed at eight postnatal day.

4.2.2 Slice preparation

Transverse organotypic hippocampal slice cultures (OHSC) were made as described previously (Stoppini *et al.*, 1991). Briefly, rats were anaesthetized by intra-peritoneal ketamine injection (100 ml/kg) followed by decapitation. Hippocampi were isolated under a microscope in ice-cold dissecting solution consisting of HBSS (Life Technologies), 33.3 mM D-Glucose, 25 mM HEPES, 4 mM $MgCl_2$, adjusted to pH 7.3~7.4. 350 μm thick transverse slices were cut on a McIlwain tissue chopper after which slices were cooled at 4 °C for an additional 20 to 30 minutes in dissecting solution. Slices were then plated to and cultured on Millicell CM membranes (Millipore) in a six-well plate for approximately two to four weeks at 35 °C and 5 % CO_2. Each well contained two or three slices per insert in 1.1 ml OHSC medium. The OHSC medium

was replaced one day after slice preparation, and then changed three times weekly. A volume of 250 ml OHSC medium contained 125 ml MEM, 5 ml 32.5 % D-glucose in MEM, 60 ml EBSS, 60 ml horse serum (heat inactived), 5 ml B-27, 775 µl $MgSO_4$ (1 M; Sigma) and 50 µl $CaCl_2$ (1 M; Fluka), and 7 µM of Cytosine β-arabinofuranoside (Sigma). MEM was supplied with 25 mM of HEPES and 2 mM of GlutaMAX. Medium was adjusted to pH 7.3-7.4 and 310-320 Osm/L osmolarity, and was filtered with 0.2 µm filter unit. All components of OHSC were purchased from Life Technologies unless stated otherwise.

Slices were selected and cut from Millicell membrane under a microscope, and in an attempt to minimize spontaneous synchronous activity of CA3 cells during recording, a single cut between the DG and CA3 was made to sever PP axons (Scharfman, 1994). Slices were then transferred to a recording chamber containing artificial cerebrospinal fluid (ACSF) and immobilized by a U-shaped platinum wire.

For a minimum of 30 minutes slice preparations were superfused with oxygenated (95 % O_2 / 5 % CO_2 gas mixture) ACSF at 32 °C before proceeding to any experimental manipulation. The ACSF contained the followings in mM concentration: 120 NaCl, 3 KCl, 2 $MgSO_4$, 3 $CaCl_2$, 1.2 NaH_2PO_4, 23 $NaHCO_3$, 11 glucose, and 1-2 Trolox (Sigma). Each day the osmolarity of the recording ACSF and OHSC media was measured and if needed the osmolarity of the ASCF was adjusted to that of the OHSC media by adding extra glucose.

4.2.3 Imaging and electrophysiology

Imaging was carried out with an upright fixed-stage epifluorescence microscope (Olympus, BX51WI) using a 60x NA 1.0 IR water immersion objective (Olympus) and an MRC1024MP laser scanner (Bio-Rad Microscience, Hemel Hempstead, UK) with nondescanned PMT detectors. Two-photon excitation wavelength was 800 nm supplied by a MIRA-900 titanium:sapphire laser (Coherent).

CA3 pyramidal cells were located using widefield visible light transmission microscopy and impaled under visual control by sharp microelectrodes with resistance of 50 to 80 MΩ. Electrode tips were filled with 5 mM of fluorescent indicators in 4 M KCl and 20 mM HEPES (pH adjusted to 7.24), and backfilled with 3 M KCl in 20 mM HEPES. The presynaptic pipette contained Alexa 568 (Molecular Probes) while the postsynaptic contained Asante Calcium Green (Teflabs Inc., Austin, Texas). AxoGraph software (AxoGraph Scientific, Sydney, Australia) was used to acquire and analyze all electrophysiological data, and LaserSharp (Biorad Microscience, Hemel Hempstead, UK) and ImageJ (http://rsb.info.nih.gov/ij) softwares were used to collect and analyze images.

4.2.4 Paired recordings

Recordings were made from two nearby pyramidal cells (up to 80 μm apart; discussed in more details in Chapter 5). Synaptic connections were confirmed in the direction of presynaptic (Alexa-filled) to the postsynaptic (Asante Calcium Green-filled)

cell by injecting depolarizing current into the presynaptic cell and recording the corresponding postsynaptic EPSPs. Fluorescent indicators were introduced to cells by applying intermittent (200 ms) hyperpolarizing currents of -50 to -200 pA for 10 to 45 minutes using a Multiclamp 700B amplifier (Molecular devices, California) and adequate dye filling was confirmed visually.

4.2.5 Localizing an active synapse

To localize the active synapse between the CA3 pair the dendritic tree of the postsynaptic Asante Calcium Green-filled cell was imaged and systematically searched for a spine with an evoked postsynaptic calcium transient (EPSCaT) while stimulating the presynaptic cell via direct current injection. Double- or triple-pulse presynaptic current injections separated by 50 ms interstimulus intervals were used for the spine search to increase the likelihood of finding spines with even low release probability (P_r). For the duration of data collection single or double pulses were used.

4.2.6 Baseline data collection

Somatically recorded baseline EPSPs and line scan images of EPSCaT for estimating P_r were collected followed by a baseline z-scan of the active synapse. Line scans were collected over the responsive spine and if possible also a segment of the dendritic shaft or soma. EPSCaTs were expressed as percent fractional change in

fluorescence: % $\Delta F/F = 100 (F_{transient} - F_{initial})/(F_{initial} - F_{background})$, where $F_{initial}$ is the mean fluorescence intensity of the imaged spine over a 50 to 100 ms period prior to stimulation, and $F_{transient}$ was measured over 40 to 50 ms. Z-stack images were collected over ± 2 μm from the focal point of the synapse in 0.5 μm steps.

4.2.7 Inducing plasticity

To induce plasticity, spike timing-dependent plasticity (STDP) protocols were used, where pre- and postsynaptic action potentials were evoked by direct current injection (Bi & Poo, 1998, 2001; Feldman, 2012). LTP-inducing protocols consisted of a single presynaptic action potential followed by one to three postsynaptic action potentials at a delay of 10 to 30 msec, repeated 100 times at 0.3 Hz. For LTD induction, the order of firing was reversed so that the postsynaptic action potentials preceded the presynaptic one by ~15 msec. LTP induction was carried out when initial release probability was low or moderate, and LTD was induced when baseline P_r was already high, to avoid ceiling and floor effects (Bolshakov & Siegelbaum, 1995).

4.2.8 Post-STDP data collection

After the STDP protocol, a second z-scan was acquired, as well as a collection of post-STDP EPSPs and EPSCaTs for P_r measures. Z-scans were recorded at one to two minutes upon completion of STDP. EPSP and EPSCaT recordings commenced at 15 to

25 minutes post STDP at 30 second intervals for 10 to 20 minutes. After each experiment, images of the CA3 pairs were also collected. EPSPs were measured at the soma with an intracellular sharp microeletrode, and expressed as mean ± S.E.M. P_r values are calculated by the success or failure of EPSCaT at the imaged spine (Emptage *et al.*, 1999; Reid *et al.*, 2001; Enoki *et al.*, 2009). Spine and bouton sizes were measured in grey scale plots of the fluorescent z-stacks images and the number of pixels occupied by the fluorescent peaks corresponding to the spine or bouton structure were compared before and after LTD induction in x and y directions (Figures 4.6, 4.7 and 4.8).

4.2.9 Statistical analysis

Statistical analyses were performed with IBM SPSS statistical predictor software (htpp://www.ibm.com/analytics/us/en/technology/spss); p values refer to two-tailed t tests.

4.2.10 Experimental steps summarized

i. Paired recordings are made from nearby CA3 pyramidal cells
ii. Synaptic connection between pair confirmed (with preferred direction)
iii. Load cells with indicators
iv. Localization of active synapse by imaging synaptically-evoked calcium transients in the dendritic spine

v. Record baseline EPSP, EPSCaT, z-scan

vi. Induce synaptic plasticity by STDP

vii. Post-STDP z-scan, EPSP, EPSCaT

viii. Data analysis

4.3 Results

Applying our multifaceted approach (Figure 4.1) we were able to get coincident readouts of somatically recorded EPSPs; optically recorded EPSCaTs at the active synapse, and thus get a readout of P_r; could induce plasticity in pairs of CA3 pyramidal cells; observe and locate the cell pair and exact location of synapse; and importantly monitor each of these parameters as the cell pair experienced plasticity induction. Completed full experiments are labeled I, II, and III and are summarized in Table 4.1.

4.3.1 Synaptic connections between nearby CA3 cells can be routinely observed

Recording intracellularly from pairs of pyramidal neurons in the CA3 region of rat OHSC (Figure 4.1) we find a high likelihood of synaptic connection between nearby CA3 cell pairs. On average 50 to 70 % of paired recordings were coupled via chemical synapses; approximately half of those were connected in one way only and the other half were connected both ways (for further details see Chapter 5). Thus, upon recording from any given two cells in the above-mentioned way we approximately had a 35 % to 55 % chance to proceed with our experiments in the intended way: that is, with cytoplasmic marker in the presynaptic cell and calcium indicator in the postsynaptic cell.

4.3.2 Localization of an active synapse by imaging synaptically-evoked calcium transients in the dendritic spine

Loading both neurons with structural or calcium-sensitive dyes, we can visualize the neuron pair, and consequently localize the active synapse by functional imaging of the EPSCaT (Figure 4.3), and can thus study morphological and functional changes in the pre- and postsynaptic compartments undergoing synaptic plasticity. We achieved this by stimulating the presynaptic cell via current injection while we systematically searched the dendritic tree of the Asante Calcium Green-filled, postsynaptic CA3 cell for a responding spine, i.e., a spine with an EPSCaT. EPSCaTs were recorded in line-scan mode and were classified as either success (Figure 4.3/C) or failure (Figure 4.3/D), with success indicating a $\Delta F/F$ value above noise level (and consequently, failures as below the noise level). Based on previous work from this laboratory, the probability of a successful EPSCaT can then be used to reliably calculate the release probability (P_r) of that synapse (Emptage *et al.*, 1999, 2003; Reid *et al.*, 2004; Enoki *et al.*, 2009). In addition to obtaining EPSCaTs we also recorded somatic EPSPs via the sharp intracellular microelectrode in response to presynaptic current injections and subsequent action potentials.

Active spines were found in various locations on the postsynaptic cell, including soma, apical and basal dendrites. However, in the case of complete experiments, the active spine was always close to the soma. Specifically, it was twice located on the soma,

and in one case the spine was found on a dendritic branch in close proximity to the cell body.

After the successful localization of an active synapse between pairs of CA3 cells, a z-scan image of the synapse was collected just before plasticity induction, right after baseline measures of EPSPs and EPSCaTs.

4.3.3 Synaptic plasticity in CA3 neuron pairs

Applying LTP- or LTD-inducing protocols to synaptically connected CA3 pairs (Figure 4.2), had varying results. While all three LTD-inducing STDP experiments resulted in a concomitant decrease of both EPSP and P_r values, the two LTP-inducing experiments did not show reliable potentiation. Therefore, out of a total of five completed experiments only the three LTD experiments were included in further analysis, labeled throughout as Experiment I, II and III (Figures 4.4, 4.5 and Table 4.1).

In the three cases of LTD induction EPSP amplitudes and P_r values decreased simultaneously after running an STDP protocol (Figures 4.4 & 4.5 and Table 4.1). In Experiment I although EPSP amplitudes decreased from 7.46 ± 0.23 to 5.74 ± 1.69 mV after the LTD-inducing STDP protocol, the variance of post-STDP EPSP amplitudes was large and values did not reach significance (Figures 4.4/A & 4.5/A). Concomitant change in P_r was from 0.9 to 0.37 (Figures 4.4/B & 4.5/B).

In Experiments II and III, the changes in EPSP and P_r values were more pronounced: EPSP amplitudes changed significantly from 2.83 ± 0.76 mV to 0.2 ± 0.43 mV in Experiment II, and 5.94 ± 0.28 mV to 2.07 ± 0.38 mV in Experiment III (Figures 4.4/A & 4.5/A), and the concomitant decrease in P_r values were from 0.76 to 0.21 and from 0.93 to 0.29 (Figure 4.4/B & 4.5/B). The mean EPSP and P_r values of all three LTD experiments before and after STDP induction changed significantly from 5.41 ± 1.67 to 2.67 ± 0.52 mV ($P < 0.0001$) and from 0.87 to 0.29 ($P < 0.0001$), respectively (Figure 4.5).

4.3.4 Structural plasticity of recurrent CA3-CA3 synapses

Once an active synapse was located, confirmed by EPSCaT restricted to the dendritic spine, z-stack images were obtained of the pre- and or postsynaptic compartment just before inducing plasticity and right after the STDP application (Figures 4.6, 4.7 and 4.8). In Experiments I and II the active spine was on the cell body where the fluorescent signal is typically most pronounced (Figures 4.6 & 4.7). It was therefore challenging to simultaneously image the presynaptic bouton without damaging the postsynaptic compartment. This was further challenged by occasional suboptimal dye-loading in the presynaptic cell as axons of CA3 cells are particularly fine and the active bouton could be far from the cell body, therefore making dye infiltration difficult. In Experiment III, however, wherein the spine was far removed from the soma, the

presynaptic, overlapping axon was clearly visible and z-scan images could be acquired (Figure 4.8).

Spine and bouton sizes were measured in grey scale plots of the fluorescent z-stacks images and the number of pixels occupied by the fluorescent peaks corresponding to the spine or bouton were compared before and after LTD induction in x and y directions (labeled by blue brackets on grey scale plots; Figures 4.6, 4.7 and 4.8). We found that neither in Experiment I (Figure 4.6) nor in Experiment II (Figure 4.7) was there a significant change in the size of the imaged spine (note that size of synapse is evaluated by pixel count and not fluorescence intensity). For Experiment I corresponding pixel sizes at baseline were from 115 to 123 in x direction and 175-186 in y direction; post-LTD these were 115-123 in x direction and 176-187 in y direction (Figure 4.6). For Experiment II baseline pixel sizes were 82-89 in x direction and 107-112 in y direction; while post-LTD the spine corresponded with pixels 83-90 and 107-111 in x and y direction, respectively (Figure 4.7). Similarly, in the one case of Experiment III where the bouton was clearly visible, its size also did not change significantly as pixels occupied by the bouton at baseline were 153-168 and 83-104 in x and y direction, respectively, and post-LTD these were 154-169 and 85-105 (Figure 4.8/A-H). In Experiment III the z-stack image of the dendritic spine is somewhat compromised (Figure 4.8/ I & J), making measurement of spine size changes ambiguous; therefore these are not included.

4.5 Discussion

The existence and degree of structural plasticity accompanying LTP or LTD has been debated for many decades now. Reports vary from no volume change to transient, to sudden, to delayed growth of the spine head as well as changes to the length and diameter of the spine neck (Lee *et al.*, 1980; Hosokawa *et al.*, 1995; Buchs & Muller, 1996; Stewart *et al.*, 2005; Harvey & Svoboda, 2007; Nägerl *et al.*, 2008; Tanaka *et al.*, 2008; Urban *et al.*, 2011; Tønnesen *et al.*, 2014; Meyer *et al.*, 2014; Tang & Yasuda, 2017). Where these reports link LTP and spine growth, or alternatively LTD and spine shrinkage, it is unclear how these phenomena relate to each other and what the functional significance of the observed structural changes might be.

Here we report an alternative approach of working with pairs of identified neurons to study the pre- and postsynaptic morphological and physiological changes at active synapses undergoing plasticity (Figure 4.1). We achieved this by using rat OHSC in which we combine electrophysiological recordings and two-photon calcium imaging of pairs of CA3 pyramidal cells. This method allows for a direct control and observation on physiological presynaptic activity on the postsynaptic cell. Furthermore it allows us to localize active synapses by monitoring EPSCaTs. Plasticity at these associational CA3 connections can be induced by precisely timing the pre- and postsynaptic action potential firing (Figure 4.2), and can be monitored simultaneously by two parameters, EPSP amplitude and P_r. These experiments were difficult and only five experiments were carried through to completion, and only three of these, all with LTD protocols, yielded

unambiguous plasticity. Even though the number of successful experiments is limited, our observations suggest that LTD induced via physiological stimulation does not cause significant changes in the size of either the spine or bouton, in keeping with some published reports (Chang & Greenough, 1984; Sorra & Harris, 1998; Bourne & Harris, 2011; Wiegert & Oertner, 2013) but not others (Okamoto *et al.*, 2004; Zhou *et al.*, 2004; Wang *et al.*, 2007; Bastrikova *et al.*, 2008; Oh *et al.*, 2013).

Evidence for non-identical induction or signaling pathways for LTD and spine shrinkage has been described (Wang *et al.*, 2007; Bastrikova *et al.*, 2008; Wiegert & Oertner, 2013). Specifically, Wang and colleagues showed that LFS in acute hippocampal slices caused LTD and a decrease in spine head diameter (Wang *et al.*, 2007). However, when they prevented spine shrinkage by blocking endogenous cofilin activation LTD expression was not affected, thus indicating that LTD does not *require* a simultaneous shrinkage of the spine. Similarly, when LTD was inhibited LFS could still reduce the size of spine heads, indicating that LTD and spine shrinkage are independent (Wang *et al.*, 2007). Furthermore, trafficking of AMPARs, previously suggested by others as possibly contributing to changes in spine size during plasticity (Park *et al.*, 2004, 2006; Kennedy *et al.*, 2010), did not lead to changes in spine size, but inhibiting actin polymerization, abolished both LTD and spine shrinkage (Wang *et al.*, 2007). Although Wang *et al.* showed that LTD and spine shrinkage could be induced independently, in contrast to our results they readily observed spine shrinkage with LFS. This difference might be due to the fact that Wang used juvenile rats for their experiments, and used a glass pipette positioned at just 20 to 30 μm away from the

imaged spines which stimulated a patch of dendrites with multiple spines. The physiological nature of these experiments is thus questionable and obtained results might not be relevant to mature spines (Macdougall & Fine, 2013).

While a few studies, including ours, do not detect spine enlargement or shrinkage upon LTP or LTD induction respectively (Hosokawa *et al.*, 1995; Stewart *et al.*, 2005; Sdrulla & Linden, 2007; Wiegert & Oertner, 2013), at present the general consensus is that LTP and LTD at simple synapses of hippocampal pyramidal cells are necessarily associated with fast, large, and selective synapse growth or shrinkage (Matsuzaki *et al.*, 2004; Harvey & Svoboda, 2007; Bosch & Hayashi, 2012; Zhang *et al.*, 2013; Meyer *et al.*, 2014; Stein *et al.*, 2015). What could potentially explain this difference? Importantly, the majority of reports supporting synapse growth in LTP or shrinkage in LTD use direct glutamate uncaging. With this method, Matsuzaki *et al*. first reported a rapid and selective enlargement of 100 % of small spines and 90 % of large spines (Matsuzaki *et al.*, 2004). These changes were often transient; in only 30 % of cases was there a persistent change in spine size. The lack of significant change regarding the size of the synapses in our experiments could perhaps be explained by considering the possibility that they all are large spines and thus less likely to be affected by structural alterations (Matsuzaki *et al.*, 2004). Alternatively, since Matsuzaki used juveniles it is likely that they imaged immature or silent synapses. Therefore their results might not be applicable to more mature synapses used in our experiments (Durand *et al.*, 1996; Matsuzaki *et al.*, 2001; Macdougall & Fine, 2013; Watson *et al.*, 2016). In addition, spine growth observed by Matsuzaki and others may have been an artifact of glutamate uncaging, which can

lead to glutamate spillover and potentially activation of extra-synaptic glutamate receptors (Scanziani *et al.*, 1997; Kullmann & Asztély, 1998; Rusakov & Kullmann, 1998; Scimemi *et al.*, 2004). Thus conclusions on structural changes in plasticity need to be based on more physiological recording and stimulating methods.

One of the more physiological LTP and LTD inducing protocols is STDP. Notwithstanding how STDP protocols are commonly used to induce LTP or LTD at pyramidal cells of the rat hippocampus (Bi & Poo, 1998; Debanne *et al.*, 1998; Meredith *et al.*, 2003; Wittenberg & Wang, 2006), our STDP results were varied: LTD induction was successful but not LTP induction. To account for this variability the following points need to be considered. Feed-forward $GABA_A$ inhibition was not controlled for in our experiments and may therefore have contributed to the lack of potentiation despite our completed STDP protocol (Meredith *et al.*, 2003). It has also been shown that some synapses are non-potentiable (Debanne *et al.*, 1999), and that LTP induction in adults require multiple postsynaptic action potentials in STDP pairing protocols (Pike & Meredith, 2004; Buchanan & Mellor, 2007) unless GABA inhibition is suppressed (Meredith *et al.*, 2003). We did in fact use three postsynaptic action potentials but no GABA blocker, which might have compromised our ability to induce LTP. In addition it has been shown before that the success of LTP induction depends on the initial strength of the synapse, as pairs with high initial EPSCs failed to potentiate (Bi & Poo, 1998). Indeed connections in our two experiments wherein potentiation failed had high summated baseline EPSP values (9.65 ± 0.55 and 11.16 ± 1.33 mV) but EPSP amplitudes for single synapses were not obtained. Moreover, it has been proposed that the location of

the active synapse might influence the effectiveness of STDP protocols, e.g., how AP back-propagation, or its possible failure, to distant synapses might alter plasticity (Kampa *et al.*, 2007; Kim *et al.*, 2012; Mishra *et al.*, 2016).

In all three LTD experiments the visualized synapse was on a spine located very close to the cell body and had an initial P_r of 0.76 or higher. Although we identified active spines further away from the soma (Figure 4.9) on second and third order branches, those recordings were lost prematurely and results could not be included in our plasticity analysis. In all completed experiments after finding the first responsive postsynaptic spine we did not search for additional active synapses simply because of the feasibility of holding reasonably healthy recordings for the required amount of time. Thus our approach is arguably biased but not limited to spines in close proximity of the cell body.

With our paired recording method, we can trigger presynaptic action potentials and report success and failure of synaptic transmission by imaging postsynaptic EPSCaT. Conversely, extracellular stimulation of axon bundles and monitoring of postsynaptic signals cannot differentiate between failure of stimulation, action potential generation, or transmitter release (Debanne *et al.*, 2008). However, even our methods are not able to identify silent synapses, excluding this population from the spine search and further manipulations (Kullmann, 1994; Isaac *et al.*, 1995; Gomperts *et al.*, 1998; Kerchner & Nicoll, 2008). Nonetheless, the number of such silent synapses decreases with longer maturation time and might not represent a large portion of missed synapses in our experiments (Liao *et al.*, 1995; Durand *et al.*, 1996; Hsia *et al.*, 1998). In addition,

structural and functional plasticity at silent synapses might employ alternative and/or developmentally restricted mechanisms not applicable to non-silent, mature spines (Isaac *et al.*, 1995; Ward *et al.*, 2006; Macdougall & Fine, 2013).

Our observations, although limited at present, suggest that synaptic plasticity and structural changes of the synapse can be dissociated. However, it does not exclude the possibility that a population of synapses (potentially silent and/or smaller spines or other than CA3-CA3 recurrent synapses) can undergo morphological changes during plasticity especially in the developing brain, or that there may be a delayed expansion or shrinkage of synapses at later time points which we did not include in our experiments (Zhou *et al.*, 2004; Wiegert & Oertner, 2013).

Most published accounts on structural plasticity use EGFP or other structural markers for labeling and measuring dendritic spines whereas we used a structural dye presynaptically and a calcium dye postsynaptically, which allowed us to identify active synapses. A potential caveat of using calcium indicators could be to misinterpret volumetric changes for changes in dye infiltration or intracellular calcium concentration dynamics. However, our spine search only commenced after visually confirming sufficient dye-filling in distal dendrites and spines, after which active dye-loading was terminated. In addition, experiments where dye saturation was detected at any time point were excluded. The presynaptic structural marker did not warrant such precautions.

The resolution limit of our two-photon microscope is ~250 nm, therefore small changes in bouton or spine sizes might have been missed with our current setup (Chéreau *et al.*, 2017). Importantly, however, published studies report spine size changes of ~200

to 400 % at one to four minutes (Matsuzaki *et al.*, 2004; Murakoshi *et al.*, 2011), a change that would have been clearly identifiable in our experiments.

Several groups have reported that with a variety of plasticity induction protocols the length and/or width of the dendritic spine neck may change (Fifkova & Anderson, 1981; Trommald *et al.*, 1990; Tanaka *et al.*, 2008; Urban *et al.*, 2011; Tønnesen *et al.*, 2014; but see Lee *et al.*, 1980; Chang & Greenough, 1984; Buchs & Muller, 1996). Tønnensen and colleagues proposed that if the spine head enlarges and the neck widens during LTP then the overall biochemical compartmentalization of the spine remains unchanged (Tønnesen *et al.*, 2014). However, the simultaneous spine neck shortening and widening may result in a significant drop in spine EPSP amplitudes and a substantial change in electrical coupling. These modifications regarding the size of the spine neck might therefore have strong implications for compartmentalization and changes of synaptic weight in LTP or LTD (Noguchi *et al.*, 2005; Gulledge *et al.*, 2012; Harnett *et al.*, 2012; Yuste, 2013). In our experiments, however, we did not investigate morphological alterations regarding the spine neck as the resolution of our two-photon microscope was inefficient. These issues, along with measurements of axonal diameter (Chéreau *et al.*, 2017), might be better addressed with super-resolution stimulated emission depletion (STED) microscopy (Hell & Wichmann, 1994; Klar *et al.*, 2000) which can provide lateral resolution of ~50 nm (Tønnesen & Nägerl, 2013).

Overall, in agreement with Wiegert and Oertner (Wiegert & Oertner, 2013) our studies provide evidence against large and short-term changes in spine and bouton morphology following LTD induction.

Figure 4.1 Paired recordings in area CA3 of organotypic hippocampal slice cultures. **(A)** Conventional electrophysiological recordings using an extracellular stimulating electrode (blue) to excite a bundle of unidentified axons (Schaffer collaterals; S/A) and a recording electrode (red). **(B)** Simultaneous recording and stimulation of pairs of identified CA3 pairs connected through recurrent axonal projections (commissural/ associational; C/A; encircled). **(C)** Example of paired recording with sharp intracellular microelectrodes attached. Presynaptic cell is loaded with a structural marker (red) and postsynaptic cell is filled with a calcium dye (green). **(D)** Representative recording from such pairs in (C). Upper trace shows direct current injection (red) and bottom trace shows over-laid postsynaptic responses to presynaptic stimulation (green).

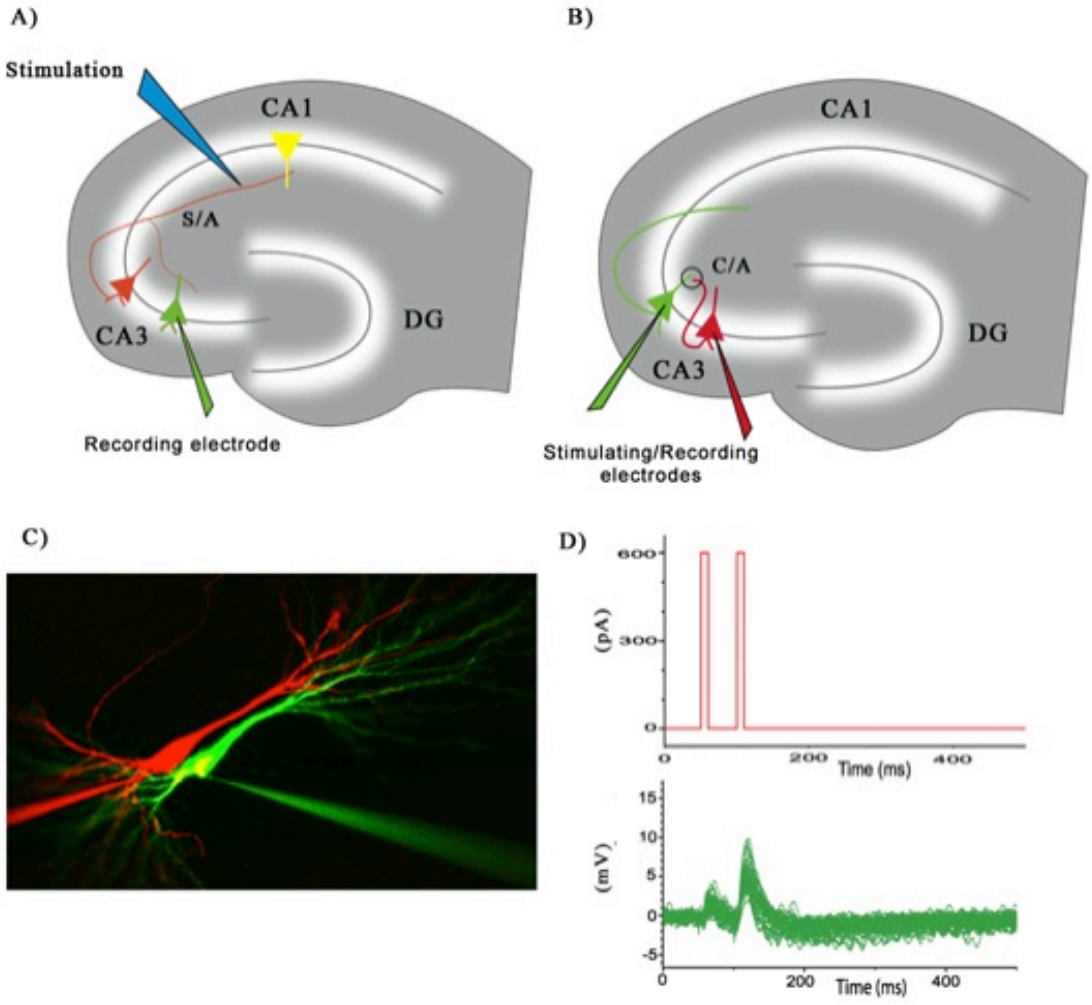

Figure 4.1 Paired recordings in area CA3 of organotypic hippocampal slice cultures.

Figure 4.2 Representative LTP-inducing spike timing-dependent plasticity (STDP) protocol in pairs of CA3 pyramidal cells. **(A)** Current command for presynaptic (red) and postsynaptic (green) cells to elicit action potentials for STDP induction. Pairing of pre- and postsynaptic action potentials are repeated 100 times. **(B)** Overlaid membrane potential changes in presynaptic (red) and postsynaptic (green) cells. **(C)** Representative EPSP recordings at baseline (blue) and after LTP-inducing STDP protocol (yellow) with mean EPSP amplitudes indicated by red dashed line.

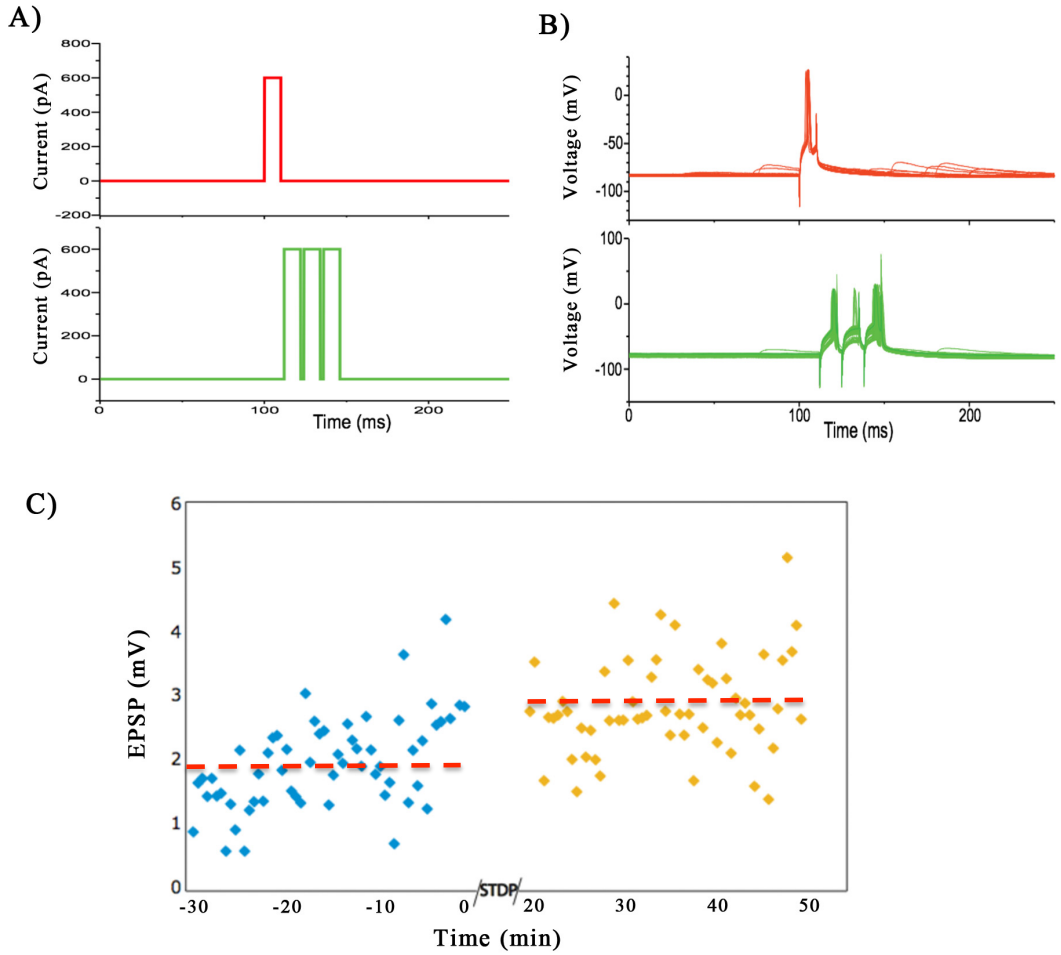

Figure 4.2 Representative LTP-inducing spike-timing-dependent plasticity in pairs of CA3 pyramidal cells.

Figure 4.3 Calcium imaging in active dendritic spine of CA3 pyramidal cells. **(A)** Fluorescent images of presynaptic (green) and postsynaptic (red) cells with sharp intracellular electrodes attached. White box indicates image in (B). **(B)** Higher magnification image of white box in (A), responsive spine encircled in white, position of line scan indicated with white dashed line. **(C)** Representative line scan image of a failure of synaptic transmission, indicated by the lack of increase in fluorescence. **(D)** Success of synaptic transmission showing EPSCaT, clearly distinguishable from failure in (C). Lower traces in (C) & (D) are unaveraged quantified fluorescence traces corresponding to failure or success, respectively. White dashed line in fluorescent traces indicate the time of presynaptic stimulation.

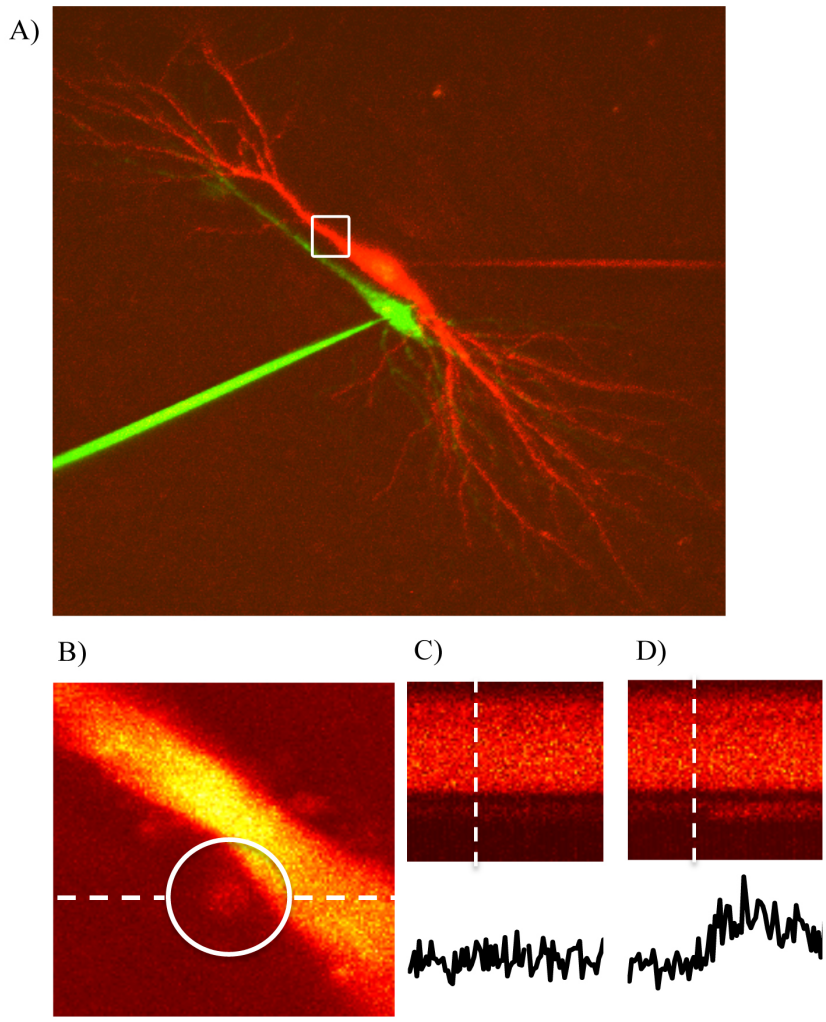

Figure 4.3 Calcium imaging in active dendritic spine of CA3 pyramidal cells.

Figure 4.4 Summary of EPSP and P_r changes with LTD-inducing STDP protocol in Experiments I, II, and III. **(A & B)** Pre-LTD EPSP and P_r values are indicated in dark grey and post-LTD EPSP and P_r values are indicated in light grey. Panel (A) shows mean EPSP values in mV ± S.E.M., and panel (B) indicates P_r values.

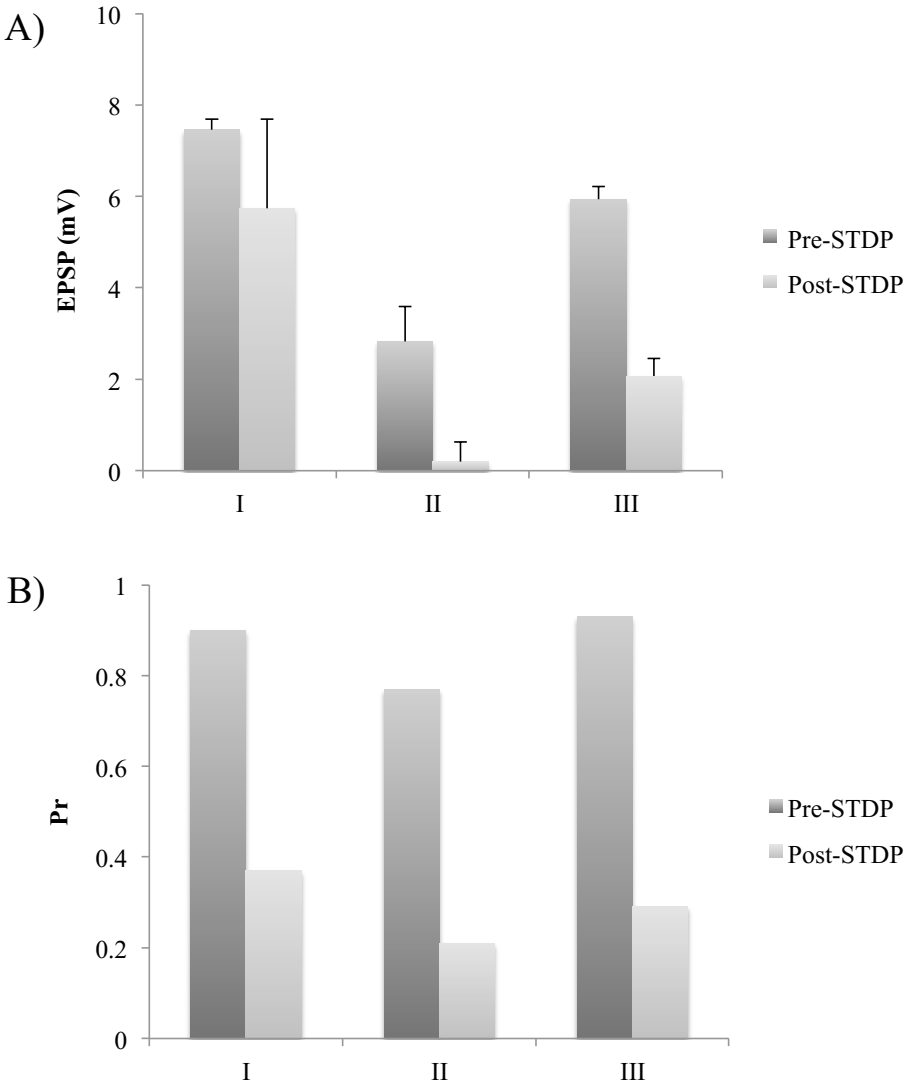

Figure 4.4 Summary of EPSP and P_r changes with LTD-inducing STDP protocol in Experiments I, II, and III.

Figure 4.5 EPSP and P_r changes at baseline and Post-STDP in all LTD experiment. **(A)** Change in EPSP amplitudes for individual LTD experiments I, II, III are shown in grey and their mean EPSP change is shown in red. **(B)** Corresponding change in P_r values for individual experiments I, II, and III are grey, their mean is in red colour. Statistical significance is indicated by P values above each graph, error bars show ± S.E.M.

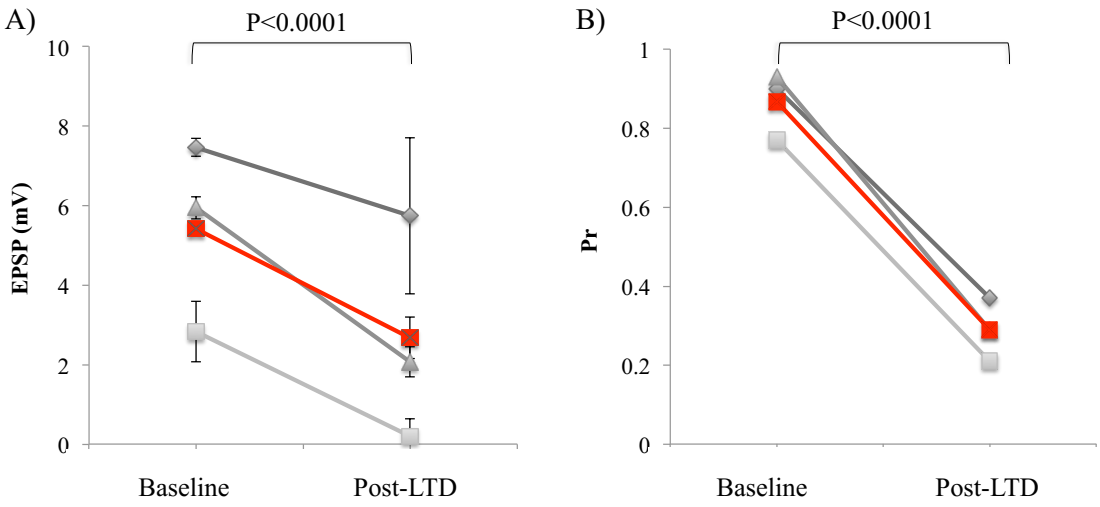

Figure 4.5 EPSP and P_r changes at baseline and Post-STDP in all LTD experiment.

Figure 4.6 Spine size measurements for Experiment I including z-stack images and corresponding grey values of the fluorescent images in x and y directions. White dashed lines on the fluorescent images indicate the location of line scans, and blue circles indicate the location of the active spine. Blue brackets in grey value graphs indicate the size of the corresponding dendritic spine, measured as number of pixels in x and y directions. Left column **(A, C, E & G)** shows images of spine at baseline, pre-LTD, whereas the right column **(B, D, F & H)** shows post-LTD images. (**A, B, C & D)** are measurements in x coordinate, and (**E, F, G, & H)** are measurements in y coordinate.

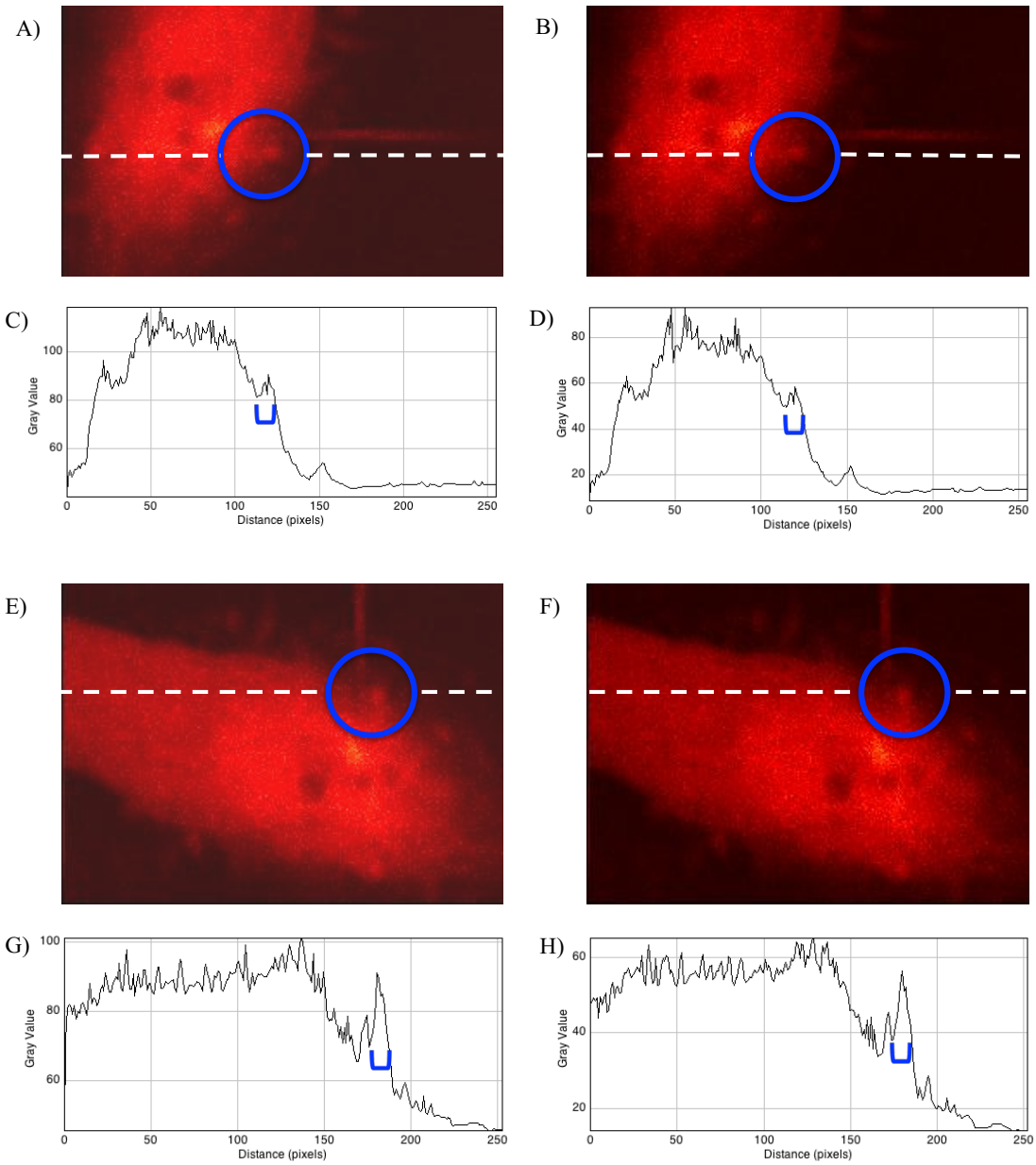

Figure 4.6 Spine size measurements for Experiment I including z-stack images and corresponding grey values of the fluorescent images in x and y directions.

Figure 4.7 Spine size measurements for Experiment II including z-stack images and corresponding grey values of the fluorescent images in x and y directions. White dashed lines on the fluorescent images indicate the location of line scans, and blue circles indicate the location of the active spine. Blue brackets in grey value graphs indicate the size of the corresponding dendritic spine, measured as number of pixels in x and y directions. Left column **(A, C, E & G)** shows images of spine at baseline, pre-LTD, whereas the right column **(B, D, F & H)** shows post-LTD images. (**A, B, C & D)** are measurements in x coordinate, and (**E, F, G, & H)** are measurements in y coordinate.

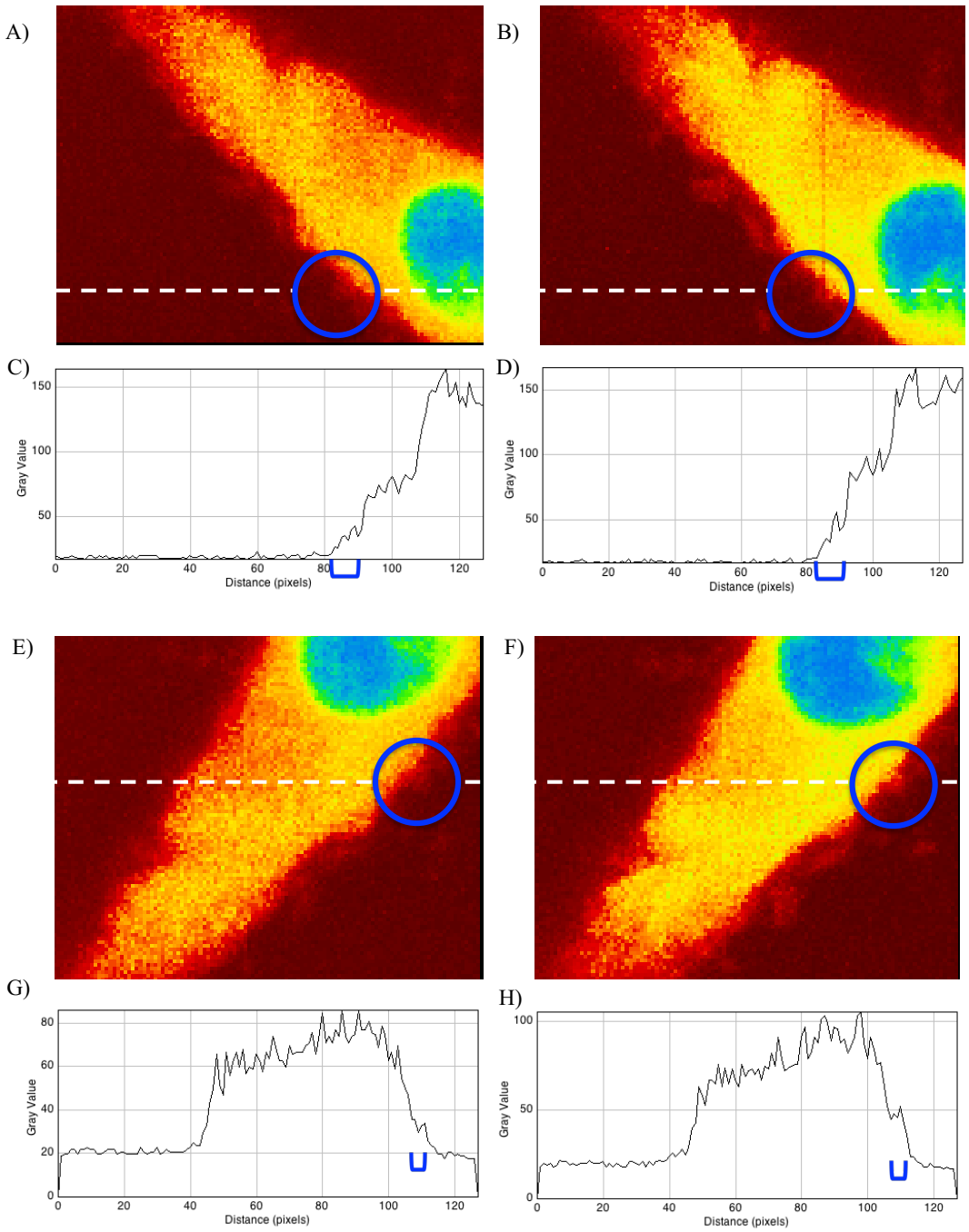

Figure 4.7 Spine size measurements for Experiment II including z-stack images and corresponding grey values of the fluorescent images in x and y directions.

Figure 4.8 Comparison of bouton and spine at baseline and post-LTD in Experiment III. Bouton measurements are shown in **(A-H)** and responding spine is shown in **(I & J)**. Bouton and spine are shown in z-stack images and corresponding grey values of the fluorescent images are indicated for the bouton. White dashed lines on the fluorescent images indicate the location of line scans, and blue circles indicate the location of the active spine. Blue brackets in grey value graphs indicate the size of the corresponding bouton, measured as number of pixels in both directions. Left column **(A, C, E, G & I)** shows images of bouton and spine at baseline, pre-LTD, whereas the right column **(B, D, F, H & J)** shows post-LTD images. **(A, B, C & D)** are measurements in x coordinate, and **(E, F, G, H)** are measurements in y coordinate.

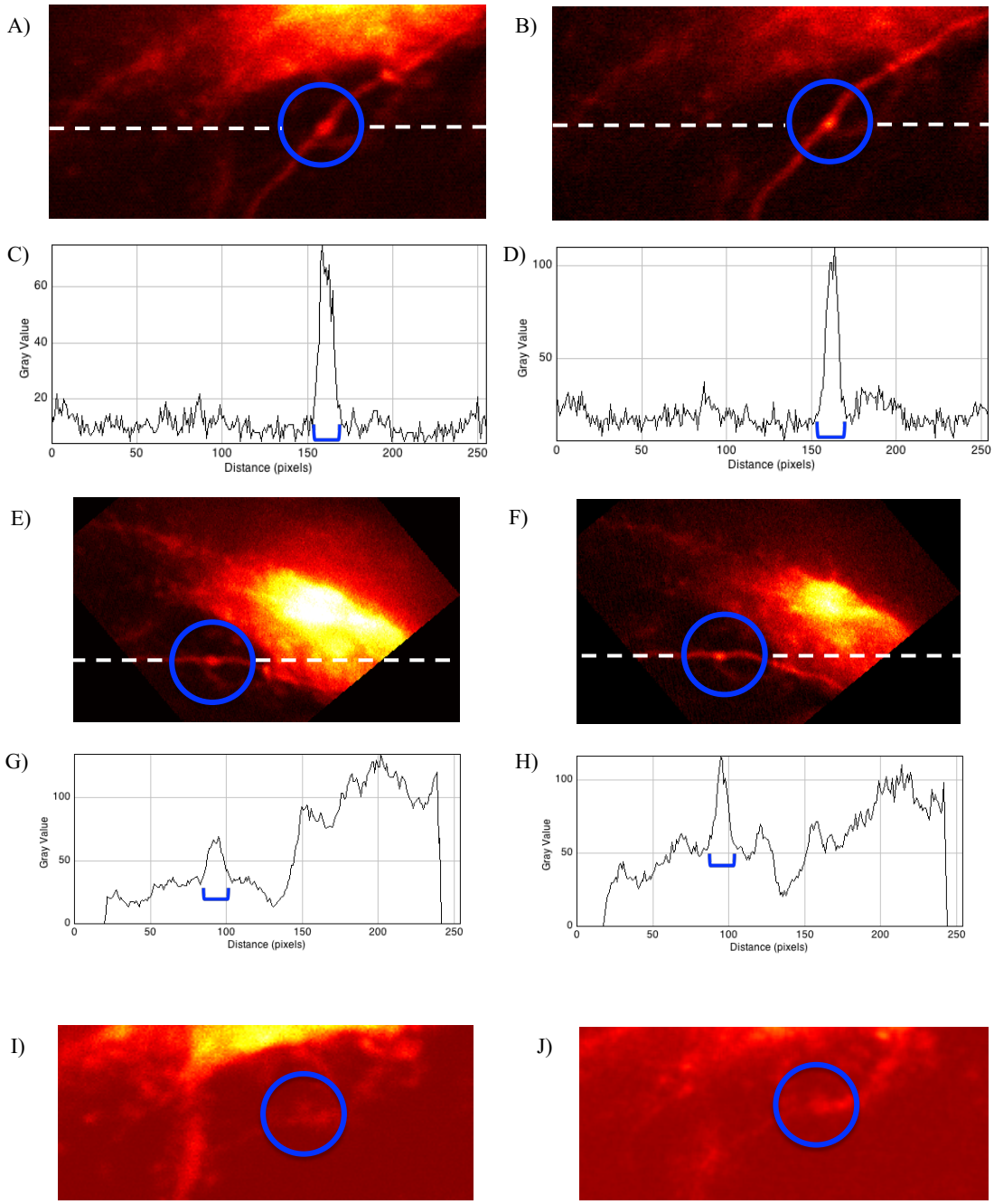

Figure 4.8 Comparison of bouton and spine at baseline and post-LTD in Experiment III.

Figure 4.9 Representative experiment with active spine located on a distal dendrite. **(A)** Presynaptic cell is labeled in red and postsynaptic cell in green. Location of active synapse in encircled in yellow, depicting both bouton and spine. **(B)** Examples of ESPCaT failure on left and success on right image. **(C)** Z-stack image of presynaptic cell, where bouton is encircled in yellow. **(D)** Z-stack image of postsynaptic cell with spine encircled in yellow.

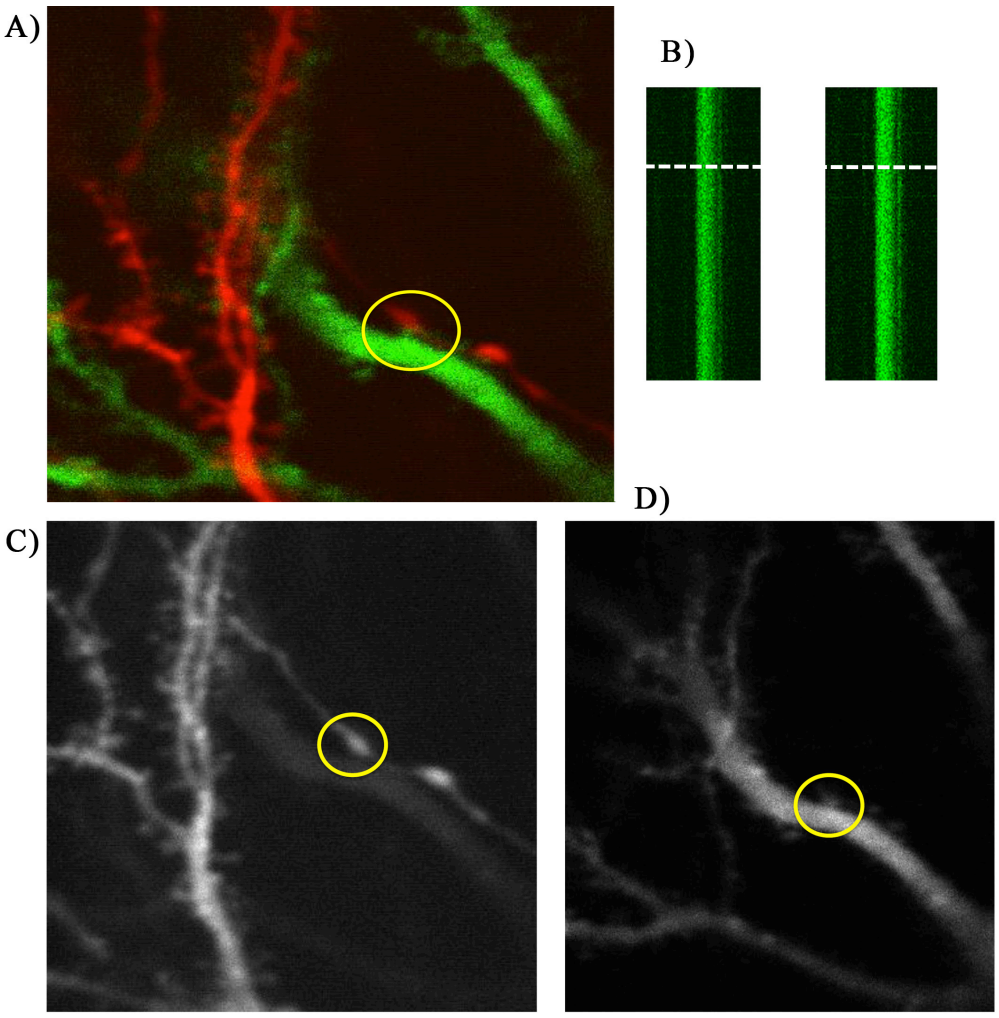

Figure 4.9 Representative experiment with active spine located on a distal dendrite.

Table 4.1 Summary table of Experiments I, II and III indicating EPSP and P_r values at baseline (Pre-STDP), and after STDP (Post-STDP), specification for STDP protocol used, and change in synapse size. All EPSP values are shown in mV, ± values indicate S.E.M.

	EPSP (mV) Pre-STDP	EPSP (mV) Post-STDP	P_r Pre-STDP	P_r Post-STDP	STDP Protocol	Change in synapse size
I.	7.46 ± 0.23	5.74 ± 1.69	0.90	0.37	LTD	No change in spine size
II.	2.83 ± 0.76	0.2 ± 0.43	0.76	0.21	LTD	No change in spine size
III.	5.94 ± 0.28	2.07 ± 0.38	0.93	0.29	LTD	No change in bouton size; Spine size?

Table 4.1 Summary table of experiments I, II, III.

CHAPTER 5

OPTIMIZATION OF PAIRED RECORDINGS IN AREA CA3 OF THE RAT ORGANOTYPIC HIPPOCAMPAL SLICE CULTURE

5.1 Introduction

The development of slice preparations from different brain regions, including the organotypic hippocampal slice cultures (OHSC) has indisputably accelerated the feasibility of paired recordings as well as modern day neuroscience as a whole (Andersen *et al.*, 2007). *In vitro* brain slice preparations were first introduced by Henry McIlwain who made horizontal neocortical and piriform cortex slices, followed by successful intracellular recordings and manipulations in such preparations (Li & McIlwain, 1957; Yamamoto & McIlwain, 1966*a*, 1966*b*; Collingridge, 1995). The technique was further advanced by the introduction of Skrede and Westgaard's transverse hippocampal slices, cut perpendicular to the longitudinal axis, which conserved the principal cell layers and the lamellar organization of major pathways of the hippocampus (Andersen *et al.*, 1971; Skrede & Westgaard, 1971). Although such acute slice preparations are arguably useful, as they are the closest to an *in vivo* scenario, long-lasting preparations are desired for a number of experiments, including investigation of chronic applications and effects of various treatments, as well as for an increased chance of obtaining paired recordings

(discussed further below). The latter is still the most irrefutable way to gain information about how one neuron effects another.

Two major avenues were taken for preparing OHSC: Gähwiler introduced the roller-tube method, in which slices are plated on glass and are slowly rotated between the gas and liquid interface providing the metabolic needs of the culture (Gähwiler, 1981*a*). This rotation thins the slices out to a monolayer over time, making this preparation particularly attractive for easy access to cells and optical studies (Gähwiler, 1981*b*). When the near three-dimensional properties and near *in vivo* characteristics of the slice is preferred, however, Stoppini's membrane interface techniques is suggested (Stoppini *et al.*, 1991). This preparation does not thin out but maintains its five to eight cell layer thickness.

Such OHSC offer unique advantages over acute slice preparations (Stoppini *et al.*, 1991; Gähwiler, 1997; Humpel, 2015). Stoppini's membrane interface OHSC maintains its three dimensional cytoarchitecture, and is allowed to recover from sectioning while in culture (Streit *et al.*, 1989; Gähwiler, 1997). Importantly, they are similar to acute slices in terms of gross tissue organization, dendritic morphology, synaptic transmission and synaptic plasticity (Gähwiler, 1997; De Simoni *et al.*, 2003). Even though projections are severed at the time of the slice preparation, this immediate loss of synaptic connections is later matched by formation of new synapses in OHSC (Sik *et al.*, 1993; De Simoni *et al.*, 2003). In fact, recurrent (and projection) synapses are substantially more pronounced in OHSC than in acute slice preparations making OHSC a particularly attractive preparation

to study pairs of CA3 cells (Miles & Wong, 1986; Sayer *et al.*, 1990; Thomson & Radpour, 1991; Debanne *et al.*, 1995, 1998, 1999).

The total length of CA3 axons is estimated to be 150 - 300 mm with an average of five to ten collaterals and 30 000 to 60 000 terminals, of which an approximately 30 - 70 % are made on other CA3 cells (Li *et al.*, 1994; Le Duigou *et al.*, 2014). However, factors such as type of preparation, time of preparation, and culturing time might alter the number of terminals and synaptic contacts significantly. Recordings from acute guinea-pig slices showed a very low, 1 to 2 % probability of recurrently connected CA3 cells (Miles & Wong, 1986). In sharp contrast to that, recurrent synapses are thought to be occurring on average in 30 to 60 % of recordings in OHSC. Pavlidis and Madison found an overall of 30 % (Pavlidis & Madison, 1999) and another study found a 56 % chance of CA3-CA3 connectivity, and a 33 % likelihood of reciprocal CA3 connections in hippocampal slice cultures (Debanne *et al.*, 1995) with some studies reporting a sub-regional difference (Ropireddy *et al.*, 2011). Moreover, the amount of synaptic connections could be increased by longer culturing time, and facilitating that is the possibility that OHSC can be maintained in culture for multiple weeks or even months (Zimmer & Gähwiler, 1984; Stoppini *et al.*, 1991). It is important to consider though that the health of the slice deteriorates over time, and that the principal cells of CA3 area are particularly sensitive to detrimental conditions (Spruston & McBain, 2007). Therefore, experiments aiming to study recurrent connections, especially of CA3-CA3, need to carefully identify a balance between healthy tissue and increased number of associational

axonal projections. This chapter aims to identify and characterize factors that make a possible contribution to the increased success of paired recordings.

Double electrophysiological recordings with simultaneous calcium imaging of nearby CA3 cells in the rat hippocampus, as it was evident in Chapter 4, are remarkably challenging. The consecutive experimental steps build on each other and cannot proceed without ideal conditions. Therefore, it is of exceptional importance to start by maximizing the likelihood of finding connected pairs in area CA3, that allow us to continue with the proceeding steps. Thus we conducted a systematic analysis of the probability of connection in OHSC relative to days *in vitro* (DIV), sub-region specificity, and distance between paired CA3 cells. The results of this study can contribute to the success of such sequential experimental approaches and gain a better understanding of such CA3-CA3 connections.

5.2 Materials and Methods

Animals used in this study were identical to those in Chapter 4. Furthermore, OHSC preparation, electrophysiological recordings and imaging were carried out as previously described in Chapter 4. The health of OHSCs was routinely accessed each day prior to recording by visually checking for smooth slice surface, lack of glia overgrowth, lack of shrunken or swollen cells, and slices visually deemed healthy were used for recordings. In addition, experiments were systematically categorized according to sub-region specificity of recordings, DIV, and the distance between the two CA3 cells from which recordings were made.

The location of each cell body was identified post-recording with lower magnification and classification of sub-region specificity was conducted according to the followings: Area CA3 was divided into three equal parts with CA3a being adjacent to CA2, followed by CA3b in the middle, and CA3c being closest to the DG (Figure 5.1). Pairs were sorted as being located in either sub-region CA3a, CA3b, CA3c, or alternatively as ambiguous, which were excluded from the analysis. Distance between cell pairs was determined between nearest edges of somas.

Statistical analyses of logistic regression, and where indicated, analysis of variance, were conducted with IBM SPSS statistical predictor software (http://www.ibm.com/analytics/us/en/technology/spss).

5.3 Results

5.3.1 Likelihood of recurrent connections between pairs of CA3 cells

A total of 106 experiments were included in the present study to assess the probability of recurrent connections between nearby CA3 cells, with n = 106 for the analysis of DIV, n = 92 for sub-region specificity, and n = 99 for evaluating effects of varying the distance between cell bodies. When impaling nearby pyramidal cells with sharp intracellular microeletrodes in area CA3 under visual control, on average 76 % of paired recordings were chemically coupled and out of that 76 % approximately 53 % were connected in one way only, and 47 % were connected both ways (Figure 5.2). Although the occurrence of electrical synapses between CA3 cells is low, occasional dye coupling, an indication of the existence of gap junctions between cells, was observed and such pairs were excluded from further analysis (MacVicar & Dudek, 1981; Perez-Velazquez *et al.*, 1994; Perez Velazquez & Carlen, 2000; Traub & Bibbig, 2000; Schmitz *et al.*, 2001).

A logistic regression analysis was conducted to ascertain the effects of DIV, sub-regional location and distance between cell bodies on the likelihood of connectivity. A test of the full logistic regression model was statistically significant (chi square = 15.941, $p < 0.005$). The analysis demonstrated that DIV made a significant contribution to the prediction ($p = 0.003$). Sub-regional location and distance between cell bodies did not reach significant values of prediction in the full model. However, an analysis of variance

on sub-regional specificity revealed that CA3c cells were significantly less likely to be connected than CA3a or CA3b ($p < 0.05$). The three factors, DIV, sub-regional location, and distance between cell pairs, and their relationship with the likelihood of recurrent connectivity, are discussed further in the sections below.

5.3.2 Correlation of days *in vitro* and the likelihood of connection

The DIV of the slice was a good predictor of the likelihood of connection between cell pairs ($p < 0.005$). By varying the maturation time of the slice in culture, we have noticed that the likelihood of connecting pairs increased over time in the following pattern (Figure 5.3). At 15 DIV or less only 56 % of CA3-CA3 pairs were connected, whereas this increased and reached even 100 % at 25 - 26 DIV when recording from healthy cells. The likelihood of connection remained high (82 to 100 %) up until 30 DIV, however by this time lesions, swollen cells, glia cells, and lack of a smooth slice surface were all more commonly observed compared to earlier time points. It appears that the health of the slice preparations were ideal around two weeks, nevertheless the chances of having connections between CA3 cells increased from 56 % to 90 % at two weeks versus at three weeks, respectively, which prompted us to propose using slices of three to four weeks in culture.

5.3.3 Sub-regional specificity

When we assessed sub-regional specificity in terms of probability of recurrent connection between pairs of CA3 cells, a clear difference was observed (Figure 5.4). The most connecting pairs at 85 % were located in sub-region b (CA3b), followed by 75 % in CA3a, and only 54 % in CA3c. Statistical analysis revealed that the likelihood of connection in CA3c sub-region was significantly lower compared to the other two ($p < 0.05$) making the middle section of CA3 area most appealing for studying pairs of CA3 cells.

5.3.4 Distance between cell pair

By altering the distance between the somas of CA3 pairs we recorded from, although not quite reaching statistical significance ($p = 0.057$), we noted the following trend: Neighboring cells are connected with 75 % probability ($n = 8$), which is only 65 % for cells with distances of 11 to 20 μm ($n = 20$). At distances of 21 to 30 μm connectivity was 82 % ($n = 22$) and between 31 to 40 μm 64 % ($n = 22$). Chance of connectivity peaked with 100 % ($n = 13$) at distances of 41 to 50 μm and was reduced to 71 % ($n = 14$) at distances above 51 μm. Thus by shifting the distance between the cell bodies of pairs of CA3 cells the likelihood of recurrent connections ranged between 64 % to 100 % (Figure 5.5).

5.4 Discussion

Taken together all relevant conditions for our experiment including the maturity, health and probability of recurrent connections of the slice preparations our paired recordings were significantly aided by considering the following parameters: DIV, sub-regional specificity of cells, and distance between cell bodies. Such paired CA3-CA3 recordings in OHSC should thus use three to four weeks old slice preparations in area CA3b with distances of 41-50 μm apart.

Reported connection probability of CA3 cells varies in the literature. Some studies show a lower connection probability within CA3-CA3 cells in OHSC compared to our results. For example Pavlidis and Madison found a 30 % overall recurrent connectivity of CA3 cells, however, their recordings were made 7 to 14 days after slice preparation, as opposed to our studies that extended to 32 DIV, by which time more connections are thought to form (Pavlidis & Madison, 1999). Another study found a 56 % chance of CA3-CA3 connectivity, and a 33 % likelihood of reciprocal CA3 connections (Debanne *et al.*, 1995). These values are on par but slightly lower than our observations. The discrepancies might be due to the fact that the lower numbers were obtained from unspecified two to four week old preparations, and as we have seen, connectivity increases during that time. It is therefore possible that lower numbers were produced by a majority of earlier time point recordings.

In our experiments, pyramidal cells of area CA3b were more likely to form recurrent synapses onto other CA3b cells (85 %) compared to CA3a (75 %) and

particularly to CA3c (54 %). Our findings are supported by the analysis of Ropireddy *et al*. of axonal branching in CA3, showing that axons of CA3c cells are more likely to project rather than to form associational connections (Ropireddy *et al.*, 2011). Similarly, other intra-hippocampal projection studies confirm the existence of preferred projections of CA3 axons based on the origin of the soma (Ishuzuka *et al.*, 1990). Together these data provide a plausible explanation to why we have found it less likely to encounter connected cells in sub-region CA3c.

Considering the space between CA3 pyramidal cell bodies, we find distances of 41 to 50 μm apart to be ideal. An earlier study found that paired recordings in OHSC resulted in about one third of recordings to be showing recurrent connections, however, when decreasing the distance between the two cells to below 100 μm, the probability increased (Pavlidis & Madison, 1999). Our most widely spaced cells were located at a distance of 79 μm, at which distance they were still connected, however we did not obtain data from cells that were > 100 μm apart. Alternatively to a spacing of 41 to 50 μm, distances of 0 to 10 μm, 21 to 30 μm, and distances above 51 μm could be also considered. However, neighboring cells can further complicate imaging and the successful localization of active synapses: small, localized calcium transients could be masked by the large fluorescent somas or by merely located "under" the soma of the other cells. In contrast, having larger distances between cells make spine searching more cumbersome, by simply needing more time, therefore more laser exposure, to travel the distance.

Taken together, optimization of our recording configurations aided us to achieve higher likelihood of connected CA3 pairs from which we are able to transition to the proceeding steps of experiments described in Chapter 4. It is a small yet important step in the direction of improving our experimental approach.

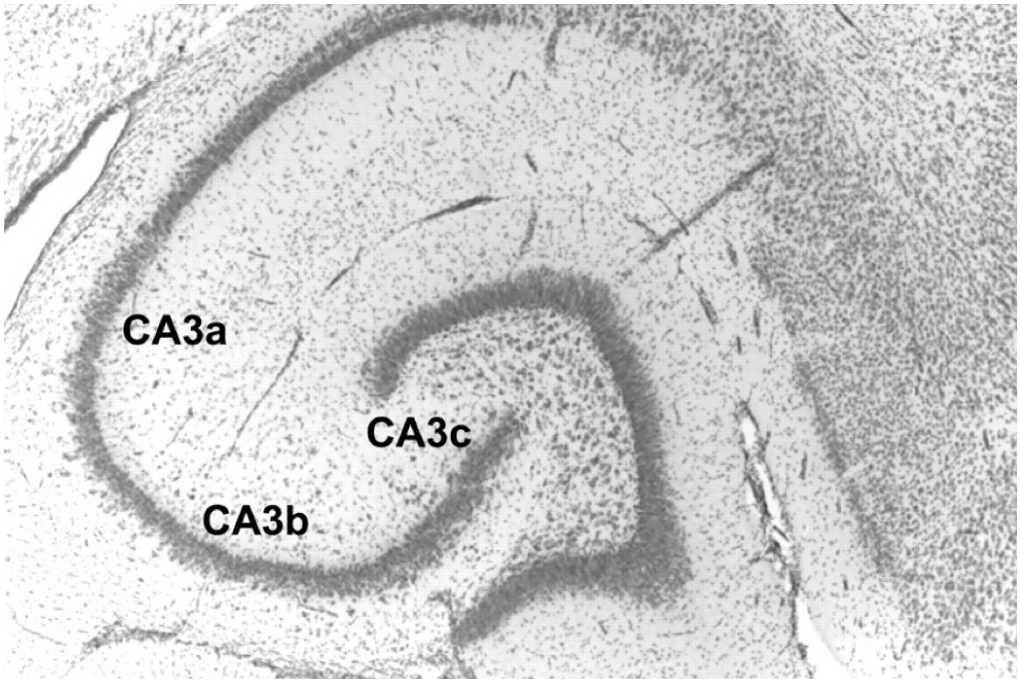

Figure 5.1 Classification of CA3 sub-regions labeling CA3a, CA3b, and CA3c in the rat hippocampus. CA3a is adjacent to CA1 and CA2, followed by CA3b, and CA3c is closest to the dentate gyrus. Photomicrograph with Nissl stain, adapted with permission from Kubota *et al.*, 2003. Reprint permission is found in Appendix A.

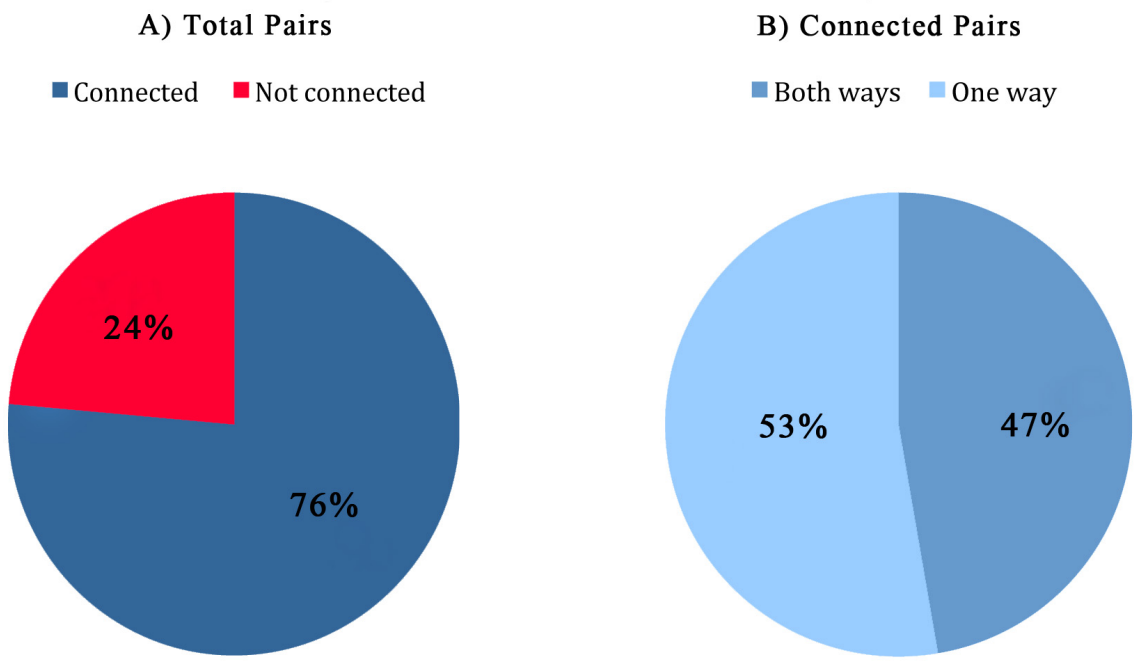

Figure 5.2 Percentage of connection between pairs of CA3 cells in OHSC. **(A)** Probability of recurrent connections onto other CA3 cells are show in dark blue (76 %; n=81), whereas red (24 %; n=25) indicates cell pairs without such connections (total n=106). **(B)** Pie chart describing the likelihood of one-way (53 %; n=39; light blue) versus reciprocal (47 %; n=35; blue) connections.

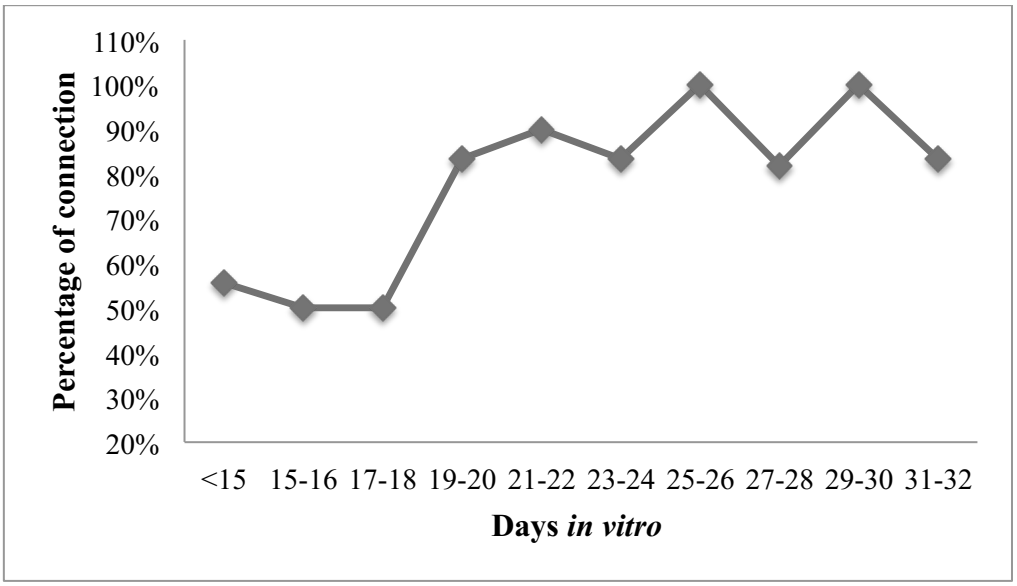

Figure 5.3 Correlations of days *in vitro* and the likelihood of connections. X-axis shows the culture's age as days *in vitro*, from less than 15 up to 31-32 days, in which recording was obtained from. Y-axis denotes the probability of finding connected pairs. Total number of experiments n= 106.

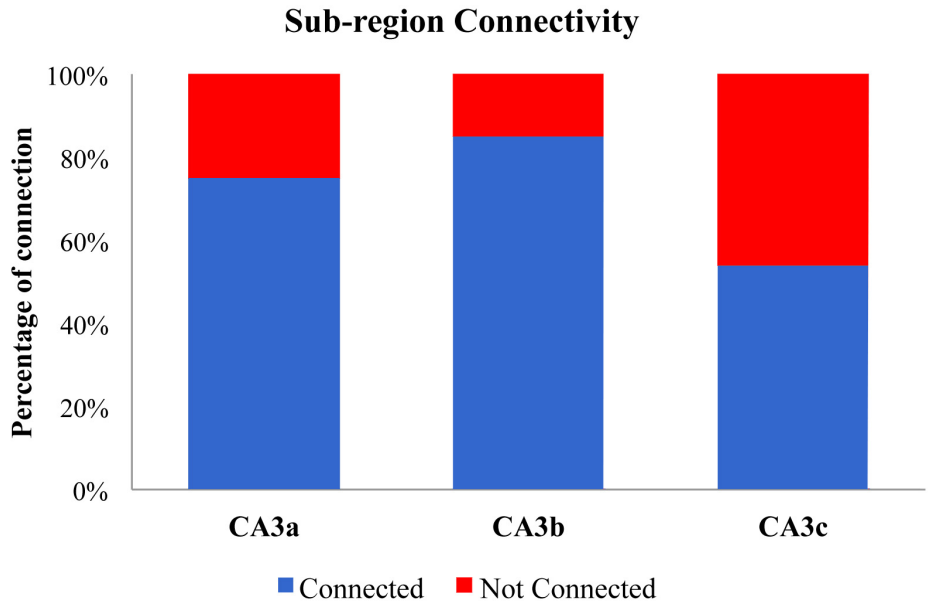

Figure 5.4 Histogram showing the likelihood of connecting pairs sorted according to sub-region localization. Blue portion of bars indicate the percentage of connected pairs whereas red portion of bars indicate the percentage of pairs that are not connected. Number of experiments were n=20 for CA3a; n=59 for CA3b; and n=13 for CA3c.

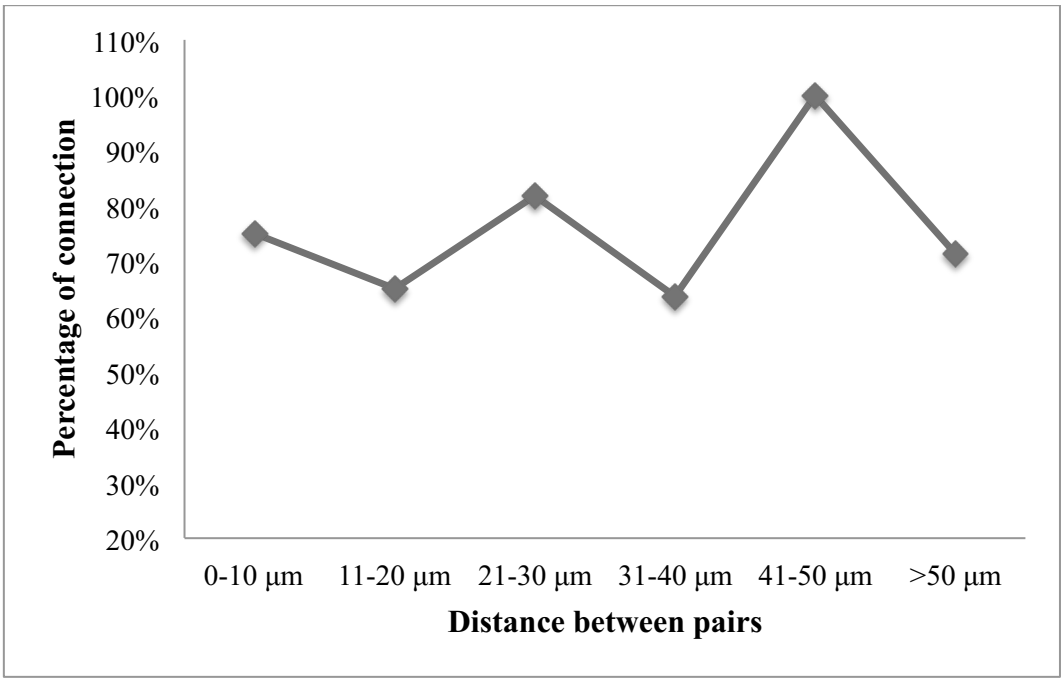

Figure 5.5 Diagram describing the intercellular distance of CA3 pairs and the probability of connection at such distances. X-axis shows the distance between cells bodies in micrometer, Y-axis indicates probability of recurrent connections expressed in percentage. Number of experiments at 0 to 10 µm n=8; 11 to 20 µm n=20; 21 to 30 µm n=22; 31 to 40 µm n= 22; 41 to 50 µm n=13; and distances above 51 µm n=14.

CHAPTER 6

OVERALL DISCUSSION

6.1 Summary of findings

The objective of this thesis was to test and apply new approaches to the study of synaptic plasticity in the rat hippocampus. Specifically, I wanted to find new ways to investigate the relationship between synaptic function and structure of individually identifiable synapses experiencing near physiological LTP and LTD stimulations. In Chapters 2 and 3 I explored the applicability of GECIs and offered a comprehensive evaluation of promising GCaMPs and GECOs, as well as newly designed faster GCaMP versions, respectively. The results indicated that although GECIs are invaluable for pursuing various important research questions, they, at present, still exhibit sub-optimal kinetics or fluorescent signals for my purposes. This propelled me to turn to other possibilities until further improvements in these GECIs transpire. Thus in Chapter 4 I introduced a multifaceted approach of sharp intracellular electrophysiological recordings from pairs of CA3 cells in organotypic hippocampal slices in combination with two-photon calcium imaging of individual synapses, induced plasticity and followed its expression mechanisms. The observations suggest that plasticity can be induced at these recurrent CA3-CA3 synapses without an obvious and rapid change in synapse size.

Finally, in Chapter 5 I show how optimization of different variables of paired recordings can enhance my success of such experiments.

Collectively, this work describes a variety of technical approaches that may be useful for the study of neuronal activity and synaptic plasticity. Innovative approaches can improve our precision over observations and control of manipulations. This thesis contributes to this by evaluating promising tools (e.g., GECIs), novel technical approaches, and optimization of such techniques, as well as offering new observations regarding structural plasticity of CA3-CA3 synapses in the rat OHSC. In closing I will discuss potential avenues for how GECIs and other genetically encoded indicators can be used to further our understanding of neuronal activity, how our observations regarding structural plasticity fit the literature at large, as well as offer a model which merges seemingly contradictory ideas.

6.2 Optical imaging with genetically encoded indicators for the study of neuronal activity in the rat hippocampus

Chapter 2 presented a standardized comparison of GECIs from the GCaMP and GECO families that we intended to use in our paired recording experiments. Although some indicators seemed promising as they clearly identified individual action potentials, they were all too slow to image fast synaptic transmission. Newly designed fast GCaMPs, described in Chapter 3, have overcome this obstacle effectively, however, they

compromise bright fluorescent signals for the improved kinetics. Notwithstanding that GECIs can be useful tools, for a number of reasons we concluded that at present they would not be appropriate for our paired recording experiments. Nonetheless, new and constantly improved indicators are expected to become available, which might be able to combine strong fluorescent signals with fast on and off kinetics.

Despite the anticipated improvements in GECIs, general limitations stemming from the nature of all calcium probes might still prove problematic. Compared to the initial voltage change in neurons, the time course of the subsequent [Ca^{2+}] change is relatively slow. Thus all GECIs' ability to monitor fast voltage changes is indirect and limited, and can be further restricted by suboptimal on/off kinetics of some sensors. Importantly, inhibitory synaptic activity or other events that are not associated with a calcium transient cannot be monitored by GECIs. Overcoming these limitations that calcium monitoring poses might be possible with genetically encoded voltage indicators (GEVIs).

First introduced in 1997 (Siegel & Isacoff, 1997) GEVIs are designed to report membrane potential changes, thus these probes provide direct readouts of neuronal activity. Unlike GECIs, they do not rely on secondary mechanisms such as Ca^{2+} influx, induced by electrical signals. This has distinct advantages. First, it potentially increases the temporal and spatial resolution of voltage indicators compared to GECIs. Second, GEVIs are theoretically not only able to monitor depolarizing but also hyperpolarizing potential changes.

Generally, GEVIs are structurally based on a voltage-gated ion channel or simply its voltage-sensing domain that senses and transduces membrane potential changes to an attached fluorescent protein (or protein pair). In all classes of GEVIs the probe is located within close proximity of the plasma membrane, and only then it is able to monitor voltage changes across the membrane. Therefore targeting and localization of GEVIs is of major importance. Particularly, targeting GEVIs specifically to the plasma membrane is crucial, as most of a cell's membranes are intracellular. Unspecific membrane targeting, i.e. to membrane structures of the endoplasmic reticulum (ER) or Golgi apparatus, will result in high background levels and thus poor signals. In addition to targeting and localization, imaging membrane potential with GEVIs has its challenges with introducing extra capacitive load, toxicity, photodamage, kinetics, and ΔF/F values to overcome (Siegel & Isacoff, 1997; Ataka & Pieribone, 2002; Chanda *et al.*, 2005; Dimitrov *et al.*, 2007; Baker *et al.*, 2007; DiFranco *et al.*, 2007; Akemann *et al.*, 2010; Kralj *et al.*, 2011).

Since the prototype of GEVIs (FlaSh, (Siegel & Isacoff, 1997)), we have seen several varieties with substantial improvements (Sakai *et al.*, 2001; Ataka & Pieribone, 2002; Knöpfel *et al.*, 2003; Tsutsui *et al.*, 2008; Lundby *et al.*, 2008; Kralj *et al.*, 2012). Most of the indicators, however, still produce small fluorescence changes, and rarely provide a sub-millisecond temporal resolution, which requires averaging several trials to resolve individual action potentials, not to mention sub-threshold changes (Looger & Griesbeck, 2011; Mutoh *et al.*, 2012; Nakajima *et al.*, 2016). However, hVOS (hybrid voltage sensor (Chanda *et al.*, 2005), ArcLight (Jin *et al.*, 2012) and ASAP-1

(Accelerated Sensor of Action Potentials 1 (St-Pierre *et al.*, 2014) achieved significant improvement in respect to both the detectable optical signal and temporal resolution, increasing their usefulness for imaging neuronal activity in brain slices. Notwithstanding, at present there is no perfect GEVI capable of identifying and differentiating EPSPs, IPSPs, and action potentials in single trials *in vivo* (Nakajima *et al.*, 2016). As further improvements are expected, GEVIs, along with GECIs, will be invaluable tools for neuroscience. The following section will thus briefly introduce a select few areas where GECIs and GEVIs may contribute significantly.

6.3 Future applications of GECIs and GEVIs

The optical readout of electrical activities in a subset of cells could help in mapping neural circuit behaviour and monitor its functions in a non-invasive way (Lin & Schnitzer, 2016). This method would aid in answering how different types of neurons connect to form networks, and how specific behaviours propagate through a network of cells. Being able to detect locations and times of synaptic activity in a cell in relation to the structure of the circuit will be useful to assess the functions of cells in such circuits.

Also, GEVIs and GECIs could be useful for studying the plasticity of neural networks under physiological and pathological conditions, and allow us to understand disruptions of calcium homeostasis in diseases such as Alzheimer's disease or cancers (Fedrizzi & Carafoli, 2011; Prevarskaya *et al.*, 2011).

The investigation of Ca^{2+} signaling and voltage changes in presynaptic and postsynaptic compartments of synapses is another area of great interest (Sabatini *et al.*, 2001; Higley & Sabatini, 2008; Peterka *et al.*, 2011; Sala & Segal, 2014). The presynaptic Ca^{2+} signal is crucial for vesicle release, and monitoring it would be invaluable in identifying the factors involved and responsible for changes in transmitter release probability during LTP and LTD. Sy-GCaMP2, which combines G-CaMP2 (Tallini *et al.*, 2006) and the synaptic vesicle protein synaptophysin, was already successfully used to monitor Ca^{2+} changes in the presynaptic bouton of cultured hippocampal neurons by localizing it to synaptic vesicles (Dreosti *et al.*, 2009). For postsynaptic events, GECIs and GEVIs will help to discover the possible differences in amplitudes of excitatory postsynaptic potentials (EPSP) at different sites along a dendrite, and the changes in unitary EPSP amplitude during plasticity. In addition, they could be used to map the temporal and spatial distribution of synaptic input sites on identified neurons responding to specific stimuli (Gulyás *et al.*, 2016).

Long-standing questions regarding how electrical signals flow between dendritic spines, dendrites, and the soma, as well as the rules and roles of dendritic signal integration could be addressed by using voltage sensors (Acker *et al.*, 2016). Currently, experimental access to the dendritic spine to monitor the amplitude of EPSPs at the location of origin is technically very challenging. Therefore, there are only assumptions about the initial magnitude of EPSPs and the degree of attenuation and integration during their propagation to the soma. Use of GECIs or GEVIs would allow addressing this fundamental question. Improved GEVIs that are able to resolve sub-threshold

postsynaptic potentials at the dendritic spine, will allow to record the magnitude of the EPSPs at the location of origin, at the merge of dendritic branches, and in the soma. EPSPs generated by uncaging neurotransmitters on two different, identified spines will be helpful to determine the spatial and temporal summation of resulting EPSPs with no recording electrode required.

Also, optical sensors monitoring voltage or Ca^{2+} changes are not in any way limited to study neuronal behaviour. Real time readouts of voltage changes or Ca^{2+} oscillations are also crucial in understanding cardiac and muscle physiology, where Ca^{2+} is an absolute necessity for controlling contraction. Calcium is also an important regulator of functions in subcellular compartments such as the mitochondria. Therefore, advances made in the development of GECIs and GEVIs are greatly applicable to other research areas.

6.4 Summary of structural and functional plasticity in the rat OHSC

Over the last few decades many research groups have been investigating the relationship of structural and functional plasticity of the synapses of the CNS (Yuste & Bonhoeffer, 2001; Sala & Segal, 2014). New insights were often brought about by the advancement of new technologies, e.g., how significant contributions to the pre/post debate of the locus of LTP expression (Kullmann, 2012; MacDougall & Fine, 2013; Bliss & Collingridge, 2013) originated from the invention and combined application of a wide

range of research tools. Notwithstanding these advancements, many fundamental questions remain open, such as whether structural and functional plasticity play distinct, parallel, complementary, or obligatory roles, whether these are the same in LTP and LTD and in different types of induction and expression mechanisms, and how these might change in development.

Considerable evidence has been produced to show that some experimental manipulations known to induce LTP or LTD also have an effect on the morphology of hippocampal synapses (Chang & Greenough, 1984; Toni *et al.*, 1999; Yuste & Bonhoeffer, 2001; Nikonenko *et al.*, 2003; Wang *et al.*, 2007; Govindarajan *et al.*, 2011; Zhang *et al.*, 2013; Bell *et al.*, 2014; Bosch *et al.*, 2014). The most compelling support for structural reorganization of the dendritic spine and possibly the bouton comes from low or high frequency glutamate uncaging, leading to synapse shrinkage or growth, respectively (Matsuzaki *et al.*, 2004; Murakoshi *et al.*, 2011; Oh *et al.*, 2013; Meyer *et al.*, 2014). The working model describing the relationship of such structural and functional changes of synapses under glutamate uncaging-induced plasticity proposes the followings: induction of LTP (and partially LTD) along with structural changes depend on the activation of NMDARs, subsequent influx of Ca^{2+}, CaMKII and small GTPase proteins after which they seem to be governed by different but parallel mechanisms (Murakoshi *et al.*, 2011; Lisman *et al.*, 2012; Smirnov *et al.*, 2017; but see Stein *et al.*, 2015). Structural and functional plasticity are thought to be merging through the above-mentioned steps (Bosch & Hayashi, 2012; Caroni *et al.*, 2012; Nishiyama & Yasuda, 2015), but it is believed that the reorganization of actin filaments and addition or

elimination of new AMPARs are the main forces behind dendritic spine size changes, which are subsequently mirrored by the presynaptic bouton (Lamprecht & LeDoux, 2004; Murakoshi & Yasuda, 2012; Choquet & Triller, 2013).

However, a substantial body of work is arguing for a different model (Skrede & Malthe-Sørenssen, 1981; Kullmann *et al.*, 1996; Emptage *et al.*, 2003; Lisman & Raghavachari, 2006; Ahmed & Siegelbaum, 2009; Lamanna *et al.*, 2015). For example, there has been clear evidence showing that hippocampal LTP and LTD of Schaffer collateral or associational mature synapses onto CA1 cells are expressed presynaptically by an increase or decrease of P_r, respectively, and not postsynaptically by addition or elimination and modifications of AMPARs (Enoki *et al.*, 2009). Therefore, if synapse growth was evident the addition of extra AMPARs would not be responsible for that, or alternatively it might explain how no change in synapse size can occur despite changes in synaptic efficacy.

Indeed, there have been numerous reports showing a dissociation between structural and functional plasticity or divergent molecular mechanisms at hippocampal synapses (Zhou *et al.*, 2004; Wang *et al.*, 2007; Bastrikova *et al.*, 2008; Yang *et al.*, 2008; Soares *et al.*, 2013; Wiegert & Oertner, 2013; Stein *et al.*, 2015). Nonetheless, the existence of tight correlation between synaptic elements argue for an important role of synapse size in their efficacy (Harris & Stevens, 1989; Takumi *et al.*, 1999; Matsuzaki *et al.*, 2001; Nishiyama & Yasuda, 2015). However, changes in spine size and PSD size have been recently reported to occur on different time scale, where PSD size only increased hours later after volume change in LTP (De Roo *et al.*, 2008; Murakoshi &

Yasuda, 2012). On the other hand, spine and PSD shrinkage happened simultaneously in LTD (Woods *et al.*, 2011). This, and other studies (Holderith *et al.*, 2012), suggest a level of decoupling between changes in spine volume and PSD size, and between bouton and spine size, respectively.

Another argument used often when advocating for structural changes of the synapse in plasticity is that dendritic spines are known to be dynamic. However, this property of spines is greatly decreased with development, and thus less important to consider in more mature preparations (Parnass *et al.*, 2000; Sala *et al.*, 2008).

Crucially, a recent study used optogenetic control of various PSD molecules and noted that adding AMPARs to the PSD, as is suggested to be happening in the postivist model of LTP expression and spine enlargement, in fact did not alter synaptic strength (Sinnen *et al.*, 2017).

Based on these opposing outcomes, perhaps it is premature to announce the defeat of one and the victory of the other overruling model. Instead, let us consider possible reasons for these confounding results.

6.5 Possible origins of contradiction in structural and functional plasticity in the rodent hippocampus

The obvious contradiction in literature can stem from numerous differences. These include, but are not limited to the type of animals, strains, developmental stage and

age, housing, sex and hormone levels, brain regions and specific synapses, *in vivo* or *in vitro* observations, acute or cultured preparations, variety of recording, stimulation, and imaging configurations, temperature, induction protocols, and time points of investigations. Also, it is important to note here the remarkable variety and flexibility of LTP. Even under similar experimental conditions when many variables are controlled, factors such as postsynaptic excitability, number of activated synapses, and level of GABA inhibition can all further affect LTP or LTD (Nicoll & Roche, 2013).

Furthermore, it has been proposed that different types of memories have distinct electrophysiological and perhaps structural manifestations, and on the experimental level that LTP induction protocols lead to a variety of LTP expressions with different properties, and how, in addition, these might change over time (Johnstone & Raymond, 2011, 2013; Nicoll & Roche, 2013; Sala & Segal, 2014). Indeed, it has been postulated that LTP at silent synapses, abundant early in development, is expressed via un-silencing, a postsynaptic process involving insertion of AMPAR in the synapses, whereas mature synapses express presynaptic LTP via an increase in P_r (Macdougall & Fine, 2013).

Since both sides put compelling evidence forward for the pre- or postivist view of LTP and LTD expression as well as for the existence or absence of concomitant structural changes of the synapse, let us consider how they can both fit into an encompassing model describing the relationship of structural and functional plasticity.

6.6 Synthesis of structural and functional synaptic plasticity models

We propose that small and potentially silent spines exhibit postsynaptic LTP by un-silencing, that is with the addition of new AMPARs, their lateral diffusion, and synaptic trapping. Simultaneously, LTP at such synapses might be associated with an increase in the synapse size, partially accounted for from extra AMPARs and a reorganization of the actin cytoskeleton.

In contrast, LTP or LTD at mature, non-silent, and bigger synapses are expressed predominantly via presynaptic mechanisms resulting in an increase or decrease in P_r, respectively. This type of LTP and LTD, where postsynaptic mechanisms are negligible, might be expressed without any necessary change in the size of the synapse. This model is partially supported by our observations as well as other observations of how small and low P_r spines are more likely to undergo morphological changes (Matsuzaki *et al.*, 2004; Wiegert & Oertner, 2013), as well as how dynamic changes of the synapse are a lot more abundant at developmentally early stages (Tashiro *et al.*, 2003; Caroni *et al.*, 2012), also a time for pronounced numbers of silent synapses (Durand *et al.*, 1996). In addition, glutamate uncaging experiments reporting synapse size changes are almost exclusively carried out in juvenile preparations, around 13 PND, (Matsuzaki *et al.*, 2004; Harvey & Svoboda, 2007; Tanaka *et al.*, 2008; Oh *et al.*, 2013; Meyer *et al.*, 2014) thus reporting structural changes in non-mature synapses.

Perhaps, similarly to how the location of LTP expression can shift from a predominantly postsynaptic mechanism in silent synapses in young animals to a

predominantly presynaptic mechanism in more mature non-silent synapses (Macdougall & Fine, 2013), a switch in the requirement of plasticity associated structural changes might shift from an obligatory or permissive role to a distinct or non-existing role.

In scenarios where structural and functional plasticity is still evident in mature non-silent synapses, notably almost exclusively demonstrated by glutamate uncaging, we propose that they are likely due to stimulation artifacts.

Glutamate uncaging is the most prominent tool at present to access structural and functional plasticity and it has been shown that such stimulation at high frequency leads to an increase in AMPARs and synapse size (however, this does not exclude the possibility that presynaptic mechanisms also occur) (Nicoll & Roche, 2013). Although glutamate uncaging is reasonably controllable regarding its spatio-temporal aspects some issues remain problematic, e.g., how the size of the uncaging spot is invariably larger than that of vesicular release, the complete exclusion of the presynaptic partner, glutamate spillover, and activation of non-synaptic glutamate receptors (Sala & Segal, 2014). Furthermore, it has been postulated that potential changes in synapse morphology might be due to changes in fluorescent intensity or reorientation of synaptic structures rather than actual morphological reorganization as this issue is not always considered (Hosokawa *et al.*, 1995; Sala & Segal, 2014).

6.7 Conclusion

Although our approaches circumvent many possible confounding factors in the evaluation of the relationship between structural and functional plasticity, they are not without limitations. Notwithstanding, my work provides a basis for future studies of neuronal activity and synaptic plasticity, and leads to the hypothesis that structural and functional plasticity achieved by STDP can be dissociated at CA3-CA3 mature synapses. New experiments can benefit from the evaluation and optimization of tools and approaches presented in this thesis.

BIBLIOGRAPHY

Abe K, Chisaka O, Van Roy F & Takeichi M (2004). Stability of dendritic spines and synaptic contacts is controlled by alpha N-catenin. *Nat Neurosci* **7,** 357–363.

Abraham WC (2003). How long will long-term potentiation last? *Phil Trans R Soc* **358,** 735–744.

Acker CD, Hoyos E & Loew LM (2016). EPSPs measured in proximal dendritic spines of cortical pyramidal neurons. *eNeuro* **3,** 1–13.

Ackermann M & Matus A (2003). Activity-induced targeting of profilin and stabilization of dendritic spine morphology. *Nat Neurosci* **6,** 1194–1200.

Ahmari SE, Buchanan J & Smith SJ (2000). Assembly of presynaptic active zones from cytoplasmic transport packets. *Nat Neurosci* **3,** 445–451.

Ahmed MS & Siegelbaum SA (2009). Recruitment of N-Type Ca(2+) channels during LTP enhances low release efficacy of hippocampal CA1 perforant path synapses. *Neuron* **63,** 372–385.

Akemann W, Mutoh H, Perron A, Rossier J & Knöpfel T (2010). Imaging brain electric signals with genetically targeted voltage-sensitive fluorescent proteins. *Nat Methods* **7,** 643–649.

Akerboom J et al. (2012). Optimization of a GCaMP calcium indicator for neural activity imaging. *J Neurosci* **32,** 13819–13840.

Akerboom J, Rivera JDV, Guilbe MMR, Malavé ECA, Hernandez HH, Tian L, Hires SA, Marvin JS, Looger LL & Schreiter ER (2009). Crystal structures of the GCaMP calcium sensor reveal the mechanism of fluorescence signal change and aid rational design. *J Biol Chem* **284,** 6455–6464.

Altschuler R (1979). Morphometry of the effect of increased experience and training on synaptic density in area CA3 of the rat hippocampus. *J Histochem Cytochem* **27,** 1548–1550.

Amaral DG, Dolorfo C & Alvarez-Royo P (1991). Organization of CA1 projections to the subiculum: a PHA-L analysis in the rat. *Hippocampus* **1,** 415–435.

Amaral DG & Witter MP (1995). *The hippocampal formation. In The rat nervous system (ed. G. Paxinos)*.

Andersen P, Bliss T & Skrede K (1971). Lamellar organization of hippocampal pathways. *Exp Brain Res* **13,** 222–238.

Andersen P, Morris R, Amaral D, Bliss T & O'Keefe J (2007). *The Hippocampus Book*. Oxford University Press, Inc., New York, New York.

Aniksztejn L & Ben-Ari Y (1991). Novel form of long-term potentiation produced by a K+ channel blocker in the hippocampus. *Nature* **349,** 67–69.

Ataka K & Pieribone VA (2002). A genetically targetable fluorescent probe of channel gating with rapid kinetics. *Biophys J* **82,** 509–516.

Badura A, Sun XR, Giovannucci A, Lynch LA & Wang SS-H (2014). Fast calcium sensor proteins for monitoring neural activity. *Neurophotonics* **1,** 025008.

Bailey CH, Kandel ER & Harris KM (2015). Structural components of synaptic plasticity and memory consolidation. *Cold Spring Harb Perspect Biol* **7,** 1–30.

Bailey ME, Wang a. CJ, Hao J, Janssen WGM, Hara Y, Dumitriu D, Hof PR & Morrison JH (2011). Interactive effects of age and estrogen on cortical neurons: Implications for cognitive aging. *Neuroscience* **191,** 148–158.

Baird GS, Zacharias DA & Tsien RY (1999). Circular permutation and receptor insertion within green fluorescent proteins. *Proc Natl Acad Sci USA* **96,** 11241–11246.

Baker BJ, Lee H, Pieribone VA, Cohen LB, Isacoff EY, Knopfel T & Kosmidis EK (2007). Three fluorescent protein voltage sensors exhibit low plasma membrane expression in mammalian cells. *J Neurosci Methods* **161,** 32–38.

Bannister N & Larkman A (1995). Dendritic morphology of CA1 pyramidal neurones from the rat hippocampus: I. Branching patterns. *J Comp Neurol* **11,** 150–160.

Barria A, Muller D, Derkach V, Griffith LC & Soderling TR (1997). Regulatory phosphorylation of AMPA-type glutamate receptors by CaM-KII during long-term potentiation. *Science (80-)* **276,** 2042–2045.

Bastrikova N, Gardner GA, Reece JM, Jeromin A & Dudek SM (2008). Synapse elimination accompanies functional plasticity in hippocampal neurons. *Proc Natl Acad Sci USA* **105,** 3123–3127.

Bats C, Groc L & Choquet D (2007). The Interaction between stargazin and PSD-95 regulates AMPA receptor surface trafficking. *Neuron* **53,** 719–734.

Baubet V, Le Mouellic H, Campbell AK, Lucas-Meunier E, Fossier P & Brúlet P (2000). Chimeric green fluorescent protein-aequorin as bioluminescent Ca2+ reporters at the single-cell level. *Proc Natl Acad Sci USA* **97,** 7260–7265.

Bell ME, Bourne JN, Chirillo MA, Mendenhall JM, Kuwajima M & Harris KM (2014). Dynamics of nascent and active zone ultrastructure as synapses enlarge during long-term potentiation in mature hippocampus. *J Comp Neurol* **522,** 3861–3884.

Benke TA, Luthi A, Isaac JTR & Collingridge GL (1998). Modulation of AMPA receptor unitary conductance by synaptic activity. *Nature* **393,** 793–797.

Bi G & Poo M (1998). Synaptic modifications in cultured hippocampal neurons: dependence on spike timing, synaptic strength, and postsynaptic cell type. *J Neurosci* **18,** 10464–10472.

Bi G & Poo M (2001). Synaptic modification by correlated activity: Hebb 's postulate revisited. *Annu Rev Neurosci* **24,** 139–166.

Biou V, Brinkhaus H, Malenka RC & Matus A (2008). Interactions between drebrin and Ras regulate dendritic spine plasticity. *Eur J Neurosci* **27,** 2847–2859.

Bliss TVP, Collingridge G & Morris RG (2007). Synaptic plasticity in the hippocampus. In *The hippocampus book*, pp. 343–474.

Bliss TVP & Collingridge GL (1993). A synaptic model of memory: long-term potentiation in the hippocampus. *Nature* **361,** 31–39.

Bliss TVP & Collingridge GL (2013). Expression of NMDA receptor-dependent LTP in the hippocampus: bridging the divide. *Mol Brain* **6,** 5.

Bliss TVP & Lømo T (1973). Long-lasting potentiation of synaptic transmission in the dentate area of the anaesthetized rabbit following stimulation of the perforant path. *J Physiol* **232,** 331–356.

Blundell J, Blaiss CA, Etherton MR, Espinosa F, Tabuchi K, Walz C, Bolliger MF, Südhof TC & Powell CM (2010). Neuroligin-1 Deletion Results in Impaired Spatial Memory and Increased Repetitive Behavior. *J Neurosci* **30,** 2115–2129.

Bolshakov V & Siegelbaum S (1995). Regulation of hippocampal transmitter release during development and long-term potentiation. *Science (80-)* **269,** 1730–1734.

Borgdorff AJ & Choquet D (2002). Regulation of AMPA receptor lateral movements. *Nature* **417,** 649–653.

Bosch M, Castro J, Saneyoshi T, Matsuno H, Sur M & Hayashi Y (2014). Structural and molecular remodeling of dendritic spine substructures during long-term potentiation. *Neuron* **82,** 444–459.

Bosch M & Hayashi Y (2012). Structural plasticity of dendritic spines. *Curr Opin Neurobiol* **22,** 383–388.

Bourne JN, Chirillo MA & Harris KM (2013). Presynaptic ultrastructural plasticity along CA3→CA1 axons during LTP in mature hippocampus. *J Comp Neurol* **521,** 3898–3912.

Bourne JN & Harris KM (2011). Coordination of size and number of excitatory and inhibitory synapses results in a balanced structural plasticity along mature hippocampal CA1 dendrites during LTP. *Hippocampus* **21,** 354–373.

Bozdagi O, Wang X -b., Nikitczuk JS, Anderson TR, Bloss EB, Radice GL, Zhou Q, Benson DL & Huntley GW (2010). Persistence of Coordinated Long-Term Potentiation and Dendritic Spine Enlargement at Mature Hippocampal CA1 Synapses Requires N-Cadherin. *J Neurosci* **30,** 9984–9989.

Bozza T, McGann JP, Mombaerts P & Wachowiak M (2004). In vivo imaging of neuronal activity by targeted expression of a genetically encoded probe in the mouse. *Neuron* **42,** 9–21.

Bruckner JJ, Zhan H & O'Connor-Giles KM (2015). Advances in imaging ultrastructure yield new insights into presynaptic biology. *Front Cell Neurosci*; DOI: 10.3389/fncel.2015.00196.

Buchanan K a & Mellor JR (2007). The development of synaptic plasticity induction rules and the requirement for postsynaptic spikes in rat hippocampal CA1 pyramidal neurones. *J Physiol* **585,** 429–445.

Buchanan K a & Mellor JR (2010). The activity requirements for spike timing-dependent plasticity in the hippocampus. *Front Synaptic Neurosci* **2,** 11.

Buchs P, Stoppini L, Párducz A, Siklós L & Muller D (1994). A new cytochemical method for the ultrastructural localization of calcium in the central nervous system. *J Neurosci Methods* **54,** 83–93.

Buchs PA & Muller D (1996). Induction of long-term potentiation is associated with major ultrastructural changes of activated synapses. *Proc Natl Acad Sci USA* **93,** 8040–8045.

Buzsaki G (2002). Theta oscillation in the rat. *Neuron* **33,** 325–340.

Buzsaki G, Haas H & Anderson E (1987). Long-term potentiation induced by physiologically relevant stimulus patterns. *Brain Res* **435,** 331–333.

Calabrese B, Saffin J-M & Halpain S (2014). Activity-dependent dendritic spine shrinkage and growth involve downregulation of cofilin via distinct mechanisms. *PLoS One* **9,** e94787.

Caroni P, Donato F & Muller D (2012). Structural plasticity upon learning: regulation and functions. *Nat Rev* **13,** 478–490.

Carroll RC, Lissin D V, von Zastrow M, Nicoll RA & Malenka RC (1999). Rapid redistribution of glutamate receptors contributes to long-term depression in hippocampal cultures. *Nat Neurosci* **2,** 454–460.

Carter AG & Sabatini BL (2004). State-dependent calcium signalling in dendritic spines of striatal medium spiny neurons. *Neuron* **44,** 483–493.

Chanda B, Blunck R, Faria LC, Schweizer FE, Mody I & Bezanilla F (2005). A hybrid approach to measuring electrical activity in genetically specified neurons. *Nat Neurosci* **8,** 1619–1626.

Chang F & Greenough W (1984). Transient and enduring morphological correlates of synaptic activity and efficacy change in the rat hippocampal slice. *Brain Res* **309,** 35–46.

Chang J-Y, Parra-Bueno P, Laviv T, Szatmari EM, Lee S-JR & Yasuda R (2017). CaMKII autophosphorylation is necessary for optimal integration of Ca2+ signals during LTP induction, but not maintenance. *Neuron* **94,** 800–808.e4.

Chen T-W, Wardill TJ, Sun Y, Pulver SR, Renninger SL, Baohan A, Schreiter ER, Kerr RA, Orger MB, Jayaraman V, Looger LL, Svoboda K & Kim DS (2013). Ultrasensitive fluorescent proteins for imaging neuronal activity. *Nature* **499,** 295–300.

Chéreau R, Saraceno GE, Angibaud J, Cattaert D & Nägerl UV (2017). Superresolution imaging reveals activity-dependent plasticity of axon morphology linked to changes in action potential conduction velocity. *Proc Natl Acad Sci USA* **114,** 201607541.

Chicurel M & Harris K (1992). Three-dimensional analysis of the structure and composition of CA3 branched dendritic spines and their synaptic relationships with mossy fiber boutons in the rat hippocampus. *J Comp Neurol* **8,** 169–182.

Choi S, Klingauf J & Tsien R (2000). Postfusional regulation of cleft glutamate concentration during LTP at "silent synapses." *Nat Neurosci* **3,** 330–336.

Choquet D & Triller A (2013). The dynamic synapse. *Neuron* **80,** 691–703.

Coan E, Saywood W & Collingridge G (1987). MK-801 blocks NMDA receptor-mediated synaptic transmission and long-term potentiation in rat hippocampal slices. *Neurosci Lett* **80,** 111–114.

Collingridge GL (1995). The brain slice preparation: a tribute to the pioneer Henry McIlwain. *J Neurosci Methods* **59,** 5–9.

Collingridge GL, Isaac JTR & Wang YT (2004). Receptor trafficking and synaptic plasticity. *Nat Rev Neurosci* **5,** 952–962.

Collingridge GL, Peineau S, Howland JG & Wang YT (2010). Long-term depression in the CNS. *Nat Rev Neurosci* **11,** 459–473.

Cooke BM & Woolley CS (2005). Gonadal hormone modulation of dendrites in the mammalian CNS. *J Neurobiol* **64,** 34–46.

Cooper SJ (2005). Donald O. Hebb's synapse and learning rule: a history and commentary. *Neurosci Biobehav Rev* **28,** 851–874.

Cremer H, Chazal G, Carleton A, Goridis C, Vincent JD & Lledo PM (1998). Long-term but not short-term plasticity at mossy fiber synapses is impaired in neural cell adhesion molecule-deficient mice. *Proc Natl Acad Sci USA* **95,** 13242–13247.

Davydova D, Marini C, King C, Klueva J, Bischof F, Romorini S, Montenegro-Venegas C, Heine M, Schneider R, Schröder MS, Altrock WD, Henneberger C, Rusakov DA, Gundelfinger ED & Fejtova A (2014). Bassoon specifically controls presynaptic P/Q-type Ca(2+) channels via RIM-binding protein. *Neuron* **82,** 181–194.

Deadwyler S, West M & Lynch G (1979). Activity of dentate granule cells during learning: differentiation of perforant path input. *Brain Res* **15,** 29–43.

Debanne D, Boudkkazi S, Campanac E, Cudmore RH, Giraud P, Fronzaroli-Molinieres L, Carlier E & Caillard O (2008). Paired-recordings from synaptically coupled cortical and hippocampal neurons in acute and cultured brain slices. *Nat Protoc* **3,** 1559–1568.

Debanne D, Gähwiler BH & Thompson SM (1998). Long-term synaptic plasticity between pairs of individual CA3 pyramidal cells in rat hippocampal slice cultures. *J Physiol* **507,** 237–247.

Debanne D, Gähwiler BH & Thompson SM (1999). Heterogeneity of synaptic plasticity at unitary CA3-CA1 and CA3-CA3 connections in rat hippocampal slice cultures. *J Neurosci* **19,** 10664–10671.

Debanne D, Guerineau NC, Gähwiler BH & Thompson SM (1995). Physiology and pharmacology of unitary synaptic connections between pairs of cells in areas CA3 and CA1 of rat hippocampal slice cultures. *J Neurophysiol* **73,** 1282–1294.

Derkach V, Barria A & Soderling TR (1999). Ca2+/calmodulin-kinase II enhances channel conductance of alpha-amino-3-hydroxy-5-methyl-4-isoxazolepropionate type glutamate receptors. *Proc Natl Acad Sci USA* **96,** 3269–3274.

Desmond N & Levy W (1983). Synaptic correlates of associative potentiation/depression: an ultrastructural study in the hippocampus. *Brain Res* **265,** 21–30.

Desmond N & Levy W (1986). Changes in the postsynaptic density with long-term potentiation in the dentate gyrus. *J Comp Neurol* **22,** 476–482.

Desmond N & Levy W (1988). Synaptic interface surface area increases with long-term potentiation in the hippocampal dentate gyrus. *Brain Res* **453,** 308–314.

Desmond N, Scott C, Jane JJ & Levy W (1994). Ultrastructural identification of entorhinal cortical synapses in CA1 stratum lacunosum-moleculare of the rat. *Hippocampus* **4,** 594–600.

Dhanrajan TM, Lynch MA, Kelly A, Popov VI, Rusakov DA & Stewart MG (2004). Expression of long-term potentiation in aged rats involves perforated synapses but dendritic spine branching results from high-frequency stimulation alone. *Hippocampus* **14,** 255–264.

DiFranco M, Capote J, Quiñonez M & Vergara JL (2007). Voltage-dependent dynamic FRET signals from the transverse tubules in mammalian skeletal muscle fibers. *J Gen Physiol* **130,** 581–600.

Dimitrov D, He Y, Mutoh H, Baker BJ, Cohen L, Akemann W & Knöpfel T (2007). Engineering and characterization of an enhanced fluorescent protein voltage sensor. *PLoS One* **2,** e440.

Ding JJ, Luo AF, Hu LY, Wang DC & Shao F (2014). Structural basis of the ultrasensitive calcium indicator GCaMP6. *Sci China Life Sci* **57,** 269–274.

Dityatev A, Bukalo O & Schachner M (2008). Modulation of synaptic transmission and plasticity by cell adhesion and repulsion molecules. *Neuron Glia Biol* **4,** 197–209.

Dombeck DA, Harvey CD, Tian L, Looger LL & Tank DW (2010). Functional imaging of hippocampal place cells at cellular resolution during virtual navigation. *Nat Neurosci* **13,** 1433–1440.

Dosemeci A, Tao-Cheng JH, Vinade L, Winters CA, Pozzo-Miller L & Reese TS (2001). Glutamate-induced transient modification of the postsynaptic density. *Proc Natl Acad Sci USA* **98,** 10428–10432.

Dreosti E, Odermatt B, Dorostkar MM & Lagnado L (2009). A genetically encoded reporter of synaptic activity in vivo. *Nat Methods* **6,** 883–889.

Dudai Y (2004). The neurobiology of consolidations, or, how stable is the engram? *Annu Rev Psychol* **55,** 51–86.

Dudek SM & Bear MF (1992). Homosynaptic long-term depression in area CA1 of hippocampus and effects of N-methyl-D-aspartate receptor blockade. *Proc Natl Acad Sci USA* **89,** 4363–4367.

Le Duigou C, Simonnet J, Teleñczuk MT, Fricker D & Miles R (2014). Recurrent synapses and circuits in the CA3 region of the hippocampus: an associative network. *Front Cell Neurosci* **7,** 1–13.

Dunaevsky A (2013). Neural Development. In *Methods and Protocols, Methods in Molecular Biology*, pp. 111–118.

Dunaevsky A, Tashiro A, Majewska A, Mason C & Yuste R (1999). Developmental regulation of spine motility in the mammalian central nervous system. *Proc Natl Acad Sci* **96,** 13438–13443.

Durand GM, Kovalchuk Y & Konnerth A (1996). Long-term potentiation and functional synapse induction in developing hippocampus. *Nature* **381,** 71–75.

Ehrlich I, Klein M, Rumpel S & Malinow R (2007). PSD-95 is required for activity-driven synapse stabilization. *Proc Natl Acad Sci USA* **104,** 4176–4181.

Emptage NJ, Bliss TVP & Fine A (1999). Single synaptic events evoke NMDA receptor–mediated release of calcium from internal stores in hippocampal dendritic spines. *Neuron* **22,** 115–124.

Emptage NJ, Reid CA, Fine A & Bliss TVP (2003). Optical quantal analysis reveals a presynaptic component of LTP at hippocampal Schaffer-associational synapses. *Neuron* **38,** 797–804.

Engert F & Bonhoeffer T (1999). Dendritic spine changes associated with hippocampal long-term synaptic plasticity. *Nature* **399,** 66–70.

Enoki R, Hu Y ling, Hamilton D & Fine A (2009). Expression of long-term plasticity at individual synapses in hippocampus is graded, bidirectional, and mainly presynaptic: Optical quantal analysis. *Neuron* **62,** 242–253.

Faherty CJ, Kerley D & Smeyne RJ (2003). A Golgi-Cox morphological analysis of neuronal changes induced by environmental enrichment. *Dev brain Res* **141,** 55–61.

Fazeli M, Breen K, Errington M & Bliss T (1994). Increase in extracellular NCAM and amyloid precursor protein following induction of long-term potentiation in the dentate gyrus of anaesthetized rats. *Neurosci Lett* **169,** 77–80.

Fedrizzi L & Carafoli E (2011). Calcium dysfunction in neurodegenerative disorders: Alzheimer ’s disease. *BioFactors* **37,** 189–196.

Feldman DE (2000). Timing-Based LTP and LTD at Vertical Inputs to Layer II/III Pyramidal Cells in Rat Barrel Cortex. *Neuron* **27,** 45–56.

Feldman DE (2012). The spike-timing dependence of plasticity. *Neuron* **75,** 556–571.

Fernandez-Alfonso T, Nadella KMNS, Iacaruso MF, Pichler B, Roa H, Kirkby PA & Silver RA (2014). Monitoring synaptic and neuronal activity in 3D with synthetic and genetic indicators using a compact acousto-optic lens two-photon microscope. *J Neurosci Methods* **222,** 69–81.

Fiala JC, Feinberg M, Popov V & Harris KM (1998). Synaptogenesis via dendritic filopodia in developing hippocampal area CA1. *J Neurosci* **18,** 8900–8911.

Fifkova E & Anderson C (1981). Stimulation-induced changes in dimensions of stalks of dendritic spines in the dentate molecular layer. *Exp Neurol* **74,** 621–627.

Fischer M, Kaech S, Knutti D & Matus A (1998). Rapid actin-based plasticity in dendritic spines. *Neuron* **20,** 847–854.

Frotscher M & Léránth C (1985). Cholinergic innervation of the rat hippocampus as revealed by choline acetyltransferase immunocytochemistry: a combined light and electron microscopic study. *J Comp Neurol* **239,** 237–246.

Fukazawa Y, Saitoh Y, Ozawa F, Ohta Y, Mizuno K & Inokuchi K (2003). Hippocampal LTP is accompanied by enhanced F-actin content within the dendritic spine that is essential for late LTP maintenance in vivo. *Neuron* **38,** 447–460.

Gähwiler B (1981*a*). Morphological differentiation of nerve cells in thin organotypic cultures derived from rat hippocampus and cerebellum. *Proc R Soc L B Biol Sci* **211,** 287–290.

Gähwiler B (1981*b*). Organotypic monolayer cultures of nervous tissue. *J Neurosci Methods* **4,** 329–342.

Gähwiler B (1997). Organotypic slice cultures: a technique has come of age. *Trends Neurosci* **20,** 471–477.

Geinisman Y, Berry RW, Disterhoft JF, Power JM & Van der Zee EA (2001). Associative learning elicits the formation of multiple-synapse boutons. *J Neurosci* **21,** 5568–5573.

Golding NL & Spruston N (1998). Dendritic sodium spikes are variable triggers of axonal action potentials in hippocampal CA1 pyramidal neurons. *Neuron* **21,** 1189–1200.

Golding NL, Staff NP & Spruston N (2002). Dendritic spikes as a mechanism for cooperative long-term potentiation. *Nature* **418,** 326–331.

Gomperts SN, Rao A, Craig AM, Malenka RC & Nicoll RA (1998). Postsynaptically silent synapses in single neuron cultures. *Neuron* **21,** 1443–1451.

Gonzales R, DeLeon Galvan C, Rangel Y & Claiborne B (2001). Distribution of thorny excrescences on CA3 pyramidal neurons in the rat hippocampus. *J Comp Neurol* **12,** 357–368.

Govindarajan A, Israely I, Huang S-Y & Tonegawa S (2011). The dendritic branch is the preferred integrative unit for protein synthesis-dependent LTP. *Neuron* **69,** 132–146.

Gu J, Lee CW, Fan Y, Komlos D, Tang X, Sun C, Yu K, Hartzell HC, Chen G, Bamburg JR & Zheng JQ (2010). ADF/cofilin-mediated actin dynamics regulate AMPA receptor trafficking during synaptic plasticity. *Nat Neurosci* **13,** 1208–1215.

Gu L, Kleiber S, Schmid L, Nebeling F, Chamoun M, Steffen J, Wagner J & Fuhrmann M (2014). Long-term in vivo imaging of dendritic spines in the hippocampus reveals structural plasticity. *J Neurosci* **34,** 13948–13953.

Gulledge AT, Carnevale NT & Stuart GJ (2012). Electrical advantages of dendritic spines. *PLoS One*; DOI: 10.1371/journal.pone.0036007.

Gulyas A, Miles R, Sik A, Toth K, Tamamaki N & Freund T (1993). Hippocampal pyramidal cells excite inhibitory neurons through a single release site. *Nature* **363,** 210–211.

Gulyás AI, Freund TF & Káli S (2016). The effects of realistic synaptic distribution and 3D geometry on signal integration and extracellular field generation of hippocampal pyramidal cells and inhibitory neurons. *Front Neural Circuits* **10,** 1–24.

Guo NN & Li BM (2007). Cellular and subcellular distributions of β1- and β2-Adrenoceptors in the CA1 and CA3 regions of the rat hippocampus. *Neuroscience* **146,** 298–305.

Harnett MT, Makara JK, Spruston N, Kath WL & Magee JC (2012). Synaptic amplification by dendritic spines enhances input cooperativity. *Nature* **491,** 599–602.

Van Harreveld A & Fifkova E (1975). Swelling of dendritic spines in the fascia dentata after stimulation of the perforant fibers as a mechanism of post-tetanic potentiation. *Exp Neurol* **49,** 736–749.

Harris KM & Stevens JK (1989). Dendritic spines of CA1 pyramidal cells in the rat hippocampus: serial electron microscopy with reference to their biophysical characteristics. *J Neurosci* **9,** 2982–2997.

Harvey CD & Svoboda K (2007). Locally dynamic synaptic learning rules in pyramidal neuron dendrites. *Nature* **450,** 1195–1200.

Harvey CD, Yasuda R, Zhong H & Svoboda K (2008). The spread of Ras activity triggered by activation of a single dendritic spine. *Science (80-)* **321,** 136–140.

Hayashi Y, Shi SH, Esteban JA, Piccini A, Poncer JC & Malinow R (2000). Driving AMPA receptors into synapses by LTP and CaMKII: requirement for GluR1 and PDZ domain interaction. *Science (80-)* **287,** 2262–2267.

Helassa N, Zhang XH, Conte I, Scaringi J, Esposito E, Bradley J, Carter T, Ogden D, Morad M & Török K (2015). Fast-response calmodulin-based fluorescent indicators reveal rapid intracellular calcium dynamics. *Sci Rep* **5,** 15978.

Hell SW & Wichmann J (1994). Breaking the diffraction resolution limit by stimulated emmision: stimulated-emission-depletion fluorescence microscopy. *Opt Lett* **19,** 780–782.

Hendel T, Mank M, Schnell B, Griesbeck O, Borst A & Reiff DF (2008). Fluorescence changes of genetic calcium indicators and OGB-1 correlated with neural activity and calcium in vivo and in vitro. *J Neurosci* **28,** 7399–7411.

Henderson MJ, Baldwin HA, Werley CA, Boccardo S, Whitaker LR, Yan X, Holt GT, Schreiter ER, Looger LL, Cohen AE, Kim DS & Harvey BK (2015). A low affinity GCaMP3 variant (GCaMPer) for imaging the endoplasmic reticulum calcium store. *PLoS One* **10,** 1–17.

Henkemeyer M, Itkis OS, Ngo M, Hickmott PW & Ethell IM (2003). Multiple EphB receptor tyrosine kinases shape dendritic spines in the hippocampus. *J Cell Biol* **163,** 1313–1326.

Higley MJ & Sabatini BL (2008). Calcium signaling in dendrites and spines: practical and functional considerations. *Neuron* **59,** 902–913.

Hirano S, Kimoto N, Shimoyama Y, Hirohashi S & Takeichi M (1992). Identification of a neural α-catenin as a key regulator of cadherin function and multicellular organization. *Cell* **70,** 293–301.

Holderith N, Lorincz A, Katona G, Rózsa B, Kulik A, Watanabe M & Nusser Z (2012). Release probability of hippocampal glutamatergic terminals scales with the size of the active zone. *Nat Neurosci* **15,** 988–997.

Holtmaat A & Svoboda K (2009). Experience-dependent structural synaptic plasticity in the mammalian brain. *Nat Rev Neurosci* **10,** 647–658.

Honkura N, Matsuzaki M, Noguchi J, Ellis-Davies GCR & Kasai H (2008). The subspine organization of actin fibers regulates the structure and plasticity of dendritic spines. *Neuron* **57,** 719–729.

Horn R & Marty A (1988). Muscarinic activation of ionic currents measured by a new whole-cell recording method. *J Gen Physiol* **92,** 145–159.

Hörtnagl H, Berger M, Sperk G & Pifl C (1991). Regional heterogeneity in the distribution of neurotransmitter markers in the rat hippocampus. *Neuroscience* **45,** 261–272.

Hosokawa T, Mitsushima D, Kaneko R & Hayashi Y (2015). Stoichiometry and phosphoisotypes of hippocampal AMPA-type glutamate receptor phosphorylation. *Neuron* **85,** 60–68.

Hosokawa T, Rusakov D, Bliss T & Fine A (1995). Repeated confocal imaging of individual dendritic spines in the living hippocampal slice: evidence for changes in length and orientation associated with chemically induced LTP. *J Neurosci* **15,** 5560–5573.

Hsia A, Malenka R & Nicoll R (1998). Development of excitatory circuitry in the hippocampus. *J Neurophysiol* **79,** 2013–2024.

Huganir RL & Nicoll RA (2013). AMPARs and synaptic plasticity: The last 25 years. *Neuron* **80,** 704–717.

Humpel C (2015). Neuroscience forefront review. Organotypic brain slice cultures: A review. *Neuroscience* **305,** 86–98.

Isaac JTR, Nicoll RA & Malenka RC (1995). Evidence for silent synapses: Implications for the expression of LTP. *Neuron* **15,** 427–434.

Ishuzuka N, Weber J & Amaral D (1990). Organization of intrahippocampal projections originating from CA3 pyramidal cells in the rat. *J Comp Neurol* **295,** 580–623.

Jin L, Han Z, Platisa J, Wooltorton JRA, Cohen LB & Pieribone VA (2012). Single action potentials and subthreshold electrical events imaged in neurons with a fluorescent protein voltage probe. *Neuron* **75,** 779–785.

Johnston SA (1990). Biolistic transformation: microbes to mice. *Nature* **346,** 776–777.

Johnstone VP & Raymond CR (2011). A protein synthesis and nitric oxide-dependent presynaptic enhancement in persistent forms of long-term potentiation. *Learn Mem* **18,** 625–633.

Johnstone VP & Raymond CR (2013). Postsynaptic protein synthesis is required for presynaptic enhancement in persistent forms of long-term potentiation. *Front Synaptic Neurosci* **5,** 1–10.

Kampa BM, Letzkus JJ & Stuart GJ (2007). Dendritic mechanisms controlling spike-timing-dependent synaptic plasticity. *Trends Neurosci* **30,** 456–463.

Kandler K, Katz LC & Kauer JA (1998). Focal photolysis of caged glutamate produces long-term depression of hippocampal glutamate receptors. *Nat Neurosci* **1,** 119–123.

Karra D & Dahm R (2010). Transfection techniques for neuronal cells. *J Neurosci* **30,** 6171–6177.

Katayama H, Kogure T, Mizushima N, Yoshimori T & Miyawaki A (2011). A sensitive and quantitative technique for detecting autophagic events based on lysosomal delivery. *Chem Biol* **18,** 1042–1052.

Kennedy MJ, Davison IG, Robinson CG & Ehlers MD (2010). Syntaxin-4 defines a domain for activity-dependent exocytosis in dendritic spines. *Cell* **141,** 524–535.

Kerchner GA & Nicoll RA (2008). Silent synapses and the emergence of a postsynaptic mechanism for LTP. *Nat Rev Neurosci* **9,** 813–825.

Kesner RP (2007). Behavioral functions of the CA3 subregion of the hippocampus. *Learn Mem* **14,** 771–781.

Kim IH, Racz B, Wang H, Burianek L, Weinberg R, Yasuda R, Wetsel WC & Soderling SH (2013). Disruption of Arp2/3 results in asymmetric structural plasticity of dendritic spines and progressive synaptic and behavioral abnormalities. *J Neurosci* **33,** 6081–6092.

Kim S, Guzman SJ, Hu H & Jonas P (2012). Active dendrites support efficient initiation of dendritic spikes in hippocampal CA3 pyramidal neurons. *Nat Neurosci* **15,** 600–606.

Klar TA, Jakobs S, Dyba M, Egner A & Hell SW (2000). Fluorescence microscopy with diffraction resolution barrier broken by stimulated emission. *Proc Natl Acad Sci* **97,** 8206–8210.

Knöpfel T, Tomita K, Shimazaki R & Sakai R (2003). Optical recordings of membrane potential using genetically targeted voltage-sensitive fluorescent proteins. *Methods* **30,** 42–48.

Kopec CD, Li B, Wei W, Boehm J & Malinow R (2006). Glutamate receptor exocytosis and spine enlargement during chemically induced long-term potentiation. *J Neurosci* **26,** 2000–2009.

Kornau H-C, Schenker LT, Kennedy MB & Seeburg PH (1995). Domain Interaction between NMDA Receptor Subunits and the Postsynaptic Density Protein PSD-95. *Science (80-)* **269,** 1737–1740.

Korobova F & Svitkina T (2010). Molecular architecture of synaptic actin cytoskeleton in hippocampal neurons reveals a mechanism of dendritic spine morphogenesis. *Mol Biol Cell* **21,** 4042–4056.

Kralj JM, Douglass AD, Hochbaum DR, Maclaurin D & Cohen AE (2012). Optical recording of action potentials in mammalian neurons using a microbial rhodopsin. *Nat Methods* **9,** 90–95.

Kralj JM, Hochbaum DR, Douglass AD & Cohen AE (2011). Electrical spiking in Escherichia coli probed with a fluorescent voltage-indicating protein. *Science (80-)* **333,** 345–348.

Krucker T, Siggins GR & Halpain S (2000). Dynamic actin filaments are required for stable long-term potentiation (LTP) in area CA1 of the hippocampus. *Proc Natl Acad Sci USA* **97,** 6856–6861.

Kubota D, Colgin LL, Casale M, Brucher FA & Lynch G (2003). Endogenous waves in hippocampal slices. *J Neurophysiol* **89,** 81–89.

Kullmann DM (1994). Amplitude fluctuations of dual-component EPSCs in hippocampal pyramidal cells: implications for long-term potentiation. *Neuron* **12,** 1111–1120.

Kullmann DM (2012). The mother of all battles 20 years on: is LTP expressed pre- or postsynaptically? *J Physiol* **590,** 2213–2216.

Kullmann DM & Asztély F (1998). Extrasynaptic glutamate spillover in the hippocampus: evidence and implications. *Trends Neurosci* **21,** 8–14.

Kullmann DM, Erdemli G & Asztély F (1996). LTP of AMPA and NMDA receptor-mediated signals: evidence for presynaptic expression and extrasynaptic glutamate spill-over. *Neuron* **17,** 461–474.

Kwon H-B & Sabatini BL (2011). Glutamate induces de novo growth of functional spines in developing cortex. *Nature* **474,** 100–104.

Lamanna J, Signorini MG, Cerutti S & Malgaroli A (2015). A pre-docking source for the power-law behavior of spontaneous quantal release: application to the analysis of LTP. *Front Cell Neurosci* **9,** 1–13.

Lamprecht R & LeDoux J (2004). Structural plasticity and memory. *Nat Rev Neurosci* **5,** 45–54.

Lang C, Barco A, Zablow L, Kandel ER, Siegelbaum SA & Zakharenko SS (2004). Transient expansion of synaptically connected dendritic spines upon induction of hippocampal long-term potentiation. *Proc Natl Acad Sci USA* **101,** 16665–16670.

Lazarevic V, Schoene C, Heine M, Gundelfinger ED & Fejtova A (2011). Extensive remodeling of the presynaptic cytomatrix upon homeostatic adaptation to network activity silencing. *J Neurosci* **31,** 10189–10200.

Lee H, Barbarosie M, Kameyama K, Bear M & Huganir R (2000). Regulation of distinct AMPA receptor phosphorylation sites during bidirectional synaptic plasticity. *Nature* **405,** 955–959.

Lee K, Oliver M, Schottler F, Creager R & Lynch G (1979). Ultrastructural effects of repetitive synaptic stimulation in the hippocampal slice preparation: a preliminary report. *Exp Neurol* **65,** 278–280.

Lee KS, Schottler F, Oliver M & Lynch G (1980). Brief bursts of high-frequency stimulation produce two types of structural change in rat hippocampus. *J Neurophysiol* **44,** 247–258.

Lee S-JR, Escobedo-Lozoya Y, Szatmari E & Yasuda R (2009). Activation of CaMKII in single dendritic spines during long-term potentiation. *Nature* **458,** 299–306.

Leuner B, Falduto J & Shors TJ (2003). Associative memory formation increases the observation of dendritic spines in the hippocampus. *J Neurosci* **23,** 659–665.

Li C & McIlwain H (1957). Maintenance of resting membrane potentials in slices of mammalian cerebral cortex and other tissues in vitro. *J Physiol* **139,** 178–190.

Li X, Somogyi P, Ylinen A & Buzsaki G (1994). The hippocampal CA3 network: an in vivo intracellular labeling study. *J Comp Neurol* **339,** 181–208.

Liao D, Hessler NA & Malinow R (1995). Activation of postsynaptically silent synapses during pairing-induced LTP in CA1 region of hippocampal slice. *Nature* **375,** 400–404.

Liebscher S, Keller GB, Goltstein PM, Bonhoeffer T & Hübener M (2016). Selective persistence of sensorimotor mismatch signals in visual cortex of behaving Alzheimer's disease mice. *Curr Biol* **26,** 956–964.

Lin MZ & Schnitzer MJ (2016). Genetically encoded indicators of neuronal activity. *Nat Neurosci* **19,** 1142–1153.

Lisman J & Raghavachari S (2006). A unified model of the presynaptic and postsynaptic changes during LTP at CA1 synapses. *Sci STKE*.

Lisman J, Yasuda R & Raghavachari S (2012). Mechanisms of CaMKII action in long-term potentiation. *Nat Rev Neurosci* **13,** 169–182.

Lisman JE (2009). The pre/post LTP debate. *Neuron* **63,** 281–284.

Lo DC et al. (2014). Neuronal transfection in brain slices using particle-mediated gene transfer. *Neuron* **5,** 9–11.

Lo DC, McAllister KA & Katz LC (1994). Neuronal transfection in brain slices using particle-mediated gene transfer. *Neuron* **13,** 1263–1268.

Lock JT, Parker I & Smith IF (2015). A comparison of fluorescent Ca2+ indicators for imaging local Ca2+ signals in cultured cells. *Cell Calcium* **58,** 638–648.

Looger LL & Griesbeck O (2011). Genetically encoded neural activity indicators. *Curr Opin Neurobiol* **22,** 18–23.

Lu WY, Man HY, Ju W, Trimble WS, MacDonald JF & Wang YT (2001). Activation of synaptic NMDA receptors induces membrane insertion of new AMPA receptors and LTP in cultured hippocampal neurons. *Neuron* **29,** 243–254.

Lundby A, Mutoh H, Dimitrov D, Akemann W & Knöpfel T (2008). Engineering of a genetically encodable fluorescent voltage sensor exploiting fast Ci-VSP voltage-sensing movements. *PLoS One* **3,** e2514.

Lüthl A, Laurent JP, Figurov A, Muller D & Schachner M (1994). Hippocampal long-term potentiation and neural cell adhesion molecules L1 and NCAM. *Nature* **372,** 777–779.

Lynch G, Larson J, Kelso S, Barrionuevo G & Schottler F (1983). Intracellular injections of EGTA block induction of hippocampal long-term potentiation. *Nature* **305,** 719–721.

Macdougall MJ & Fine A (2013). The expression of long-term potentiation: reconciling the preists and the postivists. *Phil Trans R Soc*.

MacVicar B & Dudek F (1981). Electrotonic coupling between pyramidal cells: a direct demonstration in rat hippocampal slices. *Science (80-)* **213,** 782–785.

Magee JC & Johnston D (1997). A synaptically controlled, associative signal for Hebbian plasticity in hippocampal neurons. *Science (80-)* **275,** 209–213.

Mahmmoud RR, Sase S, Aher YD, Sase A, Gröger M, Mokhtar M, Höger H & Lubec G (2015). Spatial and working memory is linked to spine density and mushroom spines. *PLoS One* **10,** 1–15.

Maisak MS, Haag J, Ammer G, Serbe E, Meier M, Leonhardt A, Schilling T, Bahl A, Rubin GM, Nern A, Dickson BJ, Reiff DF, Hopp E & Borst A (2013). A directional tuning map of Drosophila elementary motion detectors. *Nature* **500,** 212–216.

Makino H & Malinow R (2009). AMPA receptor incorporation into synapses during LTP: The role of lateral movement and exocytosis. *Neuron* **64,** 381–390.

Malenka R, Kauer J, Perkel D, Mauk M, Kelly P, Nicoll R & Waxham M (1989). An essential role for postsynaptic calmodulin and protein kinase activity in long-term potentiation. *Nature* **340,** 554–557.

Maletic-Savatic M, Malinow R & Svoboda K (1999). Rapid dendritic morphogenesis in CA1 hippocampal dendrites induced by synaptic activity. *Science (80-)* **283,** 1923–1927.

Malgaroli A, Ting A, Wendland B, Bergamaschi A, Villa A, Tsien R & RH S (1995). Presynaptic component of long-term potentiation visualized at individual hippocampal synapses. *Science (80-)* **268,** 1624–1628.

Malgaroli A & Tsien RW (1992). Glutamate-induced long-term potentiation of the frequency of miniature synaptic currents. *Nature* **357,** 242–244.

Malinow R & Malenka RC (2002). AMPA receptor trafficking and synaptic plasticity. *Annu Rev Neurosci* **25,** 103–126.

Malinow R, Schulman H & Tsien R (1989). Inhibition of postsynaptic PKC or CaMKII blocks induction but not expression of LTP. *Science (80-)* **245,** 862–866.

Manahan-Vaughan D, Kulla A & Frey JU (2000). Requirement of translation but not transcription for the maintenance of long-term depression in the CA1 region of freely moving rats. *J Neurosci* **20,** 8572–8576.

Mank M & Griesbeck O (2008). Genetically encoded calcium indicators. *Chem Rev* **108,** 1550–1564.

Markram H (2011). A history of spike-timing-dependent plasticity. *Front Synaptic Neurosci* **3,** 1–24.

Markram H, Lubke J, Frotscher M & Sakmann B (1997). Regulation of synaptic efficacy by coincidence of postysnaptic AP and EPSP. *Science (80-)* **275,** 213–215.

Marr D (1971). Simple memory: A theory for archicortex. *Phil Trans R Soc* **262,** 23–81.

Matsuzaki M, Ellis-Davies GC, Nemoto T, Miyashita Y, Iino M & Kasai H (2001). Dendritic spine geometry is critical for AMPA receptor expression in hippocampal CA1 pyramidal neurons. *Nat Neurosci* **4,** 1086–1092.

Matsuzaki M, Honkura N, Ellis-Davies GCR & Kasai H (2004). Structural basis of long-term potentiation in single dendritic spines. *Nature* **429,** 761–766.

Matus A (2000). Actin-based plasticity in dendritic spines. *Science (80-)* **290,** 754–759.

McAllister KA (2000). Biolistic transfection of neurons. *Sci STKE* **2000,** pl1.

Medvedev NI, Dallérac G, Popov VI, Rodriguez Arellano JJ, Davies HA, Kraev I V, Doyère V & Stewart MG (2014). Multiple spine boutons are formed after long-lasting LTP in the awake rat. *Brain Struct Funct* **219,** 407–414.

Medvedev NI, Popov VI, Rodriguez Arellano JJ, Dallérac G, Davies HA, Gabbott PL, Laroche S, Kraev I V., Doyère V & Stewart MG (2010). The N-methyl-d-aspartate receptor antagonist CPP alters synapse and spine structure and impairs long-term potentiation and long-term depression induced morphological plasticity in dentate gyrus of the awake rat. *Neuroscience* **165,** 1170–1181.

Megias M, Emri Z, Freund T & Gulyas A (2001). Total number and distribution of inhibitory and excitatory synapses on hippocampal CA1 pyramidal cells. *Neuroscience* **102,** 527–540.

Meredith RM, Floyer-Lea AM & Paulsen O (2003). Maturation of long-term potentiation induction rules in rodent hippocampus: Role of GABAergic inhibition. *J Neurosci* **23,** 11142–11146.

Meyer D, Bonhoeffer T & Scheuss V (2014). Balance and stability of synaptic structures during synaptic plasticity. *Neuron* **82,** 430–443.

Michel K, Müller JA, Oprişoreanu A-M & Schoch S (2015). The presynaptic active zone: A dynamic scaffold that regulates synaptic efficacy. *Exp Cell Res* **335,** 157–164.

Miles R, Tóth K, Gulyás AI, Hájos N & Freund TF (1996). Differences between somatic and dendritic inhibition in the hippocampus. *Neuron* **16,** 815–823.

Miles R & Wong R (1986). Excitatory synaptic interactions between CA3 neurones in the guinea-pig hippocampus. *J Physiol* **373,** 397–418.

Mishra RK, Kim S, Guzman SJ & Jonas P (2016). Symmetric spike timing-dependent plasticity at CA3–CA3 synapses optimizes storage and recall in autoassociative networks. *Nat Commun* **7,** 11552.

Mittmann W, Wallace DJ, Czubayko U, Herb JT, Schaefer AT, Looger LL, Denk W & Kerr JND (2011). Two-photon calcium imaging of evoked activity from L5 somatosensory neurons in vivo. *Nat Neurosci* **14,** 1089–1093.

Miyawaki A, Llopis J, Heim R, Mccaffery JM, Adams JA, Ikurak M & Tsien RY (1997). Fluorescent indicators for Ca2+ based on green fluorescent proteins and calmodulin. *Lett to Nat* **388,** 882–887.

Molnár E (2011). Long-term potentiation in cultured hippocampal neurons. *Semin Cell Dev Biol* **22,** 506–513.

Morgan SL & Teyler TJ (2001). Electrical stimuli patterned after the theta-rhythm induce multiple forms of LTP. *J Neurophysiol* **86,** 1289–1296.

Morris RGM, Anderson E, Lynch GS & Baudry M (1986). Selective impairment of learning and blockade of long-term potentiation by an N-methyl-D-aspartate receptor antagonist, AP5. *Nature* **319,** 774–776.

Moser EI, Kropff E & Moser M-B (2008). Place cells, grid cells, and the brain's spatial representation system. *Annu Rev Neurosci* **31,** 69–89.

Moser M-B, Trommald M & Andersen P (1994). An increase in dendritic spine density on hippocampal CA1 pyramidal cells following spatial learning in adult rats suggests the formation of new synapses. *Proc Natl Acad Sci USA* **91,** 12673–12675.

Moser M-B, Trommald M, Egeland T & Andersen P (1997). Spatial training in a complex environment and isolation alter the spine distribution differently in rat CA1 pyramidal cells. *J Comp Neurol* **380,** 373–381.

Mulkey R, Herron C & Malenka R (1993). An essential role for protein phosphatases in hippocampal long-term depression. *Science (80-)* **261,** 1051–1055.

Murakoshi H, Wang H & Yasuda R (2011). Local, persistent activation of Rho GTPases during plasticity of single dendritic spines. *Nature* **472,** 100–104.

Murakoshi H & Yasuda R (2012). Postsynaptic signaling during plasticity of dendritic spines. *Trends Neurosci* **35,** 135–143.

Murase S, Mosser E & Schuman EM (2002). Depolarization drives beta-catenin into neuronal spines promoting changes in synaptic structure and function. *Neuron* **35,** 91–105.

Murphy RC & Messer A (2001). Gene transfer methods for CNS organotypic cultures: A comparison of three nonviral methods. *Mol Ther* **3,** 113–121.

Musleh W, Bi X, Tocco G, Yaghoubi S & Baudry M (1997). Glycine-induced long-term potentiation is associated with structural and functional modifications of alpha-amino-3-hydroxyl-5-methyl-4-isoxazolepropionic acid receptors. *Proc Natl Acad Sci USA* **94,** 9451–9456.

Muto A, Ohkura M, Abe G, Nakai J & Kawakami K (2013). Real-time visualization of neuronal activity during perception. *Curr Biol* **23,** 307–311.

Muto A, Ohkura M, Kotani T, Higashijima S, Nakai J & Kawakami K (2011). Genetic visualization with an improved GCaMP calcium indicator reveals spatiotemporal activation of the spinal motor neurons in zebrafish. *Proc Natl Acad Sci USA* **108,** 5425–5430.

Mutoh H, Akemann W & Knöpfel T (2012). Genetically engineered fluorescent voltage reporters. *ACS Chem Neurosci* **3,** 585–592.

Nägerl U V, Willig KI, Hein B, Hell SW & Bonhoeffer T (2008). Live-cell imaging of dendritic spines by STED microscopy. *Proc Natl Acad Sci* **105,** 18982–18987.

Naisbitt S, Eunjoon K, Tu JC, Xiao B, Sala C, Valtschanoff J, Weinberg RJ, Worley PF & Sheng M (1999). Shank, a novel family of postsynaptic density proteins that binds to the NMDA receptor/PSD-95/GKAP complex and cortactin. *Neuron* **23,** 569–582.

Nakai J, Ohkura M & Imoto K (2001). A high signal-to-noise Ca(2+) probe composed of a single green fluorescent protein. *Nat Biotechnol* **19,** 137–141.

Nakajima R, Jung A, Yoon BJ & Baker BJ (2016). Optogenetic monitoring of synaptic activity with genetically encoded voltage indicators. *Front Synaptic Neurosci* **8,** 1–9.

Neves G, Cooke SF & Bliss TVP (2008). Synaptic plasticity, memory and the hippocampus: a neural network approach to causality. *Nat Rev Neurosci* **9,** 65–75.

Nicoll RA & Roche KW (2013). Long-term potentiation: peeling the onion. *Neuropharmacology* **74,** 18–22.

Niethammer M, Kim E & Sheng M (1996). Interaction between the C terminus of NMDA receptor subunits and multiple members of the PSD-95 family of membrane-associated guanylate kinases. *J Neurosci* **16,** 2157–2163.

Nikonenko I, Jourdain P & Muller D (2003). Presynaptic remodeling contributes to activity-dependent synaptogenesis. *J Neurosci* **23,** 8498–8505.

Nimchinsky EA, Yasuda R, Oetner TG & Svoboda K (2004). The number of glutamate receptors opened by synaptic stimulation in single hippocampal spines. *J Neurosci* **24,** 2054–2064.

Nishiyama J & Yasuda R (2015). Biochemical computation for spine structural plasticity. *Neuron* **87,** 63–75.

Nishiyama M, Hong K, Mikoshiba K, Poo M & Kato K (2000). Calcium stores regulate the polarity and input specificity of synaptic modification. *Lett To Nat* **408,** 584–588.

Noguchi J, Matsuzaki M, Ellis-Davies GCR & Kasai H (2005). Spine-neck geometry determines NMDA receptor-dependent Ca2+ signaling in dendrites. *Neuron* **46,** 609–622.

Nowak L, Bregestovski P, Ascher P, Herbet A & Prochiantz A (1984). Magnesium gates glutamate-activated channels in mouse central neurones. *Nature* **307,** 462–465.

Nusser Z, Lujan R, Laube G, Roberts JDB, Molnar E & Somogyi P (1998). Cell type and pathway dependence of synaptic AMPA receptor number and variability in the hippocampus. *Neuron* **21,** 545–559.

O'Keefe J & Dostrovsky J (1971). The hippocampus as a spatial map. Preliminary evidence from unit activity in the freely-moving rat. *Brain Res* **34,** 171–175.

Oh WC, Hill TC & Zito K (2013). Synapse-specific and size-dependent mechanisms of spine structural plasticity accompanying synaptic weakening. *Proc Natl Acad Sci USA* **110,** E305–E312.

Oh WC, Parajuli LK & Zito K (2015). Heterosynaptic structural plasticity on local dendritic segments of hippocampal CA1 neurons. *Cell Rep* **10,** 162–169.

Ohkura M, Matsuzaki M, Kasai H, Imoto K & Nakai J (2005). Genetically encoded bright Ca2+ probe applicable for dynamic Ca2+ imaging of dendritic spines. *Anal Chem* **77,** 5861–5869.

Ohkura M, Sasaki T, Sadakari J, Gengyo-Ando K, Kagawa-Nagamura Y, Kobayashi C, Ikegaya Y & Nakai J (2012). Genetically encoded green fluorescent Ca2+ indicators with improved detectability for neuronal Ca2+ signals. *PLoS One* **7,** e51286.

Okamoto K-I, Nagai T, Miyawaki A & Hayashi Y (2004). Rapid and persistent modulation of actin dynamics regulates postsynaptic reorganization underlying bidirectional plasticity. *Nat Neurosci* **7,** 1104–1112.

Okamoto K-I, Narayanan R, Lee SH, Murata K & Hayashi Y (2007). The role of CaMKII as an F-actin-bundling protein crucial for maintenance of dendritic spine structure. *Proc Natl Acad Sci USA* **104,** 6418–6423.

Opazo P, Labrecque S, Tigaret CM, Frouin A, Wiseman PW, De Koninck P & Choquet D (2010). CaMKII triggers the diffusional trapping of surface AMPARs through phosphorylation of stargazin. *Neuron* **67,** 239–252.

Opazo P, Sainlos M & Choquet D (2012). Regulation of AMPA receptor surface diffusion by PSD-95 slots. *Curr Opin Neurobiol* **22,** 453–460.

Otmakhov N, Khibnik L, Otmakhova N, Carpenter S, Riahi S, Asrican B & Lisman J (2004). Forskolin-induced LTP in the CA1 hippocampal region is NMDA receptor dependent. *J Neurocytol* **91,** 1955–1962.

Otto T, Eichenbaum H, Wible C & Wiener S (1991). Learning-related patterns of CA1 spike trains parallel stimulation parameters optimal for inducing hippocampal long-term potentiation. *Hippocampus* **1,** 181–192.

Ozawa M, Ringwald M & Kemler R (1990). Uvomorulin-catenin complex formation is regulated by a specific domain in the cytoplasmic region of the cell adhesion molecule. *Proc Natl Acad Sci USA* **87,** 4246–4250.

Park M, Penick EC, Edwards JG, Kauer J a & Ehlers MD (2004). Recycling endosomes supply AMPA receptors for LTP. *Science (80-)* **305,** 1972–1975.

Park M, Salgado JM, Ostroff L, Helton TD, Robinson CG, Harris KM & Ehlers MD (2006). Plasticity-induced growth of dendritic spines by exocytic trafficking from recycling endosomes. *Neuron* **52,** 817–830.

Parnass Z, Tashiro A & Yuste R (2000). Analysis of spine morphological plasticity in developing hippocampal pyramidal neurons. *Hippocampus* **10,** 561–568.

Passafaro M, Sala C, Niethammer M & Sheng M (1999). Microtubule binding by CRIPT and its potential role in the synaptic clustering of PSD-95. *Nat Neurosci* **2,** 1063–1069.

Patterson MA, Szatmari EM & Yasuda R (2010). AMPA receptors are exocytosed in stimulated spines and adjacent dendrites in a Ras-ERK-dependent manner during long-term potentiation. *Proc Natl Acad Sci USA* **107,** 15951–15956.

Pavlidis P & Madison D V (1999). Synaptic transmission in pair recordings from CA3 pyramidal cells in organotypic culture. *Am Physiol Soc*2787–2797.

Perez Velazquez JL & Carlen PL (2000). Gap junctions, synchrony and seizures. *Trends Neurosci* **23,** 68–74.

Perez-Velazquez JL, Valiante TA & Carlen PL (1994). Modulation of gap junctional mechanisms during calcium-free induced field burst activity: a possible role for electrotonic coupling in epileptogenesis. *J Neurosci* **14,** 4308–4317.

Peterka DS, Takahashi H & Yuste R (2011). Imaging voltage in neurons. *Neuron* **69,** 9–21.

Pike F & Meredith R (2004). Postsynaptic bursting is essential for "Hebbian"induction of associative long-term potentiation at excitatory synapses in rat hippocampus. *J Physiol*571–576.

Podor B, Hu Y-L, Ohkura M, Nakai J, Croll R & Fine A (2015). Comparison of genetically encoded calcium indicators for monitoring action potentials in mammalian brain by two-photon excitation fluorescence microscopy. *Neurophotonics* **2,** 021014.

Popov VI, Davies HA, Rogachevsky V V, Patrushev I V, Errington ML, Gabbott PLA, Bliss TVP & Stewart MG (2004). Remodelling of synaptic morphology but unchanged synaptic density during late phase long-term potentiation (LTP): a serial section electron micrograph study in the dentate gyrus in the anaesthetised rat. *Neuroscience* **128,** 251–262.

Prevarskaya N, Skryma R & Shuba Y (2011). Calcium in tumour metastasis: new roles for known actors. *Nat Rev Cancer* **11,** 609–618.

Prince LY, Bacon TJ, Tigaret CM & Mellor JR (2016). Neuromodulation of the feedforward dentate gyrus-CA3 microcircuit. *Front Synaptic Neurosci* **8,** 32.

Pyapali G, Sik A, Penttonen M, Buzsaki G & Turner D (1998). Dendritic properties of hippocampal CA1 pyramidal neurons in the rat: intracellular staining in vivo and in vitro. *J Comp Neurol* **16,** 335–352.

Raghavachari S & Lisman JE (2004). Properties of quantal transmission at CA1 synapses. *J Neurophysiol* **92,** 2456–2467.

Ramos JM (1998). Retrograde amnesia for spatial information: a dissociation between intra and extramaze cues following hippocampus lesions in rats. *Eur J Neurosci* **10,** 3295–3301.

Raymond CR & Redman SJ (2006). Spatial segregation of neuronal calcium signals encodes different forms of LTP in rat hippocampus. *J Physiol* **570,** 97–111.

Reid CA, Dixon DB, Takahashi M, Bliss TVP & Fine A (2004). Optical quantal analysis indicates that long-term potentiation at single hippocampal mossy fiber synapses is expressed through increased release probability, recruitment of new release sites, and activation of silent synapses. *J Neurosci* **24,** 3618–3626.

Reid CA, Fabian-Fine R & Fine A (2001). Postsynaptic calcium transients evoked by activation of individual hippocampal mossy fiber synapses. *J Neurosci* **21,** 2206–2214.

Rickgauer JP, Deisseroth K & Tank DW (2014). Simultaneous cellular-resolution optical perturbation and imaging of place cell firing fields. *Nat Neurosci* **17,** 1816–1824.

Rocca DL, Martin S, Jenkins EL & Hanley JG (2008). Inhibition of Arp2 / 3-mediated actin polymerization by PICK1 regulates neuronal morphology and AMPA receptor endocytosis. *Nat Cell Biol*; DOI: 10.1038/ncb1688.

Ron S, Dudai Y & Segal M (2012). Overexpression of PKMz alters morphology and function of dendritic spines in cultured cortical neurons. *Cereb Cortex* **22,** 2519–2528.

De Roo M, Klauser P & Muller D (2008). LTP promotes a selective long-term stabilization and clustering of dendritic spines. *PLoS Biol* **6,** e219.

Ropireddy D, Scorcioni R, Lasher B, Buzsaki G & Ascoli GA (2011). Axonal morphometry of hippocampal pyramidal neurons semi-automatically reconstructed after in vivo labeling in different CA3 locations. *Brain Struct Funct* **216,** 1–15.

Rusakov DA, Davies HA, Harrison E, Diana G, Richter-Levin G, Bliss T V & Stewart MG (1997). Ultrastructural synaptic correlates of spatial learning in rat hippocampus. *Neuroscience* **80,** 69–77.

Rusakov DA & Kullmann DM (1998). Extrasynaptic glutamate diffusion in the hippocampus: ultrastructural constraints, uptake, and receptor activation. *J Neurosci* **18,** 3158–3170.

Russo-Neustadt A, Ha T, Ramirez R & Kesslak JP (2001). Physical activity-antidepressant treatment combination: Impact on brain-derived neurotrophic factor and behavior in an animal model. *Behav Brain Res* **120,** 87–95.

Sabatini BL, Maravall M & Svoboda K (2001). Ca2+ signaling in dendritic spines. *Curr Opin Neurobiol* **11,** 349–356.

Saglietti L, Dequidt C, Kamieniarz K, Rousset MC, Valnegri P, Thoumine O, Beretta F, Fagni L, Choquet D, Sala C, Sheng M & Passafaro M (2007). Extracellular interactions between GluR2 and N-cadherin in spine regulation. *Neuron* **54,** 461–477.

Sakai R, Repunte-Canonigo V, Raj CD & Knöpfel T (2001). Design and characterization of a DNA-encoded, voltage-sensitive fluorescent protein. *Eur J Neurosci* **13,** 2314–2318.

Sala C, Cambianica I & Rossi F (2008). Molecular mechanisms of dendritic spine development and maintenance. *Prog Neurobiol* **68,** 289–304.

Sala C, Piëch V, Wilson NR, Passafaro M, Liu G & Sheng M (2001). Regulation of dendritic spine morphology and synaptic function by Shank and Homer. *Neuron* **31,** 115–130.

Sala C & Segal M (2014). Dendritic spines: the locus of structural and functional plasticity. *Physiol Rev* **94,** 141–188.

Sanders J, Cowansage K, Baumgartel K & Mayford M (2012). Elimination of dendritic spines with long-term memory is specific to active circuits. *J Neurosci* **32,** 12570–12578.

Sayer RJ, Friedlander MJ & Redman SJ (1990). The time course and amplitude of EPSPs evoked at synapses between pairs of CA3/CA1 neurons in the hippocampal slice. *J Neurosci* **10,** 826–836.

Scanziani M, Salin PA, Vogt KE, Malenka RC & Nicoll RA (1997). Use-dependent increases in glutamate concentration activate presynaptic metabotropic glutamate receptors. *Lett To Nat* **385,** 630–634.

Scharfman HE (1994). Synchronization of area CA3 hippocampal cells and non-granule cells of the dentate gyrus in bicuculline-treated rat hippocampal slices. *Neuroscience* **59,** 245–257.

Schikorski T & Stevens CF (1997). Quantitative ultrastructural analysis of hippocampal excitatory synapses. *J Neurosci* **17,** 5858–5867.

Schmitz D, Schuchmann S, Fisahn A, Draguhn A, Buhl EH, Petrasch-Parwez E, Dermietzel R, Heinemann U & Traub RD (2001). Axo-axonal coupling: A novel mechanism for ultrafast neuronal communication. *Neuron* **31,** 831–840.

Schneider C, Rasband W & Eliceiri K (2012). NIH Image to ImageJ: 25 years of image analysis. *Nat Methods* **9,** 671–675.

Scimemi A, Fine A, Kullmann DM & Rusakov DA (2004). NR2B-containing receptors mediate cross talk among hippocampal synapses. *J Neurosci* **24,** 4767–4777.

Scoville WB & Milner B (1957). Loss of recent memory after bilateral hippocampal lesions. 1957. *J Neuropsychiatry Clin Neurosci* **12,** 103–113.

Sdrulla AD & Linden DJ (2007). Double dissociation between long-term depression and dendritic spine morphology in cerebellar Purkinje cells. *Nat Neurosci* **10,** 546–548.

Shen K & Meyer T (1999). Dynamic control of CaMKII translocation and localization in hippocampal neurons by NMDA receptor stimulation. *Science (80-)* **284,** 162–166.

Shepherd GMG & Harris KM (1998). Three-dimensional structure and composition of CA3->CA1 axons in rat hippocampal slices: implications for presynaptic connectivity and compartmentalization. *J Neurosci* **18,** 8300–8310.

Sherrington C (1897). The central nervous system. In A textbook of physiology, 7th ed. (Ed. Foster M). Vol. 3.

Shigetomi E, Kracun S & Khakh BS (2010). Monitoring astrocyte calcium microdomains with improved membrane targeted GCaMP reporters. *Neuron Glia Biol* **6,** 1–9.

Shimomura O, Johnson FH & Saiga Y (1962). Extraction, purification and properties of Aequorin, a bioluminescent protein from the luminous Hydromedusan, Aequorea. *J Cell Comp Physiol* **59,** 223–239.

Shindo A, Hara Y, Yamamoto TS, Ohkura M, Nakai J & Ueno N (2010). Tissue-tissue interaction-triggered calcium elevation is required for cell polarization during Xenopus gastrulation. *PLoS One* **5,** e8897.

Shipman SL & Nicoll RA (2012). Dimerization of postsynaptic neuroligin drives synaptic assembly via transsynaptic clustering of neurexin. *Proc Natl Acad Sci USA* **109,** 19432–19437.

Siegel MS & Isacoff EY (1997). Probe of membrane voltage. *Neuron* **19,** 735–741.

Sik A, Tamamaki N & Freund TF (1993). Complete axon arborization of a single CA3 pyramidal cell in the rat hippocampus, and its relationship with postsynaptic parvalbumin-containing interneurons. *Eur J Neurosci* **5,** 1719–1728.

De Simoni A, Griesinger CB & Edwards FA (2003). Development of rat CA1 neurones in acute versus organotypic slices: role of experience in synaptic morphology and activity. *J Physiol* **550,** 135–147.

Sinnen BL, Bowen AB, Forte JS, Hiester BG, Crosby KC, Gibson ES, Dell'Acqua ML & Kennedy MJ (2017). Optogenetic control of synaptic composition and function. *Neuron* **93,** 646–660.

Sjöström P, Turrigiano G & Nelson S (2001). Rate, timing, and cooperativity jointly determine cortical synaptic plasticity. *Neuron* **32,** 1149–1164.

Skrede K & Malthe-Sørenssen D (1981). Increased resting and evoked release of transmitter following repetitive electrical tetanization in hippocampus: a biochemical correlate to long-lasting synaptic potentiation. *Brain Res* **208,** 436–441.

Skrede K & Westgaard R (1971). The transverse hippocampal slice: a well-defined cortical structure maintained in vitro. *Brain Res* **35,** 589–593.

Smirnov MS, Evans PR, Garrett TR, Yan L & Yasuda R (2017). Automated remote focusing, drift correction, and photostimulation to evaluate structural plasticity in dendritic spines. *PLoS One* **12,** 1–14.

Soares C, Lee KF, Nassrallah W & Beique JC (2013). Differential subcellular targeting of glutamate receptor subtypes during homeostatic synaptic plasticity. *J Neurosci* **33,** 13547–13559.

Song S, Miller KD & Abbott LF (2000). Competitive Hebbian learning through spike-timing-dependent synaptic plasticity. *Nat Neurosci* **3,** 919–926.

Sorra KE & Harris K (2000). Overview on the structure, composition, function, development, and plasticity of hippocampal dendritic spines. *Hippocampus* **10,** 501–511.

Sorra KE & Harris KM (1998). Stability in synapse number and size at 2 hr after long-term potentiation in hippocampal area CA1. *J Neurosci* **18,** 658–671.

Souslova EA, Belousov V V, Lock JG, Strömblad S, Kasparov S, Bolshakov AP, Pinelis VG, Labas YA, Lukyanov S, Mayr LM & Chudakov DM (2007). Single fluorescent protein-based Ca2+ sensors with increased dynamic range. *BMC Biotechnol* **7,** 37.

Spruston N & McBain C (2007). Structural and functional properties of hippocampal neurons. In *The hippocampus book*, pp. 154–222.

St-Pierre F, Marshall JD, Yang Y, Gong Y, Schnitzer MJ & Lin MZ (2014). High-fidelity optical reporting of neuronal electrical activity with an ultrafast fluorescent voltage sensor. *Nat Neurosci* **17,** 884–889.

Staley KJ, Otis TS & Mody I (1992). Membrane properties of dentate gyrus granule cells: comparison of sharp microelectrode and whole-cell recordings. *J Neurophysiol* **67,** 1346–1358.

Stanton PK, Winterer J, Bailey CP, Kyrozis A, Raginov I, Laube G, Veh RW, Nguyen CQ & Müller W (2003). Long-term depression of presynaptic release from the readily releasable vesicle pool induced by NMDA receptor-dependent retrograde nitric oxide. *J Neurosci* **23,** 5936–5944.

Star EN, Kwiatkowski DJ & Murthy VN (2002). Rapid turnover of actin in dendritic spines and its regulation by activity. *Nat Neurosci* **5,** 239–246.

Stäubli U, Chun D & Lynch G (1998). Time-dependent reversal of long-term potentiation by an integrin antagonist. *J Neurosci* **18,** 3460–3469.

Stein IS, Gray JA & Zito K (2015). Non-ionotropic NMDA receptor signaling drives activity-induced dendritic spine shrinkage. *J Neurosci* **35,** 12303–12308.

Steiner P, Higley MJ, Xu W, Czervionke BL, Malenka RC & Sabatini BL (2008). Destabilization of the postsynaptic density by PSD-95 Serine 73 phosphorylation inhibits spine growth and synaptic plasticity. *Neuron* **60,** 788–802.

Stewart MG, Medvedev NI, Popov VI, Schoepfer R, Davies HA, Murphy K, Dallérac GM, Kraev I V & Rodríguez JJ (2005). Chemically induced long-term potentiation increases the number of perforated and complex postsynaptic densities but does not alter dendritic spine volume in CA1 of adult mouse hippocampal slices. *Eur J Neurosci* **21,** 3368–3378.

Stoppini L, Buchs P & Muller D (1991). A simple method for organotypic cultures of nervous tissue. *Neurosci Methods* **37,** 173–182.

Stranahan AM, Zhou Y, Martin B & Maudsley S (2009). Pharmacomimetics of exercise: novel approaches for hippocampally-targeted neuroprotective agents. *Curr Med Chem* **16,** 4668–4678.

Streit P, Thompson S & Gähwiler B (1989). Anatomical and physiological properties of GABAergic neurotransmission in organotypic slice cultures of rat hippocampus. *Eur J Neurosci* **1,** 603–615.

Stuart GJ & Sakmann B (1994). Active propagation of somatic action potentials into neocortical pyramidal cell dendrites. *Nature* **367,** 69–72.

Südhof TC (2012). The presynaptic active zone. *Neuron* **75,** 11–25.

Sun XR, Badura A, Pacheco DA, Lynch LA, Schneider ER, Taylor MP, Hogue IB, Enquist LW, Murthy M & Wang SS (2013). Fast GCaMPs for improved tracking of neuronal activity. *Nat Commun* **4,** 2170.

Suri D & Vaidya V (2013). Glucocorticoid regulation of brain-derived neurotrophic factor: Relevance to hippocampal structural and functional plasticity. *Neuroscience* **239,** 196–213.

Suzuki J, Kanemaru K, Ishii K, Ohkura M, Okubo Y & Iino M (2014). Imaging intraorganellar Ca(2+) at subcellular resolution using CEPIA. *Nat Commun* **5,** 4153.

Takasaki K & Sabatini BL (2014). Super-resolution 2-photon microscopy reveals that the morphology of each dendritic spine correlates with diffusive but not synaptic properties. *Front Neuroanat* **8,** 1–7.

Takumi Y, Ramírez-León V, Laake P, Rinvik E & Ottersen OP (1999). Different modes of expression of AMPA and NMDA receptors in hippocampal synapses. *Nat Neurosci* **2,** 618–624.

Tallini YN, Ohkura M, Choi B-R, Ji G, Imoto K, Doran R, Lee J, Plan P, Wilson J, Xin H-B, Sanbe A, Gulick J, Mathai J, Robbins J, Salama G, Nakai J & Kotlikoff MI (2006). Imaging cellular signals in the heart in vivo: Cardiac expression of the high-signal Ca2+ indicator GCaMP2. *Proc Natl Acad Sci USA* **103,** 4753–4758.

Tamamki N & Nojyo Y (1990). Disposition of the slab-like modules formed by axon branches originating from single CA1 pyramidal neurons in the rat hippocampus. *J Comp Neurol* **291,** 509–519.

Tanaka J-I, Horiike Y, Matsuzaki M, Miyazaki T, Ellis-Davies GCR & Kasai H (2008). Protein synthesis and neurotrophin-dependent structural plasticity of single dendritic spines. *Science (80-)* **319,** 1683–1687.

Tang S & Yasuda R (2017). Imaging ERK and PKA activation in single dendritic spines during structural plasticity. *Neuron* **93,** 1315–1324.e3.

Tashiro A, Dunaevsky A, Blazeski R, Mason CA & Yuste R (2003). Bidirectional regulation of hippocampal mossy fiber filopodial motility by kainate receptors: A two-step model of synaptogenesis. *Neuron* **38,** 773–784.

Thomson A & Radpour S (1991). Excitatory connections between CA1 pyramidal cells revealed by spike triggered averaging in slices of rat hippocampus are partially NMDA receptor mediated. *Eur J Neurosci* **3,** 587–601.

Thornton JA, Rothblat LA & Murray EA (1997). Rhinal cortex removal produces amnesia for preoperatively learned discrimination problems but fails to disrupt postoperative acquisition and retention in rhesus monkeys. *J Neurosci* **17,** 8536–8549.

Tian L, Hires SA, Mao T, Huber D, Chiappe ME, Chalasani SH, Petreanu L, Akerboom J, McKinney SA, Schreiter ER, Bargmann CI, Jayaraman V, Svoboda K & Looger LL (2009). Imaging neural activity in worms, flies and mice with improved GCaMP calcium indicators. *Nat Methods* **6,** 875–881.

Tian L & Looger LL (2008). Genetically encoded fluorescent sensors for studying healthy and diseased nervous systems. *Drug Discov Today Dis Models* **5,** 27–35.

Tomita S, Stein V, Stocker TJ, Nicoll RA & Bredt DS (2005). Bidirectional synaptic plasticity regulated by phosphorylation of stargazin-like TARPs. *Neuron* **45,** 269–277.

Toni N, Buchs PA, Nikonenko I, Bron CR & Muller D (1999). LTP promotes formation of multiple spine synapses between a single axon terminal and a dendrite. *Nature* **402,** 421–425.

Tønnesen J, Katona G, Rózsa B & Nägerl UV (2014). Spine neck plasticity regulates compartmentalization of synapses. *Nat Neurosci* **17,** 678–685.

Tønnesen J & Nägerl UV (2013). Two-color STED imaging of synapses in living brain slices. *Methods Mol Biol* **950,** 65–80.

Törk I (1990). Anatomy of the serotonergic system. *Ann N Y Acad Sci* **600,** 9–34.

Török K & Trentham D (1994). Mechanism of 2-chloro-(epsilon-amino-Lys75)-[6-[4-(N,N- diethylamino)phenyl]-1,3,5-triazin-4-yl]calmodulin interactions with smooth muscle myosin light chain kinase and derived peptides. *Biochemistry* **33,** 12807–12820.

Tóth K, Borhegyi Z & Freund TF (1993). Postsynaptic targets of GABAergic hippocampal neurons in the medial septum-diagonal band of broca complex. *J Neurosci* **13,** 3712–3724.

Traub RD & Bibbig A (2000). A model of high-frequency ripples in the hippocampus based on synaptic coupling plus axon-axon gap junctions between pyramidal neurons. *J Neurosci* **20,** 2086–2093.

Trommald M & Hulleberg G (1997). Dimensions and density of dendritic spines from rat dentate granule cells based on reconstructions from serial electron micrographs. *J Comp Neurol* **377,** 15–28.

Trommald M, Hulleberg G & Andersen P (1996). Long-term potentiation is associated with new excitatory spine synapses on rat dentate granule cells. *Learn Mem* **3,** 218–228.

Trommald M, Vaaland J, Blackstad T & Andersen P (1990). Dendritic spine change in rat dentate granule cells associated with long-term potentiation. *Neurotox Excit Amin Acids* **ed. A. Gui,** 163–174.

Tsutsui H, Karasawa S, Okamura Y & Miyawaki A (2008). Improving membrane voltage measurements using FRET with new fluorescent proteins. *Nat Methods* **5,** 683–685.

Urban NT, Willig KI, Hell SW & Nägerl UV (2011). STED nanoscopy of actin dynamics in synapses deep inside living brain slices. *Biophys J* **101,** 1277–1284.

Wang H-X, Gerkin RC, Nauen DW & Bi G-Q (2005). Coactivation and timing-dependent integration of synaptic potentiation and depression. *Nat Neurosci* **8,** 187–193.

Wang Q, Shui B, Kotlikoff MI & Sondermann H (2008). Structural basis for calcium sensing by GCaMP2. *Cell* **16,** 1817–1827.

Wang X, Yang Y & Zhou Q (2007). Independent expression of synaptic and morphological plasticity associated with long-term depression. *J Neurosci* **27,** 12419–12429.

Ward B, McGuinness L, Akerman CJJ, Fine A, Bliss TVP & Emptage NJ (2006). State-dependent mechanisms of LTP expression revealed by optical quantal analysis. *Neuron* **52,** 649–661.

Watson DJ, Ostroff L, Cao G, Parker PH, Smith H & Harris KM (2016). LTP enhances synaptogenesis in the developing hippocampus. *Hippocampus* **26,** 560–576.

Wenthold RJ, Prybylowski K, Standley S, Sans N & Petralia RS (2003). Trafficking of NMDA receptors. *Annu Rev Pharmacol Toxicol* **43,** 335–358.

Wiegert JS & Oertner TG (2013). Long-term depression triggers the selective elimination of weakly integrated synapses. *Proc Natl Acad Sci USA* **110,** E4510–E4519.

Wittenberg GM & Wang SS-H (2006). Malleability of spike-timing-dependent plasticity at the CA3-CA1 synapse. *J Neurosci* **26,** 6610–6617.

Woods GF, Oh WC, Boudewyn LC, Mikula SK & Zito K (2011). Loss of PSD-95 enrichment is not a prerequisite for spine retraction. *J Neurosci* **31,** 12129–12138.

Wu J, Abdelfattah AS, Miraucourt LS, Kutsarova E, Ruangkittisakul A, Zhou H, Ballanyi K, Wicks G, Drobizhev M, Rebane A, Ruthazer ES & Campbell RE (2014). A long stokes shift red fluorescent Ca2+ indicator protein for two-photon and ratiometric imaging. *Nat Commun*.

Wu J, Liu L, Matsuda T, Zhao Y, Rebane A, Drobizhev M, Chang Y-F, Araki S, Arai Y, March K, Hughes TE, Sagou K, Miyata T, Nagai T, Li W-H & Campbell RE (2013). Improved orange and red Ca^2+ indicators and photophysical considerations for optogenetic applications. *ACS Chem Neurosci* **4,** 963–972.

Yamada Y & Mikoshiba K (2012). Quantitative comparison of novel GCaMP-type genetically encoded Ca(2+) indicators in mammalian neurons. *Front Cell Neurosci* **6,** 41.

Yamagata Y, Kobayashi S, Umeda T, Inoue A, Sakagami H, Fukaya M, Watanabe M, Hatanaka N, Totsuka M, Yagi T, Obata K & Imoto K (2009). Kinase-dead knock-in mouse reveals an essential role of kinase activity of Ca2+/ calmodulin-dependent protein kinase IIα in dendritic spine enlargement, long-term potentiation, and learning. *J Neurosci* **29,** 7607–7618.

Yamamoto C & McIlwain H (1966*a*). Potentials evoked in vitro in preparations from the mammalian brain. *Nature* **210,** 1055–5.

Yamamoto C & McIlwain H (1966*b*). Electrical activities in thin sections from the mammalian brain maintained in chemically-defined media in vitro. *J Neurochem* **13,** 1333–1343.

Yang Y, Wang X, Frerking M & Zhou Q (2008). Spine expansion and stabilization associated with long-term potentiation. *J Neurosci* **28,** 5740–5751.

Yuste R (2013). Electrical compartmentalization in dendritic spines. *Annu Rev Neurosci* **36,** 429–449.

Yuste R & Bonhoeffer T (2001). Morphological changes in dendritic spines associated with long-term synaptic plasticity. *Annu Rev Neurosci* **24,** 1071–1089.

Yuste R & Denk W (1995). Dendritic spines as basic functional units of neuronal integration. *Nature* **375,** 682–684.

Yuste R, Majewska A, Cash SS & Denk W (1999). Mechanisms of calcium influx into hippocampal spines: heterogeneity among spines, coincidence detection by NMDA receptors, and optical quantal analysis. *J Neurosci* **19,** 1976–1987.

Zakharenko S, Zablow L & Siegelbaum S (2001). Visualization of changes in presynaptic function during long-term synaptic plasticity. *Nat Neurosci* **4,** 711–717.

Zalutsky RA & Nicoll RA (1990). Comparison of two forms of long-term potentiation in single hippocampal neurons. *Science (80-)* **248,** 1619–1624.

Zhang X, Pöschel B, Faul C, Upreti C, Stanton PK & Mundel P (2013). Essential role for synaptopodin in dendritic spine plasticity of the developing hippocampus. *J Neurosci* **33,** 12510–12518.

Zhao S, Studer D, Chai X, Graber W, Brose N, Nestel S, Young C, Rodriguez EP, Saetzler K & Frotscher M (2012). Structural plasticity of hippocampal mossy fiber synapses as revealed by high-pressure freezing. *J Comp Neurol* **520,** 2340–2351.

Zhao Y, Abdelfattah AS, Zhao Y, Ruangkittisakul A, Ballanyi K, Campbell RE & Harrison DJ (2014). Microfluidic cell sorter-aided directed evolution of a protein-based calcium ion indicator with an inverted fluorescent response. *Integr Biol (Camb)* **6,** 714–725.

Zhao Y, Araki S, Wu J, Teramoto T, Chang Y-F, Nakano M, Abdelfattah AS, Fujiwara M, Ishihara T, Nagai T & Campbell RE (2011). An expanded palette of genetically encoded Ca^{2+} indicators. *Science (80-)* **333,** 1888–1891.

Zhou L, Jones E V. & Murai KK (2012). EphA signaling promotes actin-based dendritic spine remodeling through slingshot phosphatase. *J Biol Chem* **287,** 9346–9359.

Zhou Q, Homma KJ & Poo M (2004). Shrinkage of dendritic spines associated with long-term depression of hippocampal synapses. *Neuron* **44,** 749–757.

Zieliński K (2006). Jerzy Konorski on brain associations. *Acta Neurobiol Exp (Wars)* **66,** 75–84.

Zimmer J & Gähwiler B (1984). Cellular and connective organization of slice cultures of the rat hippocampus and fascia dentata. *J Comp Neurol* **228,** 432–446.

Zola-Morgan S, Squire LR & Amaral DG (1986). Human amnesia and the medial temporal region: enduring memory impairment following a bilateral lesion limited to field CA1 of the hippocampus. *J Neurosci* **6,** 2950–2967.

APPENDIX A: COPYRIGHT PERMISSION LETTERS

ELSEVIER LICENSE
TERMS AND CONDITIONS

May 20, 2017

This Agreement between Borbala Podor ("You") and Elsevier ("Elsevier") consists of your license details and the terms and conditions provided by Elsevier and Copyright Clearance Center.

License Number	4104511435238
License date	May 08, 2017
Licensed Content Publisher	Elsevier
Licensed Content Publication	Trends in Neurosciences
Licensed Content Title	Postsynaptic signaling during plasticity of dendritic spines
Licensed Content Author	Hideji Murakoshi,Ryohei Yasuda
Licensed Content Date	Feb 1, 2012
Licensed Content Volume	35
Licensed Content Issue	2
Licensed Content Pages	9
Start Page	135
End Page	143
Type of Use	reuse in a thesis/dissertation
Intended publisher of new work	other
Portion	figures/tables/illustrations
Number of figures/tables /illustrations	1
Format	both print and electronic
Are you the author of this Elsevier article?	No
Will you be translating?	No
Order reference number	
Original figure numbers	Figure 2
Title of your thesis/dissertation	NOVEL APPROACHES TO THE STUDY OF SYNAPTIC PLASTICITY IN THE RAT HIPPOCAMPUS
Expected completion date	Jun 2017
Estimated size (number of pages)	150

JOHN WILEY AND SONS LICENSE TERMS AND CONDITIONS

May 20, 2017

This Agreement between Borbala Podor ("You") and John Wiley and Sons ("John Wiley and Sons") consists of your license details and the terms and conditions provided by John Wiley and Sons and Copyright Clearance Center.

License Number	4104501149187
License date	May 08, 2017
Licensed Content Publisher	John Wiley and Sons
Licensed Content Publication	Journal of Comparative Neurology
Licensed Content Title	Dendritic morphology of CA1 pyramidal neurones from the rat hippocampus: I. Branching patterns
Licensed Content Author	N. J. Bannister,A. U. Larkman
Licensed Content Date	Sep 11, 1995
Licensed Content Pages	11
Type of use	Dissertation/Thesis
Requestor type	University/Academic
Format	Print and electronic
Portion	Figure/table
Number of figures/tables	1
Original Wiley figure/table number(s)	Figure 9
Will you be translating?	No
Title of your thesis / dissertation	NOVEL APPROACHES TO THE STUDY OF SYNAPTIC PLASTICITY IN THE RAT HIPPOCAMPUS
Expected completion date	Jun 2017
Expected size (number of pages)	150
Requestor Location	Borbala Podor 5850 College St, Room 3B-1 Dalhousie University Department of Physiology & Biophysics Halifax, NS B3H 4R2 Canada Attn: Borbala Podor
Publisher Tax ID	EU826007151
Billing Type	Invoice

ELSEVIER LICENSE
TERMS AND CONDITIONS

May 20, 2017

This Agreement between Borbala Podor ("You") and Elsevier ("Elsevier") consists of your license details and the terms and conditions provided by Elsevier and Copyright Clearance Center.

License Number	4104511268528
License date	May 08, 2017
Licensed Content Publisher	Elsevier
Licensed Content Publication	Neuron
Licensed Content Title	The Dynamic Synapse
Licensed Content Author	Daniel Choquet,Antoine Triller
Licensed Content Date	Oct 30, 2013
Licensed Content Volume	80
Licensed Content Issue	3
Licensed Content Pages	13
Start Page	691
End Page	703
Type of Use	reuse in a thesis/dissertation
Intended publisher of new work	other
Portion	figures/tables/illustrations
Number of figures/tables /illustrations	1
Format	both print and electronic
Are you the author of this Elsevier article?	No
Will you be translating?	No
Order reference number	
Original figure numbers	Figure 3/c.
Title of your thesis/dissertation	NOVEL APPROACHES TO THE STUDY OF SYNAPTIC PLASTICITY IN THE RAT HIPPOCAMPUS
Expected completion date	Jun 2017
Estimated size (number of pages)	150

ELSEVIER LICENSE
TERMS AND CONDITIONS

May 20, 2017

This Agreement between Borbala Podor ("You") and Elsevier ("Elsevier") consists of your license details and the terms and conditions provided by Elsevier and Copyright Clearance Center.

License Number	4104510844873
License date	May 08, 2017
Licensed Content Publisher	Elsevier
Licensed Content Publication	Neuron
Licensed Content Title	The Spike-Timing Dependence of Plasticity
Licensed Content Author	Daniel E. Feldman
Licensed Content Date	Aug 23, 2012
Licensed Content Volume	75
Licensed Content Issue	4
Licensed Content Pages	16
Start Page	556
End Page	571
Type of Use	reuse in a thesis/dissertation
Intended publisher of new work	other
Portion	figures/tables/illustrations
Number of figures/tables /illustrations	1
Format	both print and electronic
Are you the author of this Elsevier article?	No
Will you be translating?	No
Order reference number	
Original figure numbers	Figure 1
Title of your thesis/dissertation	NOVEL APPROACHES TO THE STUDY OF SYNAPTIC PLASTICITY IN THE RAT HIPPOCAMPUS
Expected completion date	Jun 2017
Estimated size (number of pages)	150

NATURE PUBLISHING GROUP LICENSE
TERMS AND CONDITIONS

May 08, 2017

This Agreement between Borbala Podor ("You") and Nature Publishing Group ("Nature Publishing Group") consists of your license details and the terms and conditions provided by Nature Publishing Group and Copyright Clearance Center.

License Number	4104500476206
License date	May 08, 2017
Licensed Content Publisher	Nature Publishing Group
Licensed Content Publication	Nature Reviews Neuroscience
Licensed Content Title	Synaptic plasticity, memory and the hippocampus: a neural network approach to causality
Licensed Content Author	Guilherme Neves, Sam F. Cooke and Tim V. P. Bliss
Licensed Content Date	Jan 1, 2008
Licensed Content Volume	9
Licensed Content Issue	1
Type of Use	reuse in a dissertation / thesis
Requestor type	academic/educational
Format	print and electronic
Portion	figures/tables/illustrations
Number of figures/tables /illustrations	1
High-res required	no
Figures	Figure 1. Basic anatomy of the hippocampus.
Author of this NPG article	no
Your reference number	
Title of your thesis / dissertation	NOVEL APPROACHES TO THE STUDY OF SYNAPTIC PLASTICITY IN THE RAT HIPPOCAMPUS
Expected completion date	Jun 2017
Estimated size (number of pages)	150
Requestor Location	Borbala Podor 5850 College St, Room 3B-1 Dalhousie University Department of Physiology & Biophysics Halifax, NS B3H 4R2 Canada Attn: Borbala Podor
Billing Type	Invoice

RE: Academic Permissions Request Form

Academic Permissions <Academic.permissions@oup.com>

Wed 5/24/2017 6:24 AM

To:Borbala Podor <Borbala.Podor@Dal.Ca>;

Dear Borbala,

Thank you for your request. You have our permission to use the OUP Material you list in your email below in your thesis/dissertaBon for submission to Dalhousie University.

If at some future date your thesis/dissertaBon is published it will be necessary to reEclear this permission. **Please note that if the material to be used is acknowledged to any other source, you will need to clear permission with the rights holder.**

We will also require you to include a disclaimer in the electronic ediBon which excludes OUP material from any CreaBve CommonsEstyle license that would allow onward reuse of our content, direcBng people to seek permission from OUP directly via our website: www.oup.com.

Kind regards,
Tom McKibbin
Permissions ExecuBve

EEEEOriginal MessageEEEE
From: no.reply@oup.com [mailto:no.reply@oup.com]
Sent: 20 May 2017 20:27
To: Academic Permissions
Subject: Academic Permissions Request Form

URL: /academic/rights/permissions/request

a First name: Borbala

b Last name: Podor

c InsBtuBon/Company: Dalhousie University

d Address: 5850 College Street
Department of Physiology & Biophysics
Dalhousie University
Halifax, NS

e Postcode: B3H 4R2

f Country: Canada

i Email: borbala.podor@dal.ca

G Z TheirTitle: "Novel approaches to the study of synapBc plasBcity in the rat hippocampus"
PhD dissertaBon

H Z Author: Borbala Podor

H Z Publisher: Dalhousie University

I Z Covers: Both

I Z PrintRunHard: 1

I Z pubDate: June 2017

J Z Territory: World

K Z Language: English

K Z Notes: Reprint permission of 2 figures from the Hippocampus Book, 2007, for PhD dissertaBon

L Z Media1: illustraBon

M Z Author1: Per Andersen, Richard Morris, David Amaral, Tim Bliss & John O'Keefe

M Z editedby1: Per Andersen, Richard Morris, David Amaral, Tim Bliss & John O'Keefe

M Z Title1: The Hippocampus Book

N Z Material1: Figure 5E1: CA1 dendriBc morphology, spines and synapBc inputs and outputs.
Found on Page 135, in Chapter 5: Structural and FuncBonal ProperBes of Hippocampal Neurons. Chapter by Nelson Spruston, Chris McBain

O Z OUPpubDate1: 2007

L Z Media2: illustraBon

M Z Author2: Per Andersen, Richard Morris, David Amaral, Tim Bliss & John O'Keefe

M Z editedby2: Per Andersen, Richard Morris, David Amaral, Tim Bliss & John O'Keefe

M Z Title2: The Hippocampus Book

N Z Material2: Figure 5E7: CA3 dendriBc morphology, thorny excrescences, and synapBc inputs and outputs.
Found on Page 154, in Chapter 5: Structural and FuncBonal ProperBes of Hippocampal Neurons. Chapter by Nelson Spruston, Chris McBain

O Z OUPpubDate2: 2007

M Z Title3:

W Z AddiBonal: